Cortico-thalamic interactions for head direction coding

by

Marie-Sophie Helene van der Goes

Submitted to the Department of Brain and Cognitive Sciences
in partial fulfillment of the requirements for the degree of

Doctor of Philosophy

at the

MASSACHUSETTS INSTITUTE OF TECHNOLOGY

May 2022

Author . . . . . .

Department of Brain and Cognitive Sciences
April 27, 2022

Certified by. . . . . .

Mark T. Harnett
Associate Professor of Neuroscience;
Graduate Officer, Department of Brain and Cognitive Sciences
Thesis Supervisor

Accepted by . . . . . .

Mark T. Harnett
Associate Professor of Neuroscience;
Graduate Officer, Department of Brain and Cognitive Sciences

Cortico-thalamic interactions for head direction coding

by

Marie-Sophie Helene van der Goes

Submitted to the Department of Brain and Cognitive Sciences
on April 27, 2022, in partial fulfillment of the
requirements for the degree of
Doctor of Philosophy

Abstract

The ability to orient oneself within an environment is critical for spatial navigation and thus for survival and reproductive success. Orienting depends on interactions between multiple brain areas carrying information about head and body movements as well as external sensory cues for reference. To adapt to changing environments and correct for error, head direction (HD) representations must be flexible. However, the circuit mechanisms and dynamics underlying how HD is modulated are largely unknown. Retrosplenial cortex (RSC) is a key region for spatial cognition and exhibits dense interconnection with visual and motor areas, the hippocampal formation, and diverse thalamic nuclei. Of these, the anterodorsal thalamus (ADn) is the major avenue by which HD is routed to cortex. In other cortical areas, cortico-thalamic loops have been shown to perform transformations on incoming sensory inputs for learning and behavior output. In this thesis I test the hypothesis that interactions between RSC and ADN provide a circuit substrate for flexible HD computations. In the first part, I describe experiments using simultaneous tetrode recordings in behaving mice. Through neural decoding, I show that RSC HD representation is synchronous with that of ADn, not only during the visually-guided HD reference update, but also in darkness. This coordination is supported by strong feedforward functional connectivity in the thalamo-cortical direction, suggesting that visually-guided adaptations likely emerge upstream of ADn, where angular velocity is integrated. In the second part, I confirm that ADn is devoid of recurrent excitatory connectivity, contrary to previously proposed attractor network architectures. My results suggest that inhibition, originating in thalamic reticular nucleus, likely plays a fundamental role in the control of ADn HD. Finally, I provide evidence, at the single cell level, of how long-range synaptic inputs are functionally targeted to specific dendritic domains in RSC. I speculate that this connectivity logic, together with different dendritic integration rules, may underlie high-dimensional tuning and combine visual and thalamic HD to represent global HD references. Altogether, this work suggests that ADn-RSC interactions alone cannot account for flexible HD coding, but are embedded in a network that constructs this spatial cognitive representation through transformation of multiple sensory signals.

Thesis Supervisor: Mark T. Harnett, Ph.D.
Title: Associate Professor and Graduate Officer, Department of Brain and Cognitive Sciences

Acknowledgments

Thank you to the following the funding sources for supporting my PhD: Henry E. Singleton (1940) Presidential Fellowship, James R. Killian Fellowship, Leventhal Fellowship, Jane and Sheldon (1959) Razin Fellowship, MathWorks Science Fellowship. I want to thank my thesis committee, Matthew Wilson, Ila Fiete and Michael Hasselmo for their guidance, their invaluable feedback, and their insight, which have helped me craft this thesis. I thank Hongkui Zeng, Shenqin Yao, Ali Cetin, and the Allen Institute and Ian Wickersham for sharing their rabies tracing viral constructs that have made the anatomy experiments in this thesis possible.

I want to express my gratitude to Guoping Feng for his support during my years as a technician in his lab and the beginning of graduate school. Special thanks go current and former Feng lab members Zhanyan Fu, Patricia Monteiro and Dongqing Wang from whom I learned a lot. Also, I would not have pursued this PhD in Neuroscience without the teaching and advising of my undergraduate mentors at Georgetown, Maria Donoghue and Stefano Vicini, thanks to whom I became fascinated with patch-clamp electrophysiology.

I owe a lot to my current and former members of the Harnett Lab. I want to especially thank Jakob Voigts, without whom my main project would not have been possible. Jakob so patiently and enthusiastically taught me everything I needed to know, from drive fabrication, to surgery, to tetrode recordings, to analysis and mouse behavior, and always came to the rescue with hardware and analysis issues. I made a lot of progress also thanks to Quique Toloza, with his clever and enthusiastic suggestions for data analysis, and Lukas Fischer, who shared much of his knowledge on spatial navigation and Systems Neuroscience. I am grateful to have been part of the retrosplenial dendrites project, spearheaded by Mathieu Lafourcade, as it allowed me to not lose touch with dendritic biophysics and slice physiology. The success of the RSC dendrites manuscript is largely owed to Dimitra Vardalaki, who came to the rescue with crucial revision experiments. Her friendship and company with our weekly swimming sessions also kept me in shape (and sane) in the last few months while preparing for the thesis. I also want to thank Norma Brown for her tireless contribution with anatomy experiments, and Valerio Francioni, Mila Halgren, Vincent Tang, Jaeyoung Yoon, Courtney Yaeger, my UROP Pranav Murugan and the rest of the Harnett Lab for their friendship, scientific support, and helpful discussions.

My project would not have been successful without the work of Wilson lab members Jonathan Newman and Jack Zhang, who with the help of Jakob developed the new generation ONIX acquisition system. I especially thank Jon, now head of Open Ephys, for his time and dedication to assembling the hardware for and troubleshooting issues on my recording rig, and, last but not least, for his development of the Twister3, which seriously improved the drive fabrication process.

I am immensely grateful to my advisor, Mark Harnett, for constantly inspiring and encouraging me, for being so invested in my success, for guiding me through all the steps throughout this PhD and, most importantly, teaching me how to be a scientist and how not to let difficulties stand in the way of our curiosity. I feel lucky to have had the opportunity to conduct rigorous science in the fun and productive lab that Mark has created, but also to have had the time

and freedom to learn many different techniques, ranging from whole cell electrophysiology to anatomy to in vivo tetrode recordings, under Mark's mentorship.

I want to thank all my friends that have come and gone through the Green House, my dear friends from the graduate program Rosary Lim and Xiangyu Zhang, my first housemates Giorgia Grisot and Jose de Arcos, who have filled my time in Cambridge throughout these years with fun, company, comfort, delicious dinners and bbqs.

Finally, I finally want to my partner Mathieu and my family, whose love, constant support, care and comfort have kept me motivated throughout these years.

Table of Contents

List of Figures

Chapter 1 : Introduction

1.1 The neural basis of spatial navigation

The ability of foraging animals to navigate through environments is critical to their survival. Animals exhibit a plethora of sophisticated cognitive functions that allow them to find food, shelter, mates, or migrate to known feeding and birthing grounds. These include the ability to plan and follow routes (Schwarz, Wystrach, and Cheng, 2017), memorize and recall important locations, use external cues, from celestial bodies (El Jundi, Warrant, Byrne, Khaldy, Baird, Smolka, and Dacke, 2015) to polarized light (Krapp, 2007; Wehner and Müller, 2006), magnetic fields (Lohmann, Lohmann, Ehrhart, Bagley, and Swing, 2004; Wu and Dickman, 2012), geological formations or environmental features (Harris, Graham, and Collett, 2007; Kheradmand and Nieh, 2019; Schwarz, Wystrach, and Cheng, 2017), echolocation (Ulanovsky and Moss, 2008) or movement and distance cues (Müller and Wehner, 1988) as guiding elements to goal locations. Because of its impact on the evolutionary success of many species, spatial navigation has been the focus of research in several fields, including ecology, ethology, evolutionary biology, neuroscience and finally robotics.

Several spatial navigation strategies have been outlined: route-following, beacon-following, path-integration, or dead-reckoning, and cognitive mapping (Figure 1.1) (Geva-Sagiv, Las, Yovel, and Ulanovsky, 2015). Animals, including humans, are known to perform path-integration navigation (Darwin, 1873; Etienne and Jeffery, 2004; Mittelstaedt and Mittelstaedt, 1980), whereby the distance traveled, the speed and angular velocity (AV) are continuously calculated in order to update the internal representation of self-location in an allocentric-reference frame (McNaughton, Battaglia, Jensen, Moser, and Moser, 2006). This strategy is best exemplified by the ability to triangulate through unknown routes from a purely self-movement-based estimation of location with respect to the start point of navigation. An extension of the path integration-based navigation, the spatial cognitive mapping strategy has been observed in laboratory rats (Tolman, 1948), bats (Tsoar, Nathan, Bartan, Vyssotskib, Dell'Omo, and Ulanovsky, 2011) and humans (Epstein, Patai, Julian, and Spiers, 2017). It is based on an abstract representation of the environments, originating from the translation from egocentric mapping of

external stimuli, such as the location of a stimulus in the visual field, to their allocentric, or world-centered, mapping. An additional navigational strategy identified in the birds, thanks to their sensitivity to the geomagnetic field, combines the cognitive mapping with compass navigation.

The building blocks of spatial navigation, mostly discovered from investigations in the rodent brain, comprise neurons in multiple regions carrying specific information about location, border proximity, speed, spatial periodic mapping tiling the environment and orientation. These codes shape the tuning preference, respectively, of place cells in the hippocampus (HPC) (O'Keefe and Dostrovsky, 1971; Wilson and McNaughton, 1993), border cells in the subiculum (SUB) and entorhinal cortices (Lever, Burton, Jeewajee, O'Keefe, and Burgess, 2009; Solstad, Boccara, Kropff, Moser, and Moser, 2008), speed cells in SUB and EC (Kropff, Carmichael, Moser, and Moser, 2015), grid cells in medial entorhinal cortex (MEC) (Hafting *et al.*, 2005) and finally head direction (HD) cells (Muller, Ranck and Taube, 1996) (Fig. 1.2). Many of these neural codes have been found in homologous structures in the brain of monkeys (Hori, Nishio, Kazui, Umeno, Tabuchi, Sasaki, Endo, Ono, and Nishijo, 2005; Laurens, Kim, Dickman, and Angelaki, 2016) and in humans (Ekstrom, Kahana, Caplan, Fields, Isham, Newman, and Fried, 2003; Jacobs et al., 2013; Miller et al., 2013; Shine and Wolbers, 2021) performing virtual reality navigation. Despite the different brain anatomies and different repertoires of sensory modalities influencing navigation strategies, some of these codes have also been found in insects (Pisokas, Heinze, and Webb, 2020; Seelig and Jayaraman, 2015)

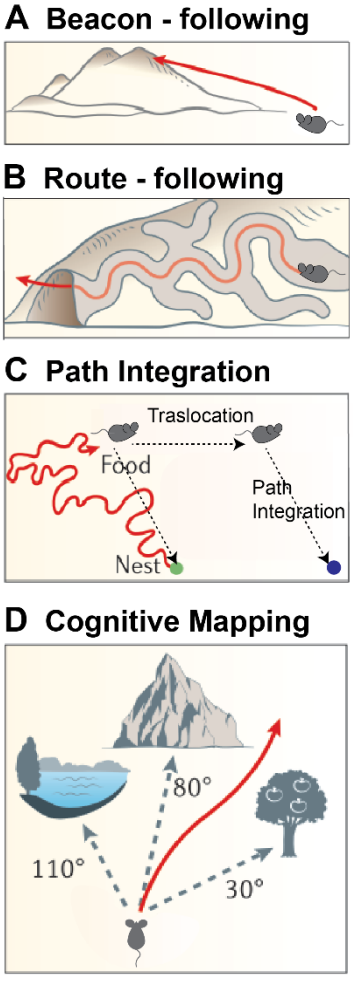

Figure 1.1 Spatial Navigation Strategies

(adapted from Geva-Sagiv Las, Yovel, and Ulanovsky, 2015) A, Navigation toward a distant cue, in this case the peak providing a visual beacon. **B**, Navigation based on following bounded routes where the change of course is determined by specific landmarks – in this case intersections. **C**, Continuous updates of self-location based on calculations of head turns and distance traveled from a starting point in the absence of landmarks. An artificial translocation will preserve the planned trajectory to the starting point obtained from triangulation. **D**, Navigation based on a mental map of the environment.

and birds (Ben-Yishay, Krivoruchko, Ron, Ulanovsky, Derdikman, and Gutfreund, 2021; Payne, Lynch, and Aronov, 2021), suggesting partially conserved circuit architectures for spatial navigation. In parallel, computational models of HD (Song and Wang, 2005; Zhang, 1996), place (Mcnaughton et al., 1996; Samsonovich and McNaughton, 1997) and grid firing (Burak and Fiete, 2009; Burgess, Barry, and O'Keefe, 2009; Fuhs and Touretzky, 2006; Stringer and Rolls, 2006), as well as artificial agents that accounted for grid tiling and visual and speed input (Banino et al., 2018), have successfully recapitulated path integration. These studies establish a direct role of these neural codes in supporting these navigation strategies, based on few assumptions about the inputs and the characteristics of neuronal firing.

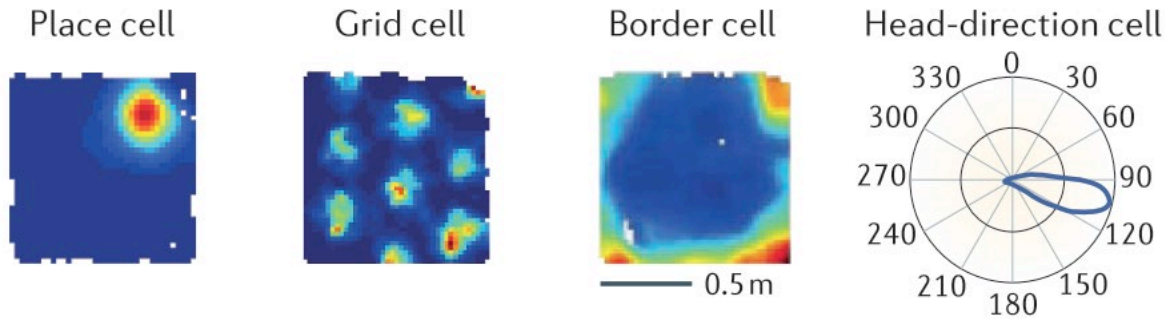

Figure 1.2 Types of spatial receptive fields in the brain (taken from Geva-Sagiv, Las, Yovel, and Ulanovsky, 2015). A hippocampal place cell selectively responds to a location in the upper right corner of a square arena (leftmost panel, data adapted from Whitlock *et al.*, 2008). An entorhinal grid cell (second panel from left, from Boccara *et al.*, 2010) fires at regular locations in a 2D environment forming an hexagonal lattice that tiles the environment with rigid periods. Border and HD cells (third and rightmost panels, respectively, from Solstad *et al.*, 2008) recorded in Pre-Subiculum respectively fire in response to environmental boundaries, at times with side preferences, and to a specific HD.

Animals, from insects to humans, are known to interchangeably use different navigational strategies depending on the contexts. Particularly, the interplay between the path integration and beacon-following strategy has been the subject of many studies in different brain areas. Common approaches included specifically probing the flexibility of spatial codes to reveal potential mechanisms of input integration (Campbell, Ocko, Mallory, Low, Ganguli, and Giocomo, 2018; Chen, King, Burgess, and O'Keefe, 2013; Fuhs, VanRhoads, Casale, McNaughton, and Touretzky, 2005; Jayakumar, Madhav, Savelli, Blair, Cowan, and Knierim, 2019; Knierim, Kudrimoti, and McNaughton, 1998; Wilber, Clark, Forster, Tatsuno, and McNaughton, 2014; Yoder, Clark,

Brown, Lamia, Valerio, Shinder, and Taube, 2011). While these studies have provided important insights into the dynamics and the behavioral conditions that favor one or the other, the neural underpinnings of this flexible use are still unknown. At the center of this conflict between internally generated spatial representations and the changing external stimuli is the nature and the origin of landmark signals for spatial navigation, or cues with a stable bearing on the spatial map. Because of its weight in human navigation and spatial cognition, vision is the dominant sensory modality tested in rodents experiments for its influence on path integration and the origin of landmark coding, however other sensory modalities can have important influences (Fischler, Joshi, Devi-Chou, Kitch, Schnitzer, Abbott, and Axel, 2019). External cues are thought to acquire landmark status as a function of exploration and reliability with respect to the allocentric and egocentric frames (Auger and Maguire, 2017; Commins and Fey, 2019; Goodridge, Dudchenko, Worboys, Golob, and Taube, 1998; Harris, Graham, and Collett, 2007; Jeffery, 1998; Jeffery, Page, and Stringer, 2016; Knierim, Kudrimoti, and Mcnaughton, 1995). However, few studies have actually characterized landmark-encoding neurons in diverse brain regions (Auger, Mullally, and Maguire, 2012; Bicanski and Burgess, 2016; Fischer, Soto-Albors, Buck, and Harnett, 2019; Jacob, Casali, Spieser, Page, Overington, and Jeffery, 2017; Page and Jeffery, 2018). Interestingly, many of these studies, from rodents to humans to computational models, suggest the Retrosplenial Cortex (RSC), a visuo-spatial cortical associative area, as a potential site of landmark coding. While tremendous advancements have been made in the fly brain navigation centers, the cellular and circuit mechanisms responsible for driving these signals and their tuning characterization are far from being fully elucidated.

HD, the signal for the animal's current head orientation, is fundamental in spatial navigation and directly influences other spatial codes. In fact, lesions of subcortical HD structures affect the stability of HPC place cells (Calton, Stackman, Goodridge, Archey, Dudchenko, and Taube, 2003), disrupt grid cell firing in MEC (Winter, Clark, and Taube, 2015), and are generally associated with impairments in memory and navigation tasks (Aggleton and Nelson, 2015). The influence of the HD signal on other spatial codes is also evident from its early emergence in rodent development, before eye opening and before place and grid firing is detected in other structures (Bjerknes, Langston, Kruge, Moser, and Moser, 2015; Langston, Ainge, Couey, Canto, Bjerknes, Witter, Moser, and Moser, 2010; Tan, Bassett, O'Keefe, Cacucci, and Wills, 2015). Finally, many of the path integration and landmark formation models require HD input. For these reasons the

HD system is a promising substrate for the integration of landmark information and the movement-based internal representation.

Understanding these processes will have important implications beyond animal navigation: homologous structures in the human brain have been reported to encode HD (Shine, Valdés-Herrera, Hegarty, and Wolbers, 2016) and human topographical disorientation and memory deficits associated with Alzheimer's disease (AD) result from disruptions to structures associated with HD coding (Coughlan, Laczó, Hort, Minihane, and Hornberger, 2018; Skelton, Ross, Nerad, and Livingstone, 2006). Interestingly, both mamillary bodies and RSC are the first regions to be affected by AD already in early stages of the disease: a marked decrease in neuron numbers and morphology, amidst minimal amyloid beta plaques, in the mamillary bodies (Grossi, Lopez, and Martinez, 1989) and reduced activity in RSC (Nestor, Fryer, Ikeda, and Hodges, 2003) were observed. The impairment of these regions and the subsequent behavioral symptoms that are hallmarks of the disease further underscore the link between HD and AV encoding and the generation of stable spatial references for navigation and memory. Understanding the causes underlying the vulnerability of these regions and the genesis of the disease will provide useful insights for the development of treatments.

In the attempt to answer this question, this thesis will provide background on the characteristics of HD coding in the brain (Chapter 1.2 to 1.7), and then focus on the interaction between a purely HD-coding thalamic region, ADn, and one of its cortical targets, RSC, with respect to the changes in HD representation in response to landmark manipulations (Chapter 2). In addition, an open question about the nature of thalamic local circuitry will be addressed and discussed in the context of possible implementation of local HD attractor architectures (Chapter 3). To establish a potential role for RSC in landmark coding, which requires directional and sensory inputs, the organization of synaptic input sources is tested in RSC pyramidal neurons (Chapter 4). Finally, concluding remarks on the technical limitations of this and current studies and suggested experiments to fill gaps in our knowledge of the local and long-range circuit architecture of the HD system will be provided (Chapter 5).

1.2 Discovery of the head direction code in the brain

HD was first identified in the Dorsal Presubiculum, or Post-Subiculum (POS), of freely moving rats (Ranck Jr, 1984; Taube, Muller, and Ranck, 1990a) via tetrode recordings of their electrical activity: these neurons were described as firing persistently in response to a specific orientation of the rat's head, with rapidly decreasing rates to neighboring directions, for a total width of ~60°, giving rise to a "triangular" shape tuning curve. Different cells preferentially fire for different directions, independently of the location within the recording arena, thus virtually providing the animal with an internal compass (Schultheiss and Redish, 2015).

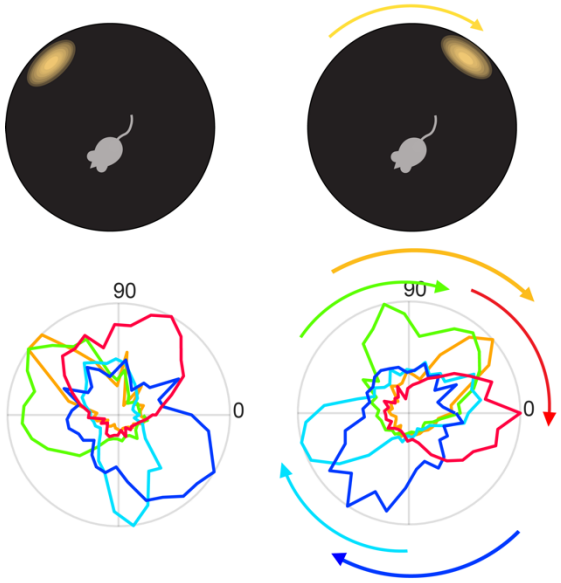

Figure 1.3 Rotations of Anterodorsal thalamic HD tuning curves in the mouse in response to a cue rotation

Top row, behavioral set up: a prominent visual cue at the outer wall of a circular arena is rotated (right) while the mouse forages. Bottom row, polar plots of tuning curves from simultaneously recorded HD cells in anterodorsal nucleus of thalamus. Note that the preferred firing directions of the HD cells rotate (right) following the rotation of the cue and by the same amount (Data from recordings analyzed in Chapter 2 of this thesis).

HD cells discharge is not related to the geomagnetic field or triggered by cues in the arena (except for particular cases later described). Passive transport and rotation leave the HD signal intact (Stackman and Taube, 1997), and, conversely, lesions of the semicircular canals ablate it (Muir, Brown, Carey, Hirvonen, DellaSantina, Minor, and Taube, 2009), suggesting that the vestibular system is necessary for the generation of the HD signal (Yoder and Taube, 2014). Angular acceleration is fundamental for path-integration-based navigation (Mittelstaedt and Mittelstaedt, 1980), and errors in homing behavior in darkness or absence of external cues are tightly correlated with heading errors (Valerio and Taube, 2012), evidence of the importance of movement-related signal in the update of the internal representation of orientation. However, rotations of a polarizing card induced rotations of the preferred firing directions of the HD cells, that were distinctively a) commensurate to the rotation angle of the

visual cue; b) similar among the HD cells ensemble (Taube, Muller, and Ranck, 1990b; Yoganarasimha, Yu, and Knierim, 2006). The systematic effect of the visual cue manipulation on all the HD cells, together with their tuning curve properties, suggested that HD encoding may be sustained by a rigid map locked to external references, with fixed relative distances among the HD units in the directional dimension (Taube, Muller, and Ranck, 1990b) (Fig. 1.3).

1.3 Anatomy, circuit connectivity and tuning properties in the HD system

Following the initial discovery, HD cells have been identified in many brain regions, mostly in what is known as the Papez circuit and in parts of the hippocampal formation (Fig. 1.4). In parallel, anatomical tracing and lesion studies have made profound efforts in mapping the wiring diagram and, based on the electrophysiological or behavioral effects in navigation tasks in rats, attributed distinct functions and hierarchy, with respect to HD information flow, to the different brain regions (Clark and Taube, 2012; Jankowski, Ronnqvist, Tsanov, Vann, Wright, Erichsen, Aggleton, and O'Mara, 2013; Laurens and Angelaki, 2018; Sharp, Blair, and Cho, 2001). The general consensus is that HD is generated in the reciprocal connections between the Dorsal Tegmental Nucleus of Gudden (DTN) and the Lateral Mamillary Nuclei (LMN) (Blair, Cho, and Sharp, 1998; Clark and Taube, 2012), with inhibitory afferents from the former and feedback excitatory inputs from the latter (Allen and Hopkins, 1989; Wirtshafter and Stratford, 1993). HD and AV signals are found in LMN and lesions of this region ablate HD in ADn (Bassett, Tullman, and Taube, 2007; Stackman and Taube, 1998). LMN-DTN activity is dependent on input from upstream brainstem nuclei carrying AV signal: these include the medial vestibular nucleus (MVN) processing "external" sensory input from the semicircular canals, but also the nucleus prepositus hypoglossi (Butler, Smith, van der Meer, and Taube, 2017) and supragenual nucleus (Clark, Brown, and Taube, 2012) conveying integrated AV with oculomotor, motor efference copy and body posture signals necessary in the generation of HD (Cullen and Taube, 2017; Laurens and Angelaki, 2018). The main target of the LMN is ADn, which contains the highest density of HD cells, with sharper tuning curves than in LMN, consistently with the idea that filtering and gain control occurs at the level of thalamic information processing (Connelly, Laing, Errington, and Crunelli, 2016; Worden, Bennett, and Neacsu, 2021). Other thalamic nuclei, mostly in the anterior and lateral groups, contain HD neurons with different properties, such as visual information-dependent responses in the laterodorsal thalamus (LD) (Mizumori and Williams, 1993) or theta-modulation in

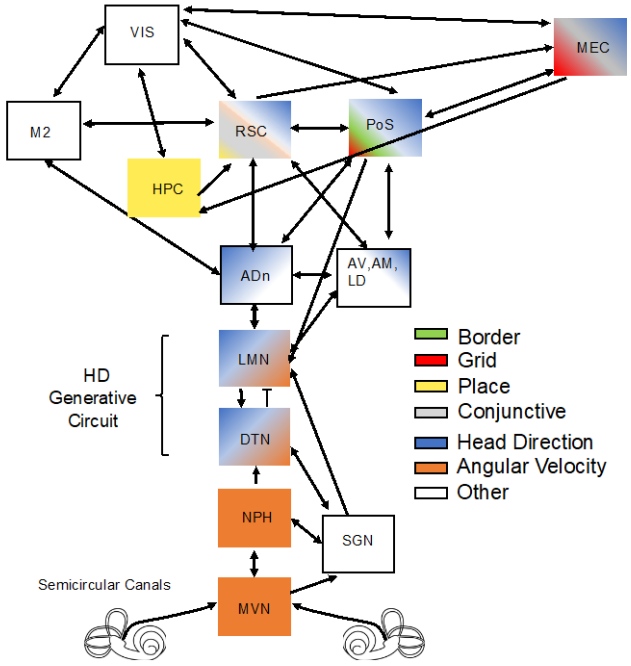

Figure 1.4 Anatomy and connectivity of brain regions involved in HD coding.

From bottom to top: Vestibular signal originating from the semicircular canals is relayed to the medial vestibular nucleus (MVN) which together with its connections to the Supragenual Nucleus (SGN) and the Nucleus Prepositus Hypoglossi (NPH) form angular velocity signals in the Dorsal Tegmental Nucleus (DTN), which contains inhibitory neurons. The reciprocal connections between DTN and the Lateral Mamillary Nuclei (LMN) are considered to be the site where HD is generated. HD tuning from LMN is then conveyed through the mammillothalamic tract to Anterodorsal Thalamus (ADn) and in other anterior thalamic nuclei. ADn mainly targets Post-Subiculum (POS), which is the main cortical site of HD coding, and Retrosplenial Cortex (RSC). RSC and POS have also reciprocal connections with other anterior thalamic nuclei. Their HD coding is also embedded and influenced by the convergence of inputs from other regions, including visual and motor areas and hippocampus. Medial Entorhinal Cortex (MEC) HD coding originates from POS projections and together with HPC feedback input sustains grid field coding.

anteroventral nucleus (AVn) (Tsanov, Chah, Vann, Reilly, Erichsen, Aggleton, and O'Mara, 2011).

ADn lesions ablate HD coding in POS (Goodridge and Taube, 1997), but ADn HD is intact after POS lesions (Goodridge and Taube, 1997; Yoder, Clark, Brown, Lamia, Valerio, Shinder, and Taube, 2011), confirming the necessity of the mamillary and vestibular origin of the HD code. HD is the dominant spatial code in POS, directly conveyed by ADn (Peyrache, Lacroix, Petersen, and Buzsaki, 2015), but with important differences: during head turns, POS HD cells firing is more aligned with the current HD, whereas ADn HD cells firing leads the true HD on average by ~25 ms (Blair, Lipscomb, and Sharp, 1997; Blair and Sharp, 1995). The function of this anticipatory firing in ADn has been postulated to derive from AV input from LMN (Blair and Sharp, 1995; Stackman and Taube, 1997) and to serve better decoding mechanisms of neuronal output of the current HD (Zirkelbach, Stemmler, and Herz, 2019). As a structure receiving dense visual and other parahippocampal inputs, HD in POS is actually mixed with other spatial codes, such as responses to environment borders (Peyrache, Schieferstein, and Buzsáki, 2017). The POS output, namely the HD-to-

spatial transformation function, might contain the stabilizing signal projected back to ADn (Goodridge and Taube, 1997), the rest of anterior thalamus, and LMN (Huang, Simonnet, Nassar, Richevaux, Lofredi, and Fricker, 2017).

Entorhinal and Retrosplenial Cortex (RSC) are the other major cortical regions exhibiting HD coding, but only RSC is directly targeted by ADn (Jankowski, Ronnqvist, Tsanov, Vann, Wright, Erichsen, Aggleton, and O'Mara, 2013; Shibata, 1993), while POS HD cells are the likely source of HD to the MEC (Preston-Ferrer, Coletta, Frey, and Burgalossi, 2016; Tukker, Tang, Burgalossi, and Brecht, 2015). Entorhinal cortex spatial code is not only limited to grid and speed firing, but is tightly coupled with HD (Raudies, Brandon, Chapman, and Hasselmo, 2014), as evidenced by the presence of conjunctive HD with position and speed cells (Sargolini, Fyhn, Hafting, McNaughton, Witter, Moser, and Moser, 2006) and by a precise dorsoventral gradient of HD information, with upper layers containing a higher density of HD-encoding cells (Giocomo, Stensola, Bonnevie, Van Cauter, Moser, and Moser, 2014). Moreover, disruption of grid fields was observed upon ADn lesion (Winter, Clark, and Taube, 2015) and conversely grid cells switched to HD coding-only upon disruption of hippocampal activity (Bonnevie, Dunn, Fyhn, Hafting, Derdikman, Kubie, Roudi, Moser, and Moser, 2013), consistent with the notion that grid firing might emerge from the convergence of HD and place code.

In RSC typical HD tuned cells comprise a small percentage of the spatial receptive fields recorded (Chen, Lin, Green, Barnes, and McNaughton, 1994a; Cho and Sharp, 2001). However, consistently with the high incidence of conjunctive encoding in cortical associative areas (Alexander and Nitz, 2015; Rigotti, Barak, Warden, Wang, Daw, Miller, and Fusi, 2013) and similarly to EC, HD is also found in conjunction with AV (Hennestad, Witoelar, Chambers, and Vervaeke, 2021), with egocentric boundary (Alexander, Carstensen, Hinman, Raudies, Chapman, and Hasselmo, 2020) and with distinct position signals (Jacob, Casali, Spieser, Page, Overington, and Jeffery, 2017). This coding strategy widely influences spatial coding in RSC and possibly underlies the emergence of landmark responses (Auger, Mullally, and Maguire, 2012; Fischer, Soto-Albors, Buck, and Harnett, 2019; Hennestad, Witoelar, Chambers, and Vervaeke, 2021; Keshavarzi, Bracey, Faville, Campagner, Tyson, Lenzi, Branco, and Margrie, 2021; Mao, Kandler, McNaughton, and Bonin, 2017a; Shine, Valdés-Herrera, Hegarty, and Wolbers, 2016). Such spatial information may also be critical for the stabilization and anchoring to visual references of HD neurons in ADn, as demonstrated by lesion studies (Clark, Bassett, Wang, and Taube, 2010).

Unlike POS HD tuning, RSC HD-tuned neurons display anticipatory firing, though highly variable, to the true HD, similarly to ADn (Lozano, Page, Jacob, Lomi, Street, and Jeffery, 2017). The mechanisms that sustain this coding strategy and the implications on spatial representations are unknown, however they are consistent with converging AV and HD inputs with potential tradeoffs in the information content.

HD has profound influences on other behavioral variables, such as motor planning and vision. It is not surprising therefore that HD tuning may be found in regions outside the hippocampal formation, as recent studies have revealed: visual cortex neurons have been shown to be modulated by 3D HD (Guitchounts, Masís, Wolff, and Cox, 2020) and fast spiking interneurons in the somatosensory cortex also bear the HD code (Long, Young, and Zhang, 2020). These findings further emphasize the idea that HD coding is a fundamental variable guiding successful motor-planning and interactions with the environment, and as such it might play a critical role in coordinating and recruiting multiple brain regions.

It is worth noting that while the initial observations and studies of HD tuning in rats and mice were restricted to the yaw, or horizontal, plane, studies in other species, such as bats (Finkelstein, Derdikman, Rubin, Foerster, Las, and Ulanovsky, 2014) and monkeys (Laurens, Kim, Dickman, and Angelaki, 2016), have revealed HD coding in 3 dimensions to account for other planes of movement, such as pitch and roll. 3D tuning of HD has recently been explored in rodents (Angelaki, Ng, Abrego, Cham, Asprodini, Dickman, and Laurens, 2020; Laurens and Angelaki, 2019), and found to explain both azimuth as well as 2D tilt tuning, whether conjunctive or in isolation, in both thalamic and cortical regions. These findings, compatible with the toroidal model of HD in the flying bat (Finkelstein, Derdikman, Rubin, Foerster, Las, and Ulanovsky, 2014) despite some unresolved differences (Taube, 2019), suggested that a new framing of HD coding in the brain that takes tilted azimuth in account is likely ubiquitous in the mammalian navigational circuitry and, as initially proposed in head-restrained monkeys (Laurens, Kim, Dickman, and Angelaki, 2016), is anchored to gravity. 3D HD tuning has also been reported in humans (Kim and Maguire, 2019), thus underscoring the importance of investigating spatial representations in the brain that take into account all 3 dimensions of body and head movement, characteristic of many land-dwelling animals. Interestingly, grid cells representations in the rat navigating a cubic lattice showed sparse and irregular grid fields (Grieves, Jedidi-Ayoub, Mishchanchuk, Liu, Renaudineau, Duvelle, and Jeffery, 2021), but in free flying bats they maintained some degree of local order

through rigid distances between grid fields (Ginosar, Aljadeff, Burak, Sompolinsky, Las, and Ulanovsky, 2021). Behavioral differences, such as movement constraints, and intrinsic mechanisms of distance travelled and velocity calculations between bats and rodents may underlie the discrepancies in the 3D grid code. Nonetheless, the loss of the striking periodicity characteristic of the 2D environmental tiling has questioned previous models that described the formation and the pattern of grid firing.

1.4 Continuous attractor network architecture for head direction coding

The initial observations of HD tuning properties, together with the persistence of firing in the absence of a salient visual cue or in darkness (Mizumori and Williams, 1993; Muller, Ranck, and Taube, 1996; Yoder and Taube, 2011) have led to the development of attractor network models (Redish, Elga, and Touretzky, 1996; Skaggs, Knierim, Kudrimoti, and McNaughton, 1995; Xie, Hahnloser, and Seung, 2002; Zhang, 1996) that could recapitulate the activity of HD cells. The common features of the proposed network architectures relied on: 1) a topological arrangement of the HD cells in a ring, with nearby cells discharging preferentially to nearby angles; 2) two additional sets of rings containing rotation cells, also called AV by HD cells, for left and right rotations triggered, respectively, by left and right vestibular cells, and connected to the HD ring by shifted connections, to ensure movement of the activity bump, i.e. the ensemble of active cells; 3) visual cells responding to specific egocentric stimuli and weakly connected to all HD cells, and responsible for the visual update of the reference 4) recurrent connectivity between nearby HD cells and inhibitory connections to farther away cells, to ensure the persistence of a single activity bump tracking the current head orientation even in the absence of movement (Fig. 1.5). These models succeeded in recapitulating the emergence of a single bump, the hallmark of attractor dynamics, and the dynamics of the gradual shifts in response to AV input, and perform path integration (Knierim and Zhang, 2012). Furthermore, they could be used to generate testable predictions about the connectivity architecture or the learning rules of the integration of visual directional references (Hahnloser, 2003; Page, Walters, Knight, Piette, Jeffery, and Stringer, 2014; Skaggs, Knierim, Kudrimoti, and McNaughton, 1995). However, while some network components were plausible given the evidence of neurons with similar features found in the brain (Chen, Lin, Green, Barnes, and McNaughton, 1994a; Sharp, Tinkelman, and Cho, 2001; Stackman and Taube, 1998; Taube, Muller, and Ranck, 1990b), others are still under investigation.

Specifically, given the initial observations on the absence of recurrent excitatory connections within LMN (Allen and Hopkins, 1989) and the reciprocal connections with the DTN, alternative network models that reflected this architecture, yet at the same time could explain the persistent activity of HD cells, were proposed (Boucheny, Brunel, and Arleo, 2005; Song and Wang, 2005). Briefly, these networks consisted in inhibitory-excitatory loops between LMN, which receives an external, possibly visual, excitatory input, and left and right DTN, which receive respectively left and right AV inputs and an external excitatory input, with the two inhibitory nuclei inhibiting each other. They succeeded in recapitulating the features of HD coding, could perform path integration based on velocity inputs and even shifted the HD reference from the ensemble neurons PFDs in response to a strong reorientation signal, thus providing a potential biologically-inspired layout of HD encoding, at least in the LMN-DTN network.

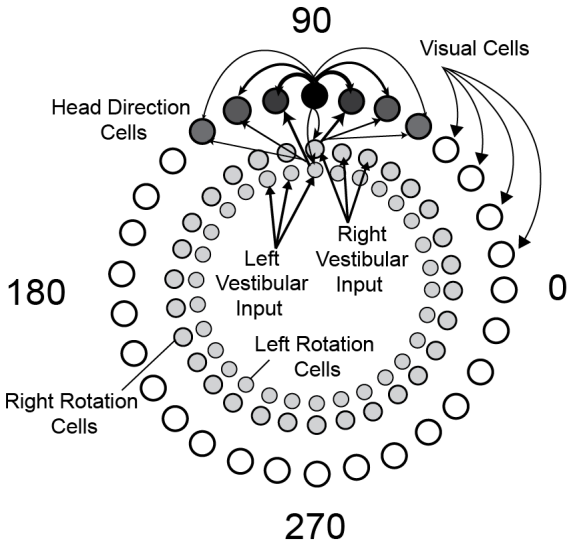

Figure 1.5 Architecture of the head direction cell model

(adapted from Skaggs, Knierim, Kudrimoti, McNaughton, 1995) HD cells with nearby preferred firing directions are arranged close by in a topological ring (outer ring). Each HD cell has strong reciprocal connections with nearby cells and weaker connections with further away cells. This arrangement allows only a single cluster of cells to be active at a time (dark shaded cells), localizing a bump of activity that tracks the current HD. Two additional rings of cells carrying rotation information (one for left rotations, one for right rotations) are each asymmetrically connected to HD cells: each receives a feedback connection from the HD cell to the left or to the right, for the rightward and leftward rotation cells, respectively, of the HD cells they target. Each Rotation cell is driven by ipsilateral vestibular input. A set of visual cells, potentially originating in cortex, sends input to all HD cells, providing stabilizing signals anchored to visual cues and that prevents the system from accumulating error.

Given the rodent anatomical evidence against recurrent excitation, studies on the cellular mechanisms of persistent activity with patch clamp slice electrophysiology demonstrated that neurons in both POS and ADn possess biophysical properties that promote persistent activity (Kulkarni, Zhang, and Kirkwood, 2011; Yoshida and Hasselmo, 2009), but whether these are sufficient in vivo is unknown. Continuous external or sensory

input is however not necessary to sustain HD firing, as demonstrated by the intact HD coding observed during sleep in ADn and POS (Peyrache, Lacroix, Petersen, and Buzsaki, 2015). While a higher degree of drift and reduced correlation between ADn and POS firing were observed in sleep (Peyrache, Duszkiewicz, Viejo, and Angeles-Duran, 2019), attractor dynamics constrained in a one dimensional topological ring described ADn neuronal activity in both sleep and awake conditions (Chaudhuri, Gerçek, Pandey, Peyrache, and Fiete, 2019). Together these findings were consistent with internally generated persistent HD coding in this structure.

Attractor dynamics do not, however, characterize HD activity in all brain structures. Notably, in MEC, where HD is found in conjunction with grid (Sargolini, Fyhn, Hafting, McNaughton, Witter, Moser, and Moser, 2006), exhibiting a precise superficial-to-deep gradient in tuning strength (Giocomo, Stensola, Bonnevie, Van Cauter, Moser, and Moser, 2014), HD cells have been shown to respond differently upon changes in prominent visual cues depending on whether they were modulated by intrinsic theta rhythms (Kornienko, Latuske, Bassler, Kohler, and Allen, 2018). Curiously, specific environmental configurations with stationary distal and rotating local cues revealed internally defined MEC HD tuning, characterized by their stability, and externally-driven HD coding that transiently switched tuning between the two references, thus highlighting the complexity of cortical HD coding (Park, Keeley, Savin, Ranck, and Fenton, 2019). Similarly, in RSC classically-defined HD cells were described, but also visually-modulated or environmentally driven HD cells were observed (Chen, Lin, Green, Barnes, and McNaughton, 1994b; Jacob, Casali, Spieser, Page, Overington, and Jeffery, 2017).

Attractor dynamics have been used to describe the spatially periodic activation of grid cells and the localized 2D bumps formed by place cells (Burak and Fiete, 2009; Samsonovich and McNaughton, 1997). However context and behaviorally relevant variables, such as the presence of reward, affect the spatial pattern of neuronal activity, by place or grid field overrepresentation around that goal (Boccara, Nardin, Stella, O'Neill, and Csicsvari, 2019; Butler, Hardcastle, and Giocomo, 2019), in striking contrast with a homogeneous tiling. While it is unclear if this strategy implies a violation of attractor dynamics in the grid code or simply a mechanism for better downstream-decoding for behavior planning, this finding suggests that the previously observed rigidity might be a feature of environments with poor-goal directed cues. This concern about the violation of rigid patterns with the increase in the dimensionality of the representations extends to the spatial signals detected in 3D navigation. A revision of original 2D attractor network models

for grid coding with classical low-dimensional hexagonal responses and low-dimensional projections of inputs showed, however, that these models can flexibly and efficiently represent many variables through mixed-selectivity and modularity (Klukas, Lewis, and Fiete, 2020). This generalization could help explain the apparent loss of the striking rigidity observed in MEC recordings in the rat navigating in a 3D environment (Grieves, Jedidi-Ayoub, Mishchanchuk, Liu, Renaudineau, Duvelle, and Jeffery, 2021) and the flying bat (Ginosar, Aljadeff, Burak, Sompolinsky, Las, and Ulanovsky, 2021). It remains, though, to integrate the gravity-anchored 3D HD tuning observed during 3D motion (Angelaki, Ng, Abrego, Cham, Asprodini, Dickman, and Laurens, 2020) with the intrinsic attractor dynamics observed in 1D manifolds of ADn neurons activity both during awake, 2D navigation, and during sleep (Chaudhuri, Gerçek, Pandey, Peyrache, and Fiete, 2019; Rubin, Sheintuch, Brande-Eilat, Pinchasof, Rechavi, Geva, and Ziv, 2019).

1.5 Insights from the Drosophila melanogaster

A model system that has that has led breakthrough insights on the building blocks of HD coding is the fruit fly. The insect central complex is a region known for navigation-related signals, and many insect species display path integration abilities (Honkanen, Adden, Da Silva Freitas, and Heinze, 2019). Leveraging on the genetic tools available to isolate specific neuronal populations in the fly brain, Seelig and Jayaraman (Seelig and Jayaraman, 2015) identified neurons in the ellipsoid body (EB) whose dendrites were arranged in a donut shape and whose activity accurately tracked the fly walking direction and was tightly anchored to a visual landmark. The activity of these neurons followed ring attractor dynamics (Kim, Rouault, Druckmann, and Jayaraman, 2017), as evidenced by the presence of a single bump at any given time, the persistence of the bump of activity in the absence of the visual cue, and the smooth transition through intermediary steps to a new location in the ring, even when artificially stimulated. Through modeling, the smooth transitions were better explained by a local recurrent excitation between the E-PG neurons and global inhibition (Kim, Rouault, Druckmann, and Jayaraman, 2017).

The connectivity offset between the reciprocal AVxHD and HD neurons, predicted by attractor network models to be responsible for driving the bump of activity around in the topological ring, was actually identified in the connection between P-EN and EPG neurons. In fact, two sets of P-EN neurons, whose dendrites occupy patches of the protocerebral bridge, innervate

the EB wedges to the left or the right, for counterclockwise and clockwise rotations respectively, of the E-PG neurons that send feedback projections to the right or left patches (Green, Adachi, Shah, Hirokawa, Magani, and Maimon, 2017; Turner-Evans, Wegener, Rouault, Franconville, Wolff, Seelig, Druckmann, and Jayaraman, 2017) (Fig. 1.6). These neurons provide the rotational velocity inputs that can push the activity bump around the ring, even in darkness.

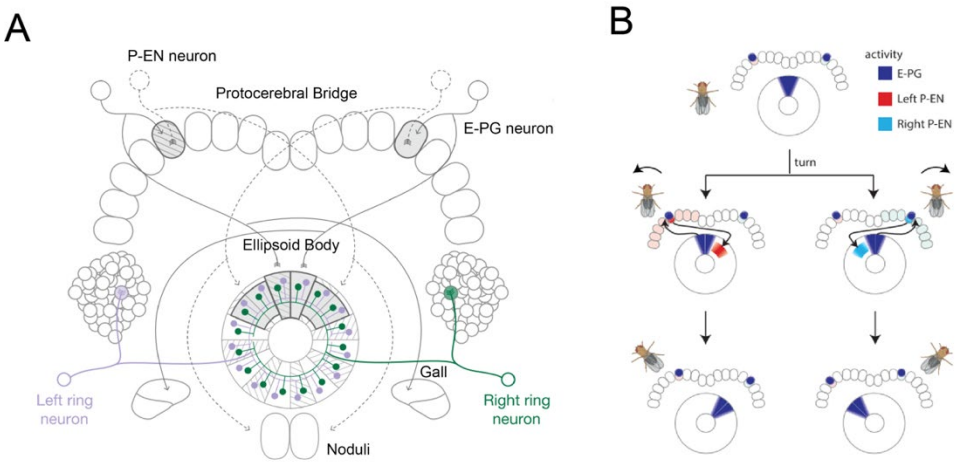

Figure 1.6 Drosophila central complex circuitry supporting HD coding and

A, Diagram of the main neuron types and their connections driving HD coding in the Drosophila central complex (taken from Kim, Rouault, Druckmann, and Jayaraman, 2019). Left and right E-PG neurons' dendrites occupy nearby wedges (16 identified, where solid grey or dashed lines indicate left and right E-PG origins) forming a ring-like structure called Ellipsoid body (EB). Activity in these dendrites has been shown to track the fly HD (Seelig and Jayaraman, 2015). E-PG neurons make synapses onto the Gall and columns of the protocerebral bridge (PB), where dendrites of left and right P-EN neurons are found. These neurons are thought to move around the EB activity in response to rotations, as a result of their crossed leftward- or rightward- shifted targets in the EB with respect to the E-PGs they receive inputs from. At the same time, left and right inhibitory ring neurons respond to stimuli in the visual space and convey this visual information by making synapses to all wedges, where local synaptic plasticity mechanisms mediate visual anchoring of HD representation (Fisher, Lu, D'Alessandro, and Wilson, 2019; Kim, Hermundstad, Romani, Abbott, and Jayaraman, 2019). **B** Schematic of the hypothesized mechanism to shift the activity bump in response to head rotation in the fly (taken from Turner-Evans, Wegener, Rouault, Franconville, Wolff, Seelig, Druckmann, and Jayaraman, 2017). The current HD is indicated by the blue bump of activity in the EB and in the left and right corresponding columns of the PB. Because of the asymmetric connectivity, a left turn would activate the left PB column and shift the HD bump to the wedge to the right of the previous bump, and vice versa for right turns.

As for mammals, unambiguous visual cues can stabilize the position of the activity bump. This input is provided by the inhibitory ring (R) neurons, which innervate all EB wedges and

whose receptive fields map the visual space. Learning of a new visual cue in the egocentric space has been shown to be mediated by long-term synaptic depression (Kim, Hermundstad, Romani, Abbott, and Jayaraman, 2019) of R-to-E-PG inhibition, thus actually driving the bump of activity to the E-PG neuron that is least inhibited (Fisher, Lu, D'Alessandro, and Wilson, 2019).

This network architecture is remarkably similar to the proposed ring attractor network models of mammalian HD (Sharp, Blair, and Cho, 2001; Skaggs, Knierim, Kudrimoti, and McNaughton, 1995) and consistent with the recent experimental evidence in the mouse ADn on the role of inhibition as a potential mechanism for mapping of the orienting visual cue to the HD (Ajabi, Keinath, Wei, and Brandon, 2021; Vantomme, Rovó, Cardis, Béard, Katsioudi, Guadagno, Perrenoud, Fernandez, and Lüthi, 2020). Moreover, experimentally addressing whether local recurrent excitation is present in the fly compass neurons could solve if indeed the basic HD generative circuit is conserved across species.

1.6 Oscillations in the HD circuitry

HD coding along regions of the Papez circuit serves important functions in memory and navigational tasks (Aggleton and Nelson, 2015; Aggleton, O'Mara, Vann, Wright, Tsanov, and Erichsen, 2010; Jankowski, Ronnqvist, Tsanov, Vann, Wright, Erichsen, Aggleton, and O'Mara, 2013). One fundamental neural mechanism for the memory consolidation found across hippocampal and cortical networks is the high frequency oscillatory burst called sharp wave ripples (SWRs), which occur during NREM sleep (Diekelmann and Born, 2010) and during quiet wakefulness, in opposition to the other prominent rhythm found in the limbic system, the theta oscillations (Buzsáki, 2015). During SWRs, temporally compressed patterns of neuronal activity from awake states, for example from explorations or navigation tasks, are reactivated in coordination between HPC and cortex (Ji and Wilson, 2007; Lee and Wilson, 2002; Wilson and Mcnaughton, 1994). These accelerated coactivations have also recently been reported for HD cells (Peyrache, Lacroix, Petersen, and Buzsaki, 2015), suggesting that HD coding might also participate in memory consolidation mechanisms. During slow wave sleep, SWRs are thought to be coordinated with neocortical spindle oscillations (Siapas and Wilson, 1998) timed by thalamocortical oscillatory dynamics resulting from fluctuations of the ensemble membrane potentials between UP, or active, and DOWN, or quiet, states (Steriade, McCormick, and Sejnowski, 1993). In addition to being a key hub for propagation of these slow oscillations (Gent,

Bandarabadi, Herrera, and Adamantidis, 2018), ADn is thought to participate in memory consolidation via coupling of HD firing to hippocampal SWRs at stable directions and with an ADn HD gain increase preceding the SWRs (Viejo and Peyrache, 2020). Furthermore, POS neurons maintain the same coordination with ADn HD firing during NREM sleep as in awake (Viejo, Cortier, and Peyrache, 2018). HD coordination may be a fundamental signal for memory consolidation processes occurring during sleep, not only across but also within structures: POS HD neuron pairs with little bias in spatial information, unlike those with higher spatial information, maintain high pairwise correlations during wakefulness as well as during sleep (Peyrache, Schieferstein, and Buzsáki, 2017).

RSCg has recently been proposed as a conduit path for SWRs coupled to CA1 to neocortex via subicular projections (Nitzan, McKenzie, Beed, English, Oldani, Tukker, Buzsáki, and Schmitz, 2020). RSC is a central hub for integrating sensory, motor and spatial information and plays a fundamental role in cognitive mapping during spatial tasks and memory (Bicanski and Burgess, 2018; Miller, Mau, and Smith, 2019; Miller, Vedder, Law, and Smith, 2014). The presence of SWRs in the superficial layers of RSCg, where subiculum and ADn axons make synapses, is further evidence of the tight connection between HD coding and this mechanism of memory consolidation.

Another rhythm characteristic of hippocampal and cortical networks, and previously recorded in RSC during spatial memory tasks (Corcoran, Frick, Radulovic, and Kay, 2016; Yoshida, Chinzorig, Matsumoto, Nishimaru, Ono, Yamazaki, and Nishijo, 2021), is the theta-range oscillation. It has been proposed to organize cortico-hippocampal interactions during memory tasks (Hasselmo, Bodelón, and Wyble, 2002; Jones and Wilson, 2005) and movement-related signals in the hippocampus during awake behavior and plays a fundamental role in spatial imagery (Buzsáki, 2002; Byrne, Becker, and Burgess, 2007; Colgin, 2016; Kay, Chung, Sosa, Schor, Karlsson, Larkin, Liu, and Frank, 2020). The link between HD coding and theta rhythms in the limbic system is heterogeneous and no unified circuit mechanisms underlying their cooccurrence, or mutual exclusion, have yet been delineated. However, theta modulation of neuronal firing in RSC is more strongly observed in the granular than in the dysgranular portion (Lomi, Mathiasen, Cheng, Zhang, Aggleton, Mitchell, and Jeffery, 2021), and a subset of egocentric boundary cells, possibly carrying important transformations between sensory information about the environment and stored memories, in RSC show phase-locking to theta

(Alexander, Carstensen, Hinman, Raudies, Chapman, and Hasselmo, 2020). HD coding in RSC (Chen, Lin, Green, Barnes, and McNaughton, 1994a; Cho and Sharp, 2001; Lozano, Page, Jacob, Lomi, Street, and Jeffery, 2017) and ADn do not show coupling to theta, but theta power increases with firing in the preferred direction of the HD cells in AVn (Tsanov, Chah, Vann, Reilly, Erichsen, Aggleton, and O'Mara, 2011). In MEC, however, theta rhythms may help organize HD cells into separate assemblies by a phenomenon called theta-cycle skipping, with important computational bearing on grid cell-periodicity (Brandon, Boogard, Schultheiss, and Hasselmo, 2013). Furthermore, MEC HD cells that are not modulated by theta rhythms, according to their autocorrelation functions, respond incoherently and with greater variance to visual cue changes than theta-rhythmic HD cells, in contrast to the homogeneity and rigidity predicted by attractor dynamics (Kornienko, Latuske, Bassler, Kohler, and Allen, 2018). Such diverse rhythm-tuning interactions might expand the regimes of possible spatial learning and memory computations at the single cell but also at the network level.

1.7 Cellular and circuit architecture of thalamic and cortical head direction

Thalamocortical loops are the basis of cognitive functions carried by cortex. They have been implicated in the refinement of behavioral responses to sensory stimuli in detection tasks (Manita et al., 2015; Pauzin and Krieger, 2018), detection of stimulus deviants (Voigts, Deister, and Moore, 2020) and more recently in executive functions, attention and rule switching (Lewis, Voigts, Flores, Ian Schmitt, Wilson, Halassa, and Brown, 2015; Rikhye, Gilra, and Halassa, 2018; Schmitt, Wimmer, Nakajima, Happ, Mofakham, and Halassa, 2017). Decades of research have identified the anatomical and neural basis of these thalamocortical loops, including features of first and high order thalamus, drivers' and modulators' synaptic connectivity, synaptic triads involving TRN-mediated inhibition and corticothalamic output (Halassa and Sherman, 2019; Sherman, 2016; Sherman and Guillery, 1996). While most of these features have been characterized for somatosensory, visual, auditory and more recently in the medio-dorsal (MD) thalamus and their cortical targets, less attention has been given to the anterior thalamic group.

Like other sensory systems, HD originating from head movement and velocity is distributed to cortex through a critical thalamic hub, ADn. This region receives excitatory inputs from LMN and cortical afferents, which, respectively, have synaptic properties that resemble typical drivers and modulators (Petrof and Sherman, 2009). However, unlike other sensory stimuli,

ADn HD coding is persistent and ADn firing shows limited shifts between tonic and burst mode (Viejo and Peyrache, 2020), possibly as a result of different cellular properties (Sheroziya and Timofeev, 2014). The underlying local and long-range circuitry that sustains this thalamic coding is unknown.

Another factor that differentiates the thalamocortical loops of ADn from other nuclei is the cortical targeting: both RSC and POS are part of periarchicortex, which, with a minimal layer (L) 4 band, have a different laminar organization than the neocortex. POS and the granular portion of RSC receive dense ADn input in L1 and L3 (Brennan, Jedrasiak-Cape, Kailasa, Rice, Sudhakar, and Ahmed, 2021; Nassar, Simonnet, Huang, Mathon, Cohen, Bendels, Beraneck, Miles, and Fricker, 2018), in contrast to the canonical L4 targeting of first order targeting in other sensory systems. L1 targeting is a path for top-down input from long-range cortico-cortical feedback connections, however thalamic targeting of L1 has also been reported for higher order nuclei, which target L2/3 neurons (Zhang and Bruno, 2019) as well as L5 (Petreanu, Mao, Sternson, and Svoboda, 2009) pyramidal cells in somatosensory cortex and prefrontal cortex (Anastasiades, Collins, and Carter, 2021). How these L1 inputs interact with other input sources to shape neuronal firing and their receptive fields is a major question in cortical processing. RSC is a highly interconnected area integrating multiple streams of information from cortical and subcortical regions (Van Groen and Wyss, 2003, 1990) and characterized by high dimensional and complex receptive fields. Revealing what input mapping and input-specific decoding strategies are implemented in single neurons in RSC would be a particularly helpful first step towards understanding conjunctive encoding and the potential cellular substrates for associative computations in RSC.

Despite the importance of HD in memory and spatial computations, little is known regarding how this signal is generated in the mammalian brain. Several computational models have tackled this questions using predictions based on the necessity of AV inputs, but also considering the importance of other signals such as optic flow, efference copy, proprioceptive and gravity signals (Boucheny, Brunel, and Arleo, 2005; Cullen and Taube, 2017; Laurens and Angelaki, 2018; Skaggs, Knierim, Kudrimoti, and McNaughton, 1995; Song and Wang, 2005; Zhang, 1996). However, the anatomy of the hypothesized HD generative circuitry in the rodent brain imposes technical challenges for applying recording and perturbation techniques, especially for the circuit

dissection, multisite in vivo recording, and single cell tracing experiments that are required to test the predictions of the initial attractor network models. This has been a serious impediment to progress on understanding how HD is represented and processed in the mammalian brain.

Another fundamental aspect of HD computations is their flexibility with respect to changing environments and/or corrections from relevant sensory stimuli. As already mentioned, visual cues provide a strong anchoring signal for HD coding, but the exact circuitry has not yet been determined. While cortical brain regions, and particularly RSC, seem likely candidates for performing the spatial computations that combine internally generated signals with visual cues (Clark, Bassett, Wang, and Taube, 2010; Maguire, 2001; Vann, Aggleton, and Maguire, 2009), the underlying circuit mechanisms and the dynamics of such updates are unknown. In other cortical areas, rule switching and/or detection of unexpected changes in sensory stimuli emerge in and are mediated by cortico-thalamic loops (Born, Schneider-Soupiadis, Erisken, Vaiceliunaite, Lao, Mobarhan, Spacek, Einevoll, and Busse, 2021; Pauzin and Krieger, 2018; Rikhye, Gilra, and Halassa, 2018; Voigts, Deister, and Moore, 2020). In this thesis, I test the hypothesis that RSC-ADn interactions contain neural activity signatures associated with the updating of the orienting references by simultaneously recording in both regions for the first time.

ADn is the major avenue for distributing HD to the rest of cortex, and thus it plays a fundamental role in spatial functions. What local circuitry can support persistent and smoothly changing HD coding? We addressed whether fundamental components of attractor network architectures, namely recurrent excitation and local inhibition, are present in ADn. These circuit components can not only be fundamental in entraining and shaping HD in ADn from upstream inputs, but can also be tuned in response to external input changes that determines the anchoring reference.

Finally, the nature of these potential anchoring signals is unknown. RSC has been suggested the key region for landmark encoding by integration of diverse input sources and several models have assigned specific activity profiles and circuit connectivity to these cells (Bicanski and Burgess, 2016; Page and Jeffery, 2018). However, the cellular and synaptic substrates of RSC encoding profile is unknown. In the 4th chapter I will address the spatial organization of a subset of synaptic input targeting to RSC L5b neurons and suggest how the connectivity logic may be used for high-dimensional spatial coding.

Chapter 2 : Coordination of Head Direction Representations in Mouse Anterodorsal Thalamic Nucleus and Retrosplenial Cortex[1]

Abstract

Our sense of location and orientation within an environment depends on knowledge of our self-motion and relevant external cues. Retrosplenial cortex is a key region for this process; it encodes several behavioral variables that guide navigation, including head direction. While much of the wiring diagram for HD is well known, the circuit dynamics and mechanisms of how visual information is used to update HD representations remain poorly understood. Here, we show that retrosplenial head direction representation is nearly synchronous with that of the anterodorsal nucleus of thalamus, the obligatory thalamic relay of head direction to cortex, during rotation of a prominent visual cue. Moreover, coordination of head direction representations in the two regions was maintained during darkness. Finally, anatomical and functional monosynaptic connectivity were consistent with a strong feedforward drive of head direction information from anterodorsal thalamus to retrosplenial cortex, with very little drive in the corticothalamic direction. Together, our results provide direct evidence for a concerted global head direction reference update across cortex and thalamus and of the underlying connectivity that supports this coordination.

Introduction

Internal representations of self-location and orientation must be updated as sensory experience and behavioral demands change in order to facilitate efficient navigation. Changes to information about the environment are known to trigger remapping of place (Muller and Kubie, 1987), grid tiling (Fyhn, Hafting, Treves, Moser, and Moser, 2007) and head direction (HD) (Taube, Muller and Ranck, 1990; Goodridge *et al.*, 1998; Knierim, Kudrimoti and McNaughton, 1998). In the insect

[1] Adapted from the work of **Marie-Sophie H. van der Goes**, Jakob Voigts, Jonathan P. Newman, Enrique H. S. Toloza, Norma J. Brown, Pranav Murugan and Mark T Harnett (manuscript in preparation)

and mammalian HD systems, remapping has been observed as rotations of the preferred firing directions of HD cells reflecting the rotations of a prominent visual cue, often in the form of a color-contrast card (Taube, Muller and Ranck, 1990; Goodridge *et al.*, 1998) or a narrow band (Seelig and Jayaraman, 2015) or scene (Kim *et al.*, 2019) of a LED screen. Hebbian synaptic plasticity mechanisms, embedded in known circuit arrangements, have been proposed to explain these phenomena in the fly ellipsoid body (Fisher, Lu, D'Alessandro, and Wilson, 2019; Kim, Hermundstad, Romani, Abbott, and Jayaraman, 2019). Network models with similar architecture have been applied to the rodent HD system (Hahnloser, 2003; Knight, Piette, Page, Walters, Marozzi, Nardini, Stringer, and Jeffery, 2014; Page, Walters, Knight, Piette, Jeffery, and Stringer, 2014; Skaggs, Knierim, Kudrimoti, and McNaughton, 1995). However, unlike the fly brain (Franconville, Beron, and Jayaraman, 2018; Hanesch, Fischbach, and Heisenberg, 1989), the circuitry that drives HD remapping in the rodent brain is not yet resolved. Several studies have indicated that cortical regions play a role in the stability and the visual anchoring of HD (Golob and Taube, 1999). Understanding the dynamics and the connectivity of visual-HD integration is the first necessary step to uncover the mechanisms that lead to remapping in the mammalian HD system.

Previous studies in the rat indicate that the HD code in the Anterodorsal Thalamic Nucleus (ADn), the necessary thalamic relay of HD to the hippocampal formation and cortex (Aggleton and Nelson, 2015; Calton, Stackman, Goodridge, Archey, Dudchenko, and Taube, 2003; Frost, Martin, Cafalchio, Islam, Aggleton, and O'Mara, 2021; Jenkins, Vann, Amin, and Aggleton, 2004; Winter, Clark, and Taube, 2015), becomes unstable and is less likely to remap to reflect cue rotations after lesions to the Retrosplenial Cortex (RSC)(Clark, Bassett, Wang, and Taube, 2010) or the Post-Subiculum (POS) (Goodridge and Taube, 1997). Both of these regions are strongly interconnected with visual areas (Sugar, Witter, van Strien, and Cappaert, 2011; Van Groen and Wyss, 2003), with each other (Kononenko and Witter, 2012; Wyss and Van Groen, 1992) and with ADn (Jankowski, Ronnqvist, Tsanov, Vann, Wright, Erichsen, Aggleton, and O'Mara, 2013; Shibata, 1998, 1993; Van Groen and Wyss, 2003, 1990; Wang, Gonzalo-Ruiz, Sanz, Campbell, and Lieberman, 1999). While HD dominates the spatial code in POS (Taube, Muller and Ranck, 1990; Peyrache, Schieferstein and Buzsáki, 2017; Laurens *et al.*, 2019), RSC is characterized by diverse visuo-spatial activity (Alexander, Carstensen, Hinman, Raudies, Chapman, and Hasselmo, 2020; Cho and Sharp, 2001; Mao, Kandler, McNaughton, and Bonin, 2017b; Powell, Connelly,

Vasalauskaite, Nelson, Vann, Aggleton, Sengpiel, and Ranson, 2020), with complex spatial receptive fields, where multiple correlates influence the firing patterns of individual neurons (Alexander, Carstensen, Hinman, Raudies, Chapman, and Hasselmo, 2020; Alexander and Nitz, 2017, 2015; Jacob, Casali, Spieser, Page, Overington, and Jeffery, 2017). As a cortical association area, RSC plays a critical role in spatial cognition (Knight and Hayman, 2014; Mitchell, Czajkowski, Zhang, Jeffery, and Nelson, 2018; Vann, Aggleton, and Maguire, 2009) and spatial memory (Miller, Mau, and Smith, 2019; Miller, Vedder, Law, and Smith, 2014): rats and humans with RSC lesions show impairments in route planning, identification and flexible use of navigational landmarks (Hindley, Nelson, Aggleton, and Vann, 2014; Maguire, 2001; Pothuizen, Aggleton, and Vann, 2008; Vann and Aggleton, 2004). Specifically, in the intact RSC, associations between egocentric and allocentric reference frames become evident with spatial tasks (Alexander, Carstensen, Hinman, Raudies, Chapman, and Hasselmo, 2020; Alexander and Nitz, 2015; Shine and Wolbers, 2021; van Wijngaarden, Babl, and Ito, 2020). These kinds of computations might underlie the emergence of navigational landmarks (Auger, Mullally, and Maguire, 2012; Fischer, Soto-Albors, Buck, and Harnett, 2019; Jacob, Casali, Spieser, Page, Overington, and Jeffery, 2017; Page and Jeffery, 2018), as sensory stimuli that appear in the egocentric view and are deemed reliable are ultimately mapped to an abstract representation of space (Barry and Burgess, 2014; Bicanski and Burgess, 2016; Yan, Burgess, and Bicanski, 2021). Altogether, this evidence strongly implicates RSC in the integration of visual orienting cues and HD. It is, however, unknown how the ensuing changes in HD representation are coordinated between cortical and sub-cortical circuits, and what the role of RSC is in this process. We sought to answer this question by performing simultaneous single unit recording in RSC and ADn in freely moving mice while a visual cue was either rotated around the arena or turned off.

Results

ADn and RSC differentially encode HD

To monitor single unit activity in RSC and ADn we implanted tetrodes targeting the two regions simultaneously in 9 mice. We additionally recorded from RSC alone in two mice, and used carbon fiber electrodes to record from ADn in one more mouse (Fig. 2.1A, sample electrolytic lesions for

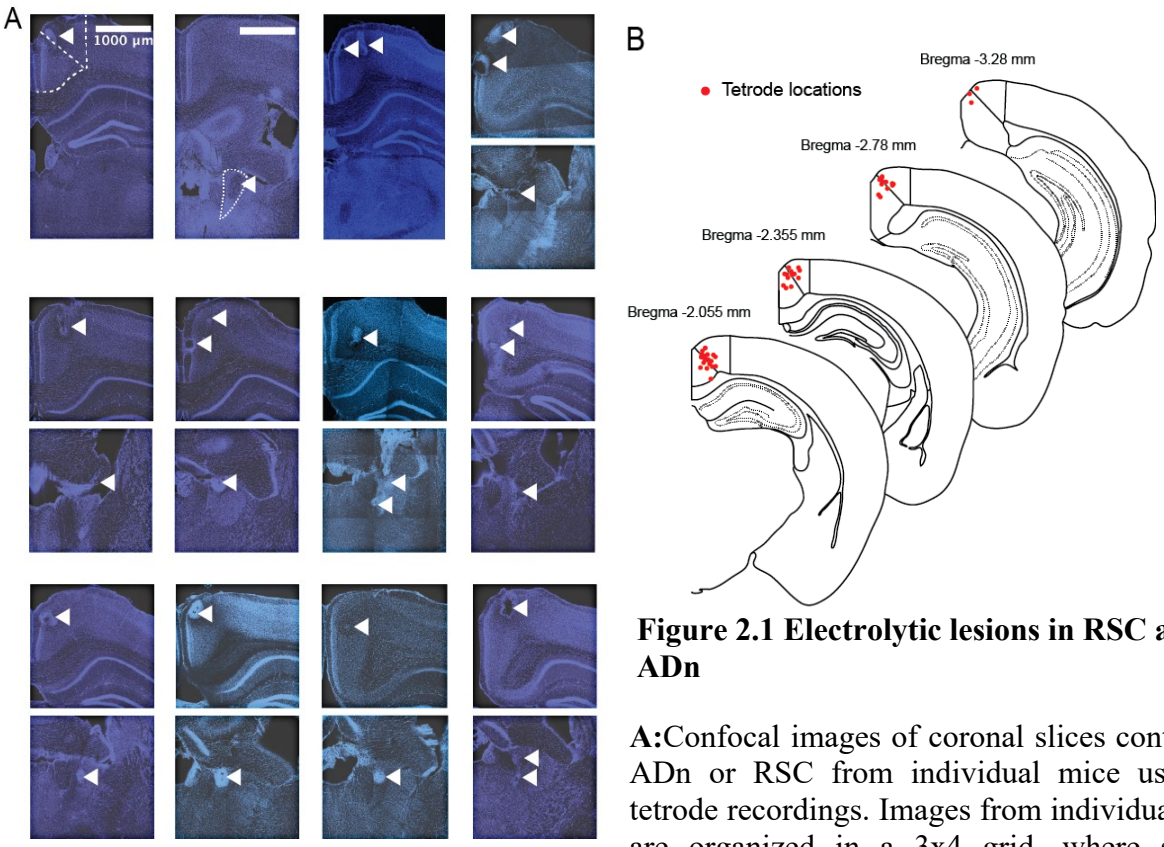

Figure 2.1 Electrolytic lesions in RSC and ADn

A:Confocal images of coronal slices containing ADn or RSC from individual mice used for tetrode recordings. Images from individual mice are organized in a 3x4 grid, where sample electrolytic lesions in RSC are presented in the top row and those in ADn in the bottom row for mice with dual site recordings. For mice with single recording site (the first 3), only one sample image is provided (in order RSC, carbon fiber-targeted ADn and RSC). ADn and RSC granular and dysgranular outlines are shown with dashed lines in the first two images. White, leftward arrows indicate the lesions, which corresponds to the locations of the recording electrodes. Scale bar 1 mm; the same scale was applied to all images. **B:** Summary of cortical tetrode locations from all mice, distributed over 4 roughly matching coronal slices from the Mouse Allen Brain Atlas.

ADn and RSC targeting for each mouse). During the recordings, mice could freely roam in a circular arena of diameter 50 cm, where the only visual cue was provided by an illuminated subset of LEDs spanning an angle of 20° which were located around the upper rim of a wider circle outside the arena. From our recordings we found that 48% of units in ADn meet our criterion for HD cells, whereas 20% in RSC do so (Fig. 2.3 B,C). Our HD cell selection method relied on the amount of directional information and magnitude of the resultant from the tuning curve (Fig 2.2 D,E) or the von Mises fit to the largest peak in multi-peak units (Fig. 2.2 A-C) against those obtained from shuffling the spikes. RSC displayed a modest HD code, in agreement with findings

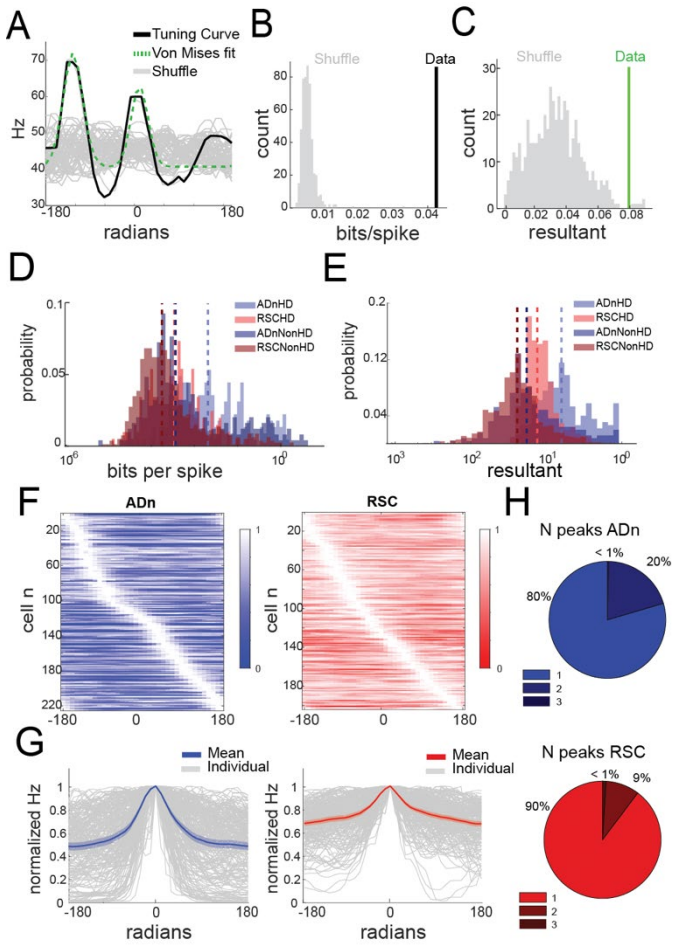

Figure 2.2 HD selection method and HD features across ADn and RSC

A: Example of von Mises fitting (green dashed) to the tuning curve (solid black) with two identified peaks in ADn, compared to the tuning curves obtained from shuffling the spikes (grey solid lines). **B:** The directional information calculated from the tuning curve in the example in A is above the 95th percentile of the shuffle distribution. **C:** The resultant of the fit to the largest peak of the tuning curve in A is above the 90th percentile of the shuffle distribution. **D:** Distributions and medians (dashed lined) of the directional information (in bits/spike) across ADn HD (0.0567, n=225) and non-HD (0.0142, n=248) and RSC HD (0.0134, n=205) and non-HD (0.0074, n=805) units ($p<0.0001$, Kruskal Wallis test, and $p<0.001$ for multiple comparisons after Bonferroni correction, except for ADn NonHD and RSC HD cells, where $p=0.0675$). **E:** Distributions and medians (dashed lines) of the resultants of the same groups of units as in D: ADn HD (0.159, n=225) and non-HD (0.055, n=248) and RSC HD (0.076, n=205) and non-HD (0.041, n=805) units ($p<0.0001$, Kruskal Wallis test, and $p<0.001$ for multiple comparisons after Bonferroni correction). **F:** Normalized tuning curves of all the HD units in Fig.1c sorted by peak location in ADn (left) and RSC (right). **G:** Individual (grey) and mean and 95% CI of normalized and peak-aligned to 0° HD tuning curves from F, ADn (left, blue) and RSC (right, red). **H:** Fraction of HD units with multiple peaks in ADn and RSC.

in rats and humans (Chen, Lin, Green, Barnes, and McNaughton, 1994a; Cho and Sharp, 2001; Shine, Valdés-Herrera, Hegarty, and Wolbers, 2016; Shine and Wolbers, 2021). However, directional information in RSC was generally lower than in ADn (bits/spike median: ADn HD=0.0567, n=225, RSC HD=0.0134, n=204, ADn NonHD=0.0142, n=248, RSC NonHD=0.0074, n=805, Kruskal Wallis test $p<0.0001$, and $p<0.001$ for multiple comparisons after Bonferroni correction, except for ADn NonHD and RSC HD cells, where $p=0.0675$) (Fig. 2.2D). This was consistent with the high incidence of conjunctive encoding observed in RSC and

the high dimensionality of individual receptive fields (Alexander and Nitz, 2015; Chen, Lin, Green, Barnes, and McNaughton, 1994a; Cho and Sharp, 2001; Laurens, Abrego, Cham, Popeney, Yu, Rotem, Aarse, Asprodini, Dickman, and Angelaki, 2019), where multiple spatial correlates, contexts and states influence HD coding.

Congruent HD response to visual cue rotation in ADn and RSC

To challenge the sense of orientation and determine whether ADn and RSC similarly update the HD frame in response to changes to visual stimuli, we rotated the LED cue around the arena by either 45° or 90° with a sudden "jump" (Fig. 2.3D) from one angular position to the next, in trials ranging from 5 to 40 minutes. Previous work with cue card rotations indicated that HD cells in ADn rotated their preferred firing directions (PFD, the circular mean of the directional tuning curve) coherently (Yoganarasimha, Yu, and Knierim, 2006), but it remains unclear if the same applies to RSC. Different studies of HD cells in posterior cortex, including RSC, reported diverse, complex responses to cue manipulations (Chen, Lin, Green, Barnes, and McNaughton, 1994b), while others compared their responses to those seen in POS and ADn (Lozano, Page, Jacob, Lomi, Street, and Jeffery, 2017). Other studies in medial entorhinal cortices have reported the presence of HD cells uncoupled to theta rhythms. These cells escape attractor dynamics, showing incoherent responses, including changes in peak firing rate upon visual cue manipulations (Kornienko, Latuske, Bassler, Kohler, and Allen, 2018). Cortical HD may be influenced by environmental cues, including the geometry, and discriminate between contexts differently from ADn, which encodes the global HD. To investigate this issue in our behavioral setting, we first calculated the angle offsets as the phase shift of maximal correlation between the tuning curves of all unique simultaneous pairs before and after cue rotation (Fig. 2.3F). As expected, the phase relationship between pairs of ADn HD neurons remained rigid after rotations of the neurons' PFD (Fig. 2.3 G,H,I, circular correlation=0.738, n= 211 trials, 4686 pairs, 10 mice). Despite the reduced amount of HD coding together with a lower resultant in HD cells in RSC compared to ADn (Fig. 2.2 E, median ADn HD cells: 0.159, non-HD cells: 0.055, RSC HD cells 0.076, non-HD cells 0.041, $p<0.0001$ for Bonferroni-corrected multiple comparisons after Kruskal Wallis test, $p<0.0001$), we observed a small, but nonetheless higher than chance correlation (0.388, n=222 trials, 17579 pairs,10 mice) between before and after cue rotations phase offsets of RSC HD neuron pairs (Fig.

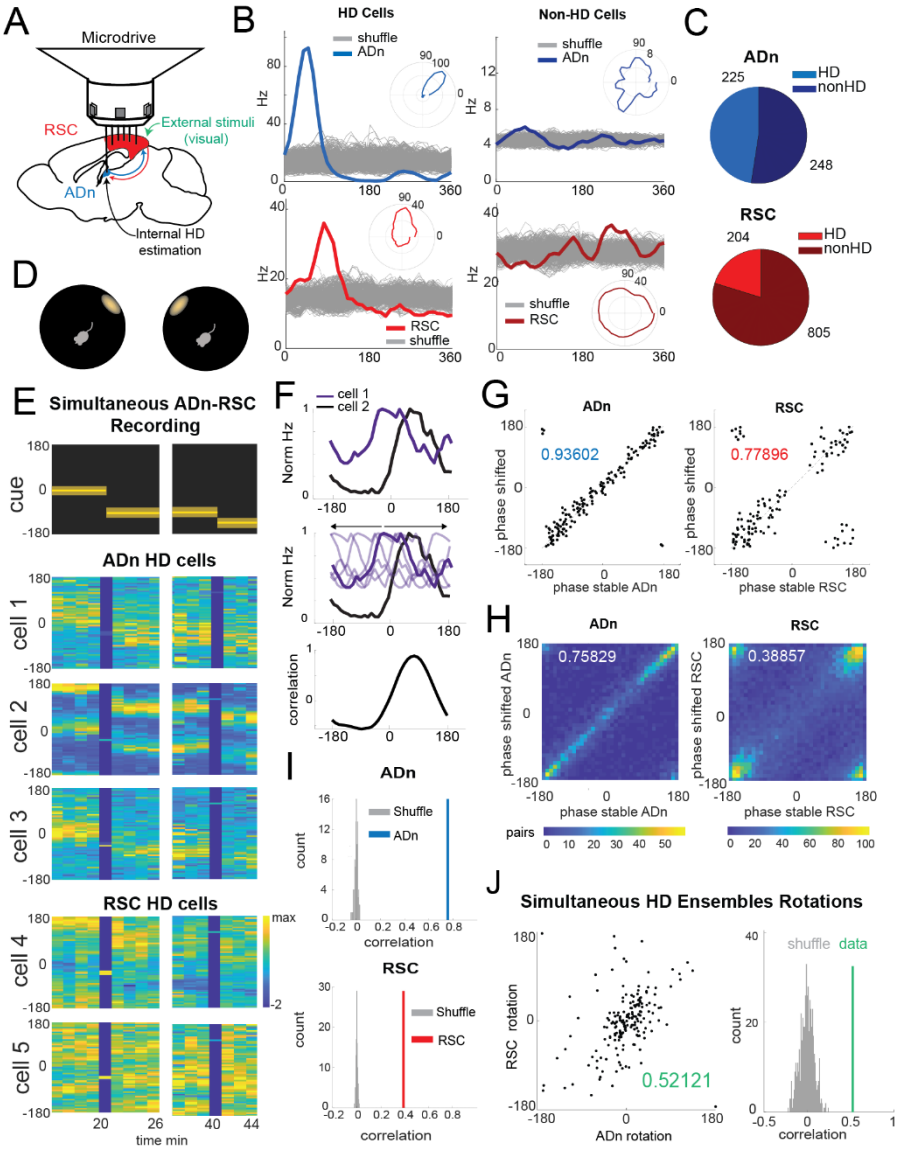

Figure 2.3 Congruent HD response to visual cue rotation in ADn and RSC, despite differences in strength of HD coding.

A: Schematic of multisite tetrode recording in the mouse brain to test the relationship between ADn (blue) and RSC (red) HD activity in response to changes in visual stimuli. **B:** Tuning curves of examples of HD (left) and non-HD (right) cells in ADn and RSC. Grey lines are the tuning curves obtained from 500 shuffles of the cells firing rates. Insets show the tuning curves in polar coordinates. **C:** Pie charts showing that 48% of cells in mouse ADn meet the HD selection criterion, but only 20% in RSC do (right) (N=12 mice, 8 with simultaneous ADn and RSC, 2 ADn only and 2 RSC only). **D:** Schematic of the arena with the only prominent LED cue before (left) and after 90-degree rotation (right). **E:** Example of a simultaneous ADn-RSC recording from a session were the cue (top) was rotated first by 90° (first segment) and then 45° (second segment). Panels from cell1 to cell5 show the tuning curves (2 min bins) over time of HD cells in the two regions, shifting the preferred firing direction (yellow bins, maximal firing rate) in register in response to the cue rotation. **F:** Schematic of the phase correlation procedure: top, tuning curves of two HD cells; middle, circular shifting of the purple tuning curve; bottom, calculated circular correlation for all phase shifts. The two cells are maximally correlated at 90° phase shift. **G:** Scatter plots of phase-difference from all ADn HD cells pairs (left) and RSC HD cells pairs (right) from example trials before vs after rotation. In blue and red the correlation between before and after rotation for ADn and RSC pairs, respectively. **H:** 2D histograms of phase-differences before vs after rotation from all HD unit pairs from all rotation trials of ADn recordings (left) and RSC recordings (right) (ADn correlation :0.738, N=211 trials, 4686 pairs, 10 mice; RSC correlation: 0.39, N= 222 trials, 17579 pairs, 10 mice). **I:** Correlation values of ADn pairs (top) and RSC (bottom) from the data in **H** are above the 99th percentile of 100 randomly drawn phases. **J:** Left, mean rotations from HD cells in ADn vs mean rotations of simultaneously recorded HD

cells in RSC. Right, correlation value from the data in the left panel (N=185 trials, 8 mice) is above the 99th percentile of 500 times shuffled rotation trial indices for each HD cell.

2.3 G,H,I). We concluded that RSC also presented a coherent HD representation, in that the reference shift was similarly reflected in the HD units PFDs, despite the higher variability.

Using our established within-region HD coherence, we calculated the mean PFD shifts for RSC and ADn HD ensembles in order to compare how both regions responded to cue rotations. Despite a bias toward the inertial HD estimate, evident through the higher density of rotation values around 0 (Fig. 2.3 J), the rotations from the simultaneously recorded ADn and RSC HD ensembles were more correlated (coefficient=0.52, n=185 trials, 8 mice) than those produced by temporally disconnecting with random shifts RSC and ADn neural activity around the cue rotations (Fig. 2.3 J). This suggested that in our behavioral paradigm the HD map, despite the differences in HD encoding between ADn and RSC, is somewhat locked between the two regions.

Synchronous shifting of ADn and RSC HD representation in response to cue rotations

Based on the individual HD cells tuning curves, we concluded that RSC and ADn encoded the same HD reference, whether they shifted with the cue rotation or disregarded the cue as an orienting landmark (Fig 2.3 J). However, were ADn and RSC also coordinated at a finer temporal scale in response to the cue rotation? To answer this question, we applied a decoding approach that infers the HD representation from the entire recorded population at a high temporal resolution (20 ms) in ADn and RSC. We implemented a linear-Gaussian generalized linear model (GLM) that related the ADn or RSC ensemble neural activity to HD obtained from behavioral tracking (Fig. 2.4 A). Specifically, for each trial we estimated the weight coefficients based on the stable cue section before rotation and tested the model on the last 80 seconds, by calculating the difference between the decoded HD and the HD from tracking. On average 75% of the decoded errors from the test period were under 60.133° ± 3.44 in ADn (n=303) and under 72.46° ± 3.44 in RSC (n=311) ($p<0.0001$, Mann-Whitney test) (Fig. 2.4 B,C).

Consistent with what has previously been reported with other decoders (Ajabi, Keinath, Wei, and Brandon, 2021; Park, Keeley, Savin, Ranck, and Fenton, 2019), the errors from the GLM decoder reflected the mean rotations that we calculated from the tuning curves both from ADn and

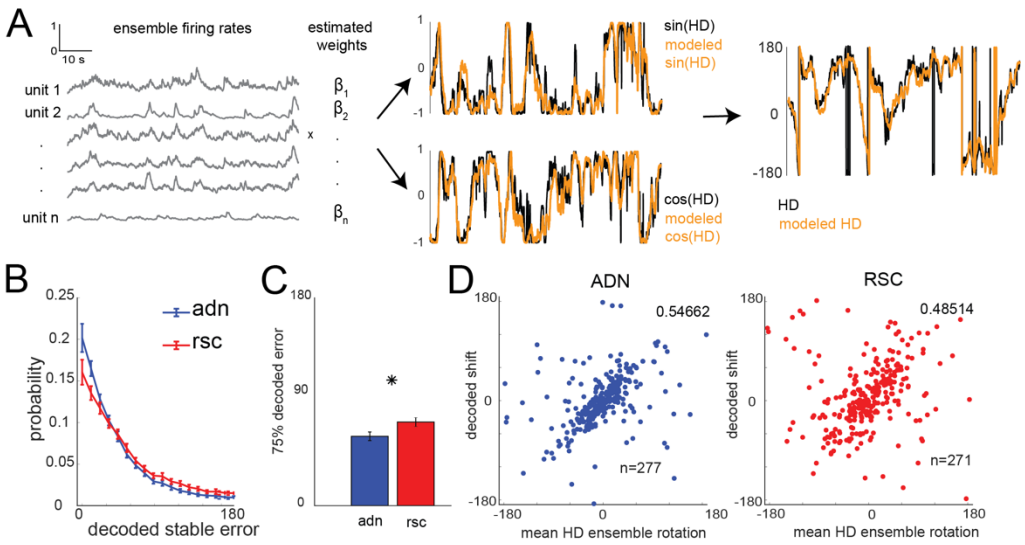

Figure 2.4 HD decoding with a linear-Gaussian GLM

A: Linear-Gaussian GLM-based decoding strategy for each trial and neuronal ensembles (See also Methods Section) with an example of modeled sin(HD) and cos(HD). **B:** Mean and 95% CI of the absolute decoding error distribution for ADn (blue) and RSC (red) from the test/before rotation period for all trials (n=303 for ADn, n=311 for RSC). **C:** Mean and 95% CI of the 75th percentile of the absolute decoded error distributions for ADn and RSC ($p<0.0001$, Mann-Whitney test). **D:** Scatter plots of the mean rotations from HD tuning curves quantified in Fig 1 vs those from the decoding for ADn (left) and RSC (right). Circular correlation values (0.54 for ADn, n=277, and 0.48 for RSC, n=271, $p<0.0001$ both) indicated that the decoding captures the changes in HD reference.

RSC (Fig. 2.4 D, 0.546 and 0.485 circular correlation coefficients for ADn, n=277, and RSC, n=271, respectively, $p<0.0001$ for both) suggesting that our method largely captured the changes in neural activity with cue rotation. The mean decoded errors after cue rotations from simultaneously recorded ADn and RSC ensembles were also correlated (Fig. 2.6 C, 0.664 circular correlation coefficient, n=213), confirming the findings from the mean tuning curves rotations (Fig. 2.3 J). We also observed a higher density of decoded rotations values around zero, despite the high number of trials for 90° as well as 45° rotations. This effect likely resulted from devaluation or bias toward internal HD representation after multiple exposures to visual and internal HD mismatches within the arena, especially for the large 90° rotations (Knierim, Kudrimoti, and McNaughton, 1998).

To investigate whether the egocentric experience of the cue influenced the rate of under-rotations, we compared rotations occurring when the cue was well outside of the visual field of the

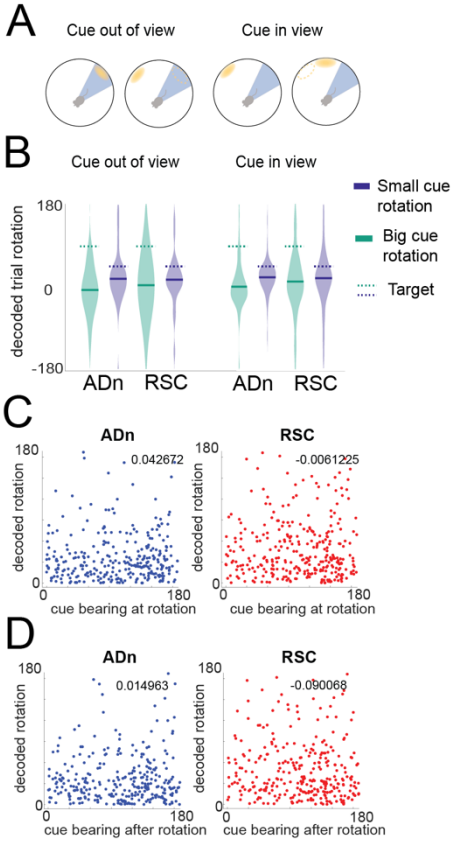

Figure 2.5 Relationship between cue bearing and decoded neural rotations

A: Schematic of the distinction between egocentric "in view" (right) and "out of view" (left) angular position of the visual cue before rotation. **B:** Violin plots of the decoded rotations from simultaneous ADn and RSC trials according to the imposed cue rotation size (at a cutoff of 67.5°) and the egocentric view of the cue before rotation. Large cue rotations resulted more often in neural rotations around 0 than the small cue rotations (multiple ways ANOVA, p=0.010 effect of the size of rotation, p>0.05 for effects of brain region and egocentric condition and for all interactions. P>0.05 for all Bonferroni-corrected multiple comparisons, between the following categories N trials and means: large/out of view: n=18, ADn=-0.127, RSC=0.0569, large/in view: n=100, ADn=-0.001, RSC=0.194; small/out of view: n=26, ADn=0.31, RSC=0.26; small/in view: n=69, ADn=0.35, RSC=0.32). **C:** Decoded rotation as a function of the egocentric bearing of the cue before rotation. **D:** Decoded rotation as a function of the egocentric bearing of the cue after rotation. P>0.05 of the Pearson's correlation coefficients, ADn n=300, RSC n=306, both in C and D.

mouse before rotation (Dräger and Olsen, 1980; Sterratt, Lyngholm, Willshaw, and Thompson, 2013) or not (>154° or >-154°, calculated at the center of the cue, with 0° aligned to the mouse' snout; Fig. 2.5 A). We found that, despite an overall effect of the size of the rotation (ANOVA with 3 factors, p>0.05 for any interaction), there were no detected differences between the groups (multiple comparison after Bonferroni correction p>0.05, cue out of view: small rotation n=26 trials, ADn 0.31, RSC 0.26, big rotation n=18 trials, ADn -0.127, RSC 0.0569; cue in view: small rotation n=69 trials, ADn 0.35, RSC 0.32, big rotation n=100 trials, ADn -0.001, RSC 0.194, Fig. 2.5 B). This suggested that even though large mismatches were more likely to result in under rotations, we could pool the results of the rotation analyses. Furthermore, we did not find any correlation between the size of the decoded rotation in ADn and RSC and the egocentric bearing of the cue before (Fig. 2.5 C, 0.043 and 0.006 correlation coefficients respectively for ADn, n=303,

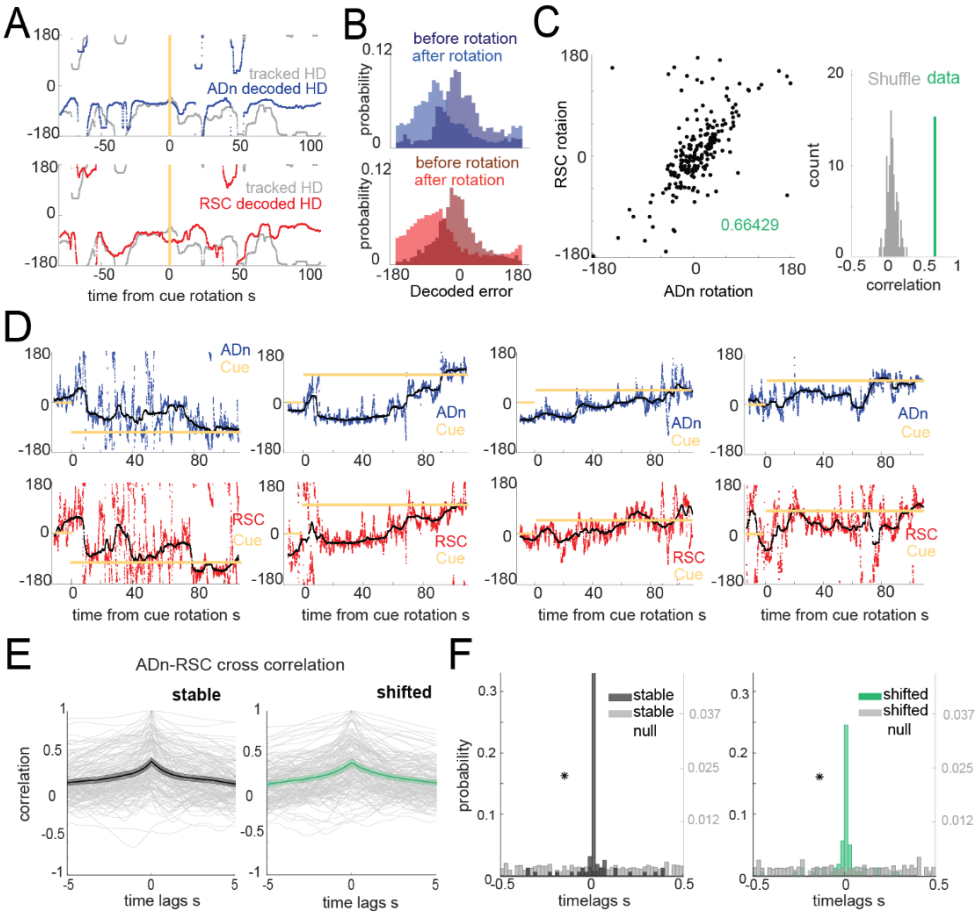

Figure 2.6 Synchronous shifting of ADn and RSC HD representation in response to cue rotation

A: Example of decoded HD in ADn (top, blue line) and RSC (bottom, red line) from a simultaneous recording in the two regions before and after cue rotation (yellow line at t= 0 s). Grey line, mouse HD from tracking. **B:** Probability normalized histograms of the difference between the tracked and the decoded HD from the example in A in ADn (top, blue) and RSC (bottom, red). Darker shades, decoded error before rotation, lighter shades after rotation. **C:** Left, decoded ADn vs paired RSC rotation (N=213 trials, 8 mice). Right, Correlation value between the decoded ADn and RSC rotation (green) is above the 99th percentile of the 100 times randomly shifted RSC decoded HD for each trial (grey). **D:** Four examples of paired ADn (top row) and RSC (bottom row) decoded HD errors aligned to the time of cue rotation (t= 0 s) drifting toward the target (yellow). Black lines, median-smoothed error over a 10 s window. The first example is the decoded error of the traces shown in A. **E:** Mean and 95% confidence intervals of temporal cross correlation between paired decoded errors before rotation (left, black) and immediately after rotation (right, green) (80 s long segments, N=159 out of 204 paired trials with mean ADn rotation >11.5°, 8 mice). Grey, individual trials. **F:** View in the -0.5 s to 0.5 s range of the probability normalized histograms (20 ms bins) of the time lags corresponding to the peak correlation values from all trials in E, left, before rotation, right, after rotation. Left y axis scaled to show the uniformity of the null distributions (grey). Asterisks indicate the real distributions are significantly different from null

(two-sample Kolmogorov-Smirnov test, $p<0.0001$ for both stable and shifted). No difference between stable and shifted trial correlations was observed (Wilcoxon Signed-Rank test $p=0.975$).

and RSC, n=311) or after rotation (Fig. 2.5 D, 0.015 and -0.090 correlation coefficients respectively for ADn and RSC). Altogether, these analyses indicated that in our behavioral setting the egocentric experience of the cue rotation was not the main factor underlying the under-rotations of the HD representation.

One fundamental question about the HD system is how quickly the reference shifts in response to changes in environmental stimuli. By applying our decoding strategy, we first observed that decoded errors drifted to the targets at variable rates, some immediate and some slower (Fig. 2.6 D and Fig. 2.7 A), but there was no relationship between the size of the rotation and the time it took for the error to settle (Fig. 2.7 B, circular correlation coefficient = 0.25) or between the size of the rotation and the trajectory of the unwrapped decoded error (circular correlation coefficient=0.29). The rotation trajectory was however highly correlated with and linearly dependent on the timing of the rotation (0.887 correlation coefficient, $p<0.05$), suggesting that despite some variability, the shifts were continuous and gradual. On average we observed similar, and mostly slow, HD reference shifts, in both ADn and RSC (Fig 2.7 E).

Interestingly, we observed closely matched trajectories to the new target offset for both ADn and RSC for simultaneously recorded neurons (Fig. 2.6 D). To quantify if any initial jitters in the drift of the HD representations were indicative of a region-specific response to the new angular position of the cue, we calculated the temporal cross correlations between simultaneous ADn and RSC decoded errors immediately after cue rotations (75 s window). To isolate the effect of successful update of the HD reference, we included only trials where the absolute mean HD shift was at least above 11.5°. While substantial trial-to-trial variability in the correlation level was observed, the majority of the trials had peaks at 0ms time lags (two-sample Kolmogorov-Smirnov test between data and null distribution, $p<0.0001$ for both stable and shifted, Fig. 2.2 G), both before and after cue rotations (Fig. 2.2 E,F) (Wilcoxon Signed-Rank test $p=0.975$, n=159 trials). Contrary to our predictions, that RSC would lead the HD reference update compared to ADn as a result of visual integration of the cue's new angular position, we found that the two regions were highly synchronized in their HD reference update. More variability was observed in the histograms

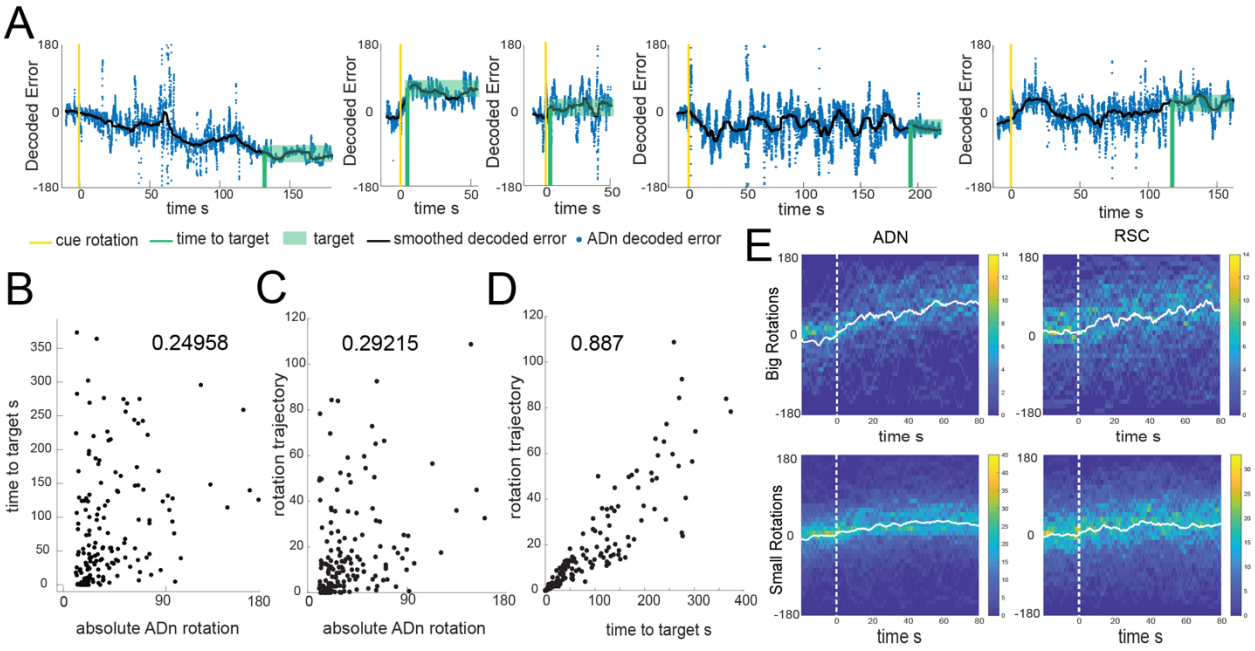

Figure 2.7 Time course of the decoded HD rotations.

A: Examples of decoded ADn HD error (blue) after perceived cue rotations (yellow line) showing variable timing (green vertical lines) and rates of the representation shift between the pre-rotation period and the target HD offset (shaded green), calculated as the circular mean of the decoded error taken between 100 and 400 s after cue rotation. In black, median-smoothed decoded error over 10 s. **B:** Scatter plot of the absolute ADn HD target offset (or neural rotation) vs the time to target in s. The Pearson correlation coefficient 0.25, $p<0.05$, indicates no pattern between the size of the rotation and the timing to target. **C:** Scatter plot of the absolute ADn HD target vs the total distance travelled, calculated as the sum of the absolute distances between consecutive points of the unwrapped decoded error after rotation, smoothed over a 5 s window. The Pearson correlation coefficient 0.29, $p<0.05$, also indicated no pattern between the size of the rotation and the trajectory. **D:** Scatterplot and correlation between the timing of the rotation and the rotation trajectory (0.887, $p<0.05$). Data in B,C,D, n=165, only absolute mean rotations larger than 11.5° with timing calculations that met the requirement of normalized circular variance over 10 s window less than 2 and mean difference from target less than 5.7 were included. **E:** 2D heatmaps of the decoded errors (in 10° bins, y axis, over 20 ms bins, x axis) from 20 s before the rotated cue entered the visual field of the mouse up to 80 s after, flipped to all have final positive target offsets. Large rotations (offset larger and equal than 67.5°) ADn n=46, RSC n=72; small rotations (offset smaller than 67.5°and larger than 11.5°) ADn n=182, RSC n=185. White lines indicate the circular means across the trials.

from the cross-correlations after cue rotation, but without a specific bias for anticipatory or delayed time lags. Variability in the neural activity, and therefore in HD decoding, could emerge following the cue rotation as a response to unexpected visual stimuli and could provide a potential explanation to the slightly decreased synchrony compared to stable cue periods.

Correlated HD drift in darkness in ADn and RSC

Visual cues influence the HD signal in ADn and POS by acting as an anchoring reference, thus counteracting the drift (Ajabi, Keinath, Wei, and Brandon, 2021; Mizumori and Williams, 1993; Valerio and Taube, 2012; Yoder, Clark, Brown, Lamia, Valerio, Shinder, and Taube, 2011) from stochastic error in angular velocity (AV) integration observed in darkness (Stackman and Taube, 1997; Zhang, 1996). RSC is also necessary for path integration-based navigation in darkness (Elduayen and Save, 2014), likely by integrating motor (Yamawaki, Radulovic, and Shepherd, 2016) and AV signals (Hennestad, Witoelar, Chambers, and Vervaeke, 2021; Keshavarzi, Bracey, Faville, Campagner, Tyson, Lenzi, Branco, and Margrie, 2021) together with the incoming HD from thalamic nuclei and POS to form a representation of orientation. However, it is unknown if visual cues are necessary for maintaining the coordination of HD representations in ADn and RSC. To resolve this issue, we challenged the sense of orientation in a subset of mice, by turning the LED cue off after a period of cue-on baseline (Fig. 2.8 A). HD cells maintained the same initial PFD while the cue was on in a stable position, but were more variable while the cue was off, and sometimes continuously drifted during prolonged darkness (Fig 2.8 B, example). On average, we observed modest levels of drift in darkness (Fig. 2.9 A, $p<0.05$ Kuiper test between total cue-on and cue off mean drift distribution, n=72 trials in ADn). When we applied the same decoding strategy (Fig. 2.8 C and Fig. 2.9 D-F) to quantify the drift in the two regions, we observed correlated HD representations between ADn and RSC both during cue on and cue off periods, as shown by the bright band across the diagonal of the column-normalized 2D histograms of the HD decoded errors. The correlations were similar between the cue on (Fig. 2.8 E) and the cue off (Fig. 2.8 F) periods, and were significantly higher than the correlations produced by a randomly shifting the RSC decoded HD (left plots, Fig. 2.8 E,F). Moreover, rotational head velocity did not affect this relationship (Fig. 2.9 B and C), suggesting that even under the challenges of greater head velocity, the coordination between the two regions is maintained. Whether local AV signals in ADn and RSC modulate and coordinate the HD code is unknown.

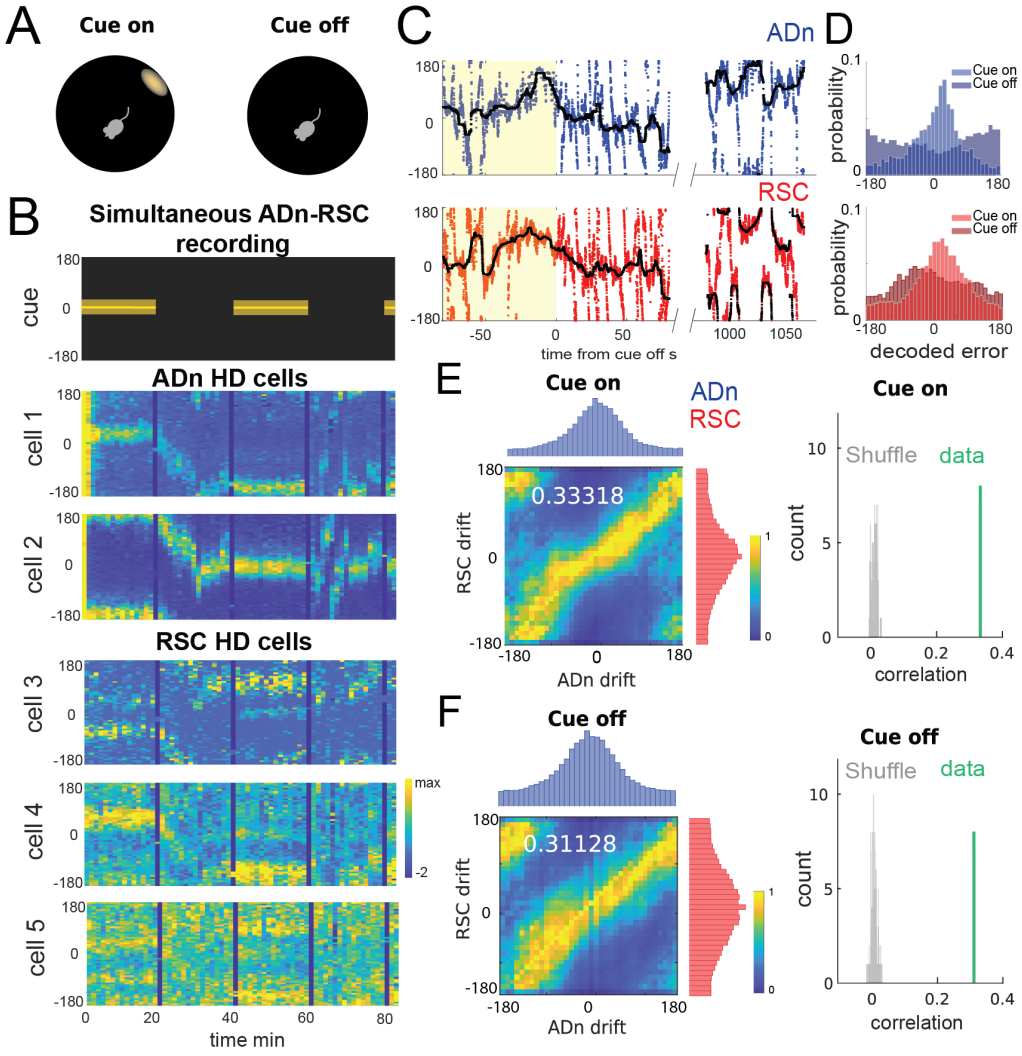

Figure 2.8 Correlated HD drift in darkness in ADn and RSC

A: Schematic of cue off trials. **B:** Example of a simultaneous ADn-RSC recording from a session were the cue (top) was turned on and off. Panels from cell1 to cell5 show the tuning curves (2 min bins) over time of HD cells in the two regions, where the preferred firing direction (yellow bins, maximal firing rate) is stable during while the cue is on, but shifts similarly in all cells in darkness. **C:** Simultaneous ADn and RSC decoded HD errors from the first cue on (yellow shaded) and off trial of the example shown in B. For illustrative purposes, only the initial and middle segments of the cue off are shown here. **D:** Probability normalized histograms of the decoded HD error from the example in **C** in ADn (blue, top) and RSC (red, bottom). The lighter shaded histograms are from the cue-on segments, the darker shaded from the cue-off. **E:** Left: 2D histogram of simultaneous ADn and RSC decoded errors from cue on, normalized by the maximum column value per bin (i.e. in the ADn dimension); above and on the side, marginal distributions of ADn and RSC drift, respectively. Right: Correlation value (green) from the not-normalized data in the left is above the 99th percentile of the distribution obtained after randomly shifting the RSC drift in each trial (grey), both for the cue on (top) and cue off (bottom) segments. **F:** Same 2-D histogram and marginal distributions during cue-off on the left, and correlation of the real data vs shuffle on the right. (N= 33 trials, 3 mice).

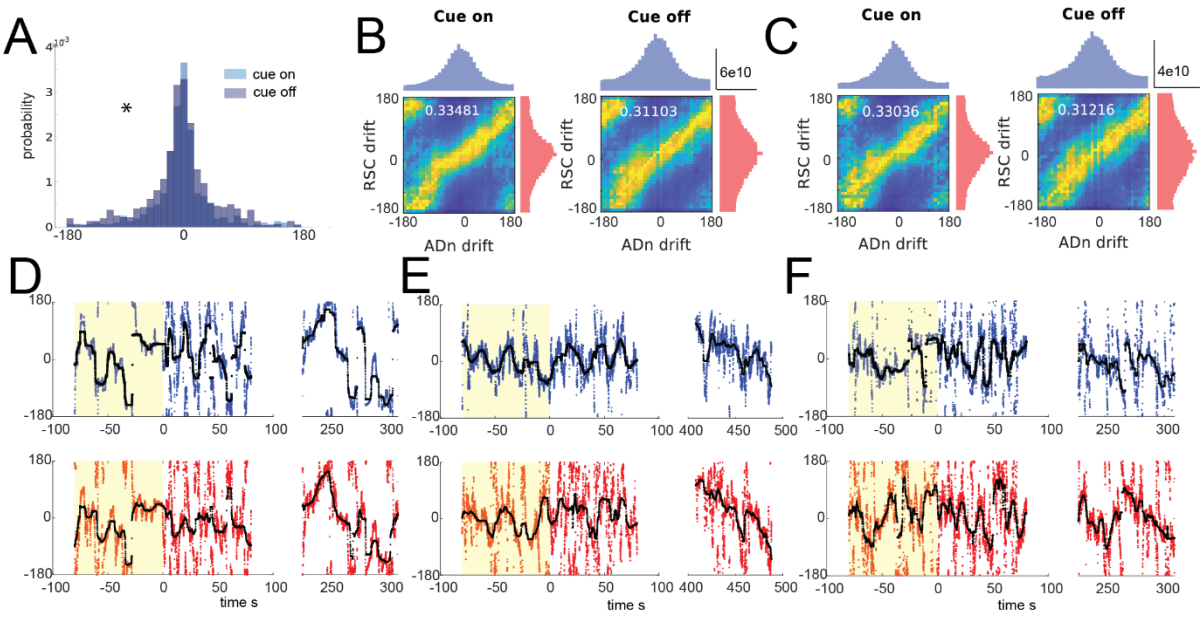

Figure 2.9 HD drift in darkness in ADn and RSC.

A: Distribution of the ADn HD ensemble mean of the differences between the PFDs from the first 4 minutes of cue on and either the subsequent cue on (lighter shade) and cue off (darker shade) periods calculated every 2 minutes ($p<0.001$ Kuipers test, 72 trials, 5 mice). **B-C** Column-normalized 2D histogram of the decoded HD drift from ADn vs RSC while the cue was on (left) or off (right) and marginal histograms of the regional drifts on the sides, with scale bar of the histogram counts, and value of circular cross-correlation. B comes from periods of head immobility and slow rotational velocity (< 30°/s) and C from periods with rotational velocity higher than 30°/s. **D-F:** Examples of decoded HD representations from simultaneously recorded ADn and RSC during cue on (yellow shade) and cue off. In black, the median-smoothed decoded errors over a 5 s window.

Our results indicate that the HD representation is also coordinated between ADn and RSC in the absence of a visual input and in periods of HD instability.

Asymmetry in the RSC-to-ADn and ADn-to-RSC connectivity

Temporal coordination of HD representation at timescale of 20 ms or less across different structures could be accomplished by direct monosynaptic connections or by concurrent input from different areas, particularly for the visual update of HD. To begin investigating the anatomical substrate for direct connectivity between ADn and RSC, we performed retrograde monosynaptic rabies tracing (Wickersham and Sullivan, 2015) experiments in ADn and RSC. We found that cells

from similar RSC regions to those from our tetrode recordings (Fig. 2.1 A,B) received dense anterior thalamic inputs, and particularly ADn (Fig. 2.10 A). Conversely, the RSC cells that made synapses onto ADn were sparse, more frequently localized in the granular and ventral portion of RSC (Fig. 2.10 B). These results were consistent with previous studies in the rat, which revealed reciprocal, but similarly asymmetric connectivity between ADn and RSC (Shibata, 1998, 1993; Van Groen and Wyss, 1990).

We next examined whether the HD coordination we observed in our recordings could emerge from ensembles in RSC or ADn that were functionally connected and could convey updated or visually-anchoring HD information. To this end, we performed spike cross correlation between all possible ADn-RSC pairs, considering the spikes occurring during cue-on trials. Putative monosynaptic connections were identified in the cross correlograms as sharp peaks above the baseline (Fig. 2.10 C) between 1 and 5 ms from the time of ADn unit firing (Fig. 2.10 D). Using this metric (Peyrache, Lacroix, Petersen, and Buzsaki, 2015; Stark and Abeles, 2009), we identified 6.4% of all possible pairs with a monosynaptic connection in the ADn to RSC direction (522 out of 8083, in 6 mice) and only 0.08% in the RSC to ADn direction (7 out of 8083, from 2 mice). In terms of unit counts, 107 out of 424 ADn units had at least one connection to RSC, while only 4 out of 811 RSC units had a connection with ADn (Fig. 2.10 E). The ADn-to-RSC connectivity was divergent, with a mean number of RSC synaptic partners of 4.64 for ADn HD cells and 3.33 for non-HD cells. When we focused on the connectivity during darkness, we found similar results: 45 out of 226 units in ADn (3 mice) had at a connection, and no RSC units were connected. The generally lower connectivity rate was likely due to the reduced sample size of cue off trials, but suggested that even in the absence of visual cues corticothalamic projections were not a substrate for HD coordination.

ADn's dense connectivity largely originated from identified HD cells (284 connected pairs from ADn HD cells versus 118 from non-HD ADn cells) and included HD and non-HD partner cells in RSC (Fig. 2.10 F). HD-coding was a feature of both RS and FS units in RSC (Fig. 2.11) and both groups received ADn connections (Fig. 2.10 G, left plot). Finally, the distribution of the PFD differences between ADn HD-coding units and their HD-coding synaptic partners in RSC showed a small but significant bias toward similar tuning (Fig. 2.10 G left polar plot, n=102 units, 60 RS and 42 FS, 6 mice, Rayleigh test for non-uniformity $p=0.0086$ for the RS synaptic partners, circular mean -7.44°). This similarity was not observed for the PFD differences between the same

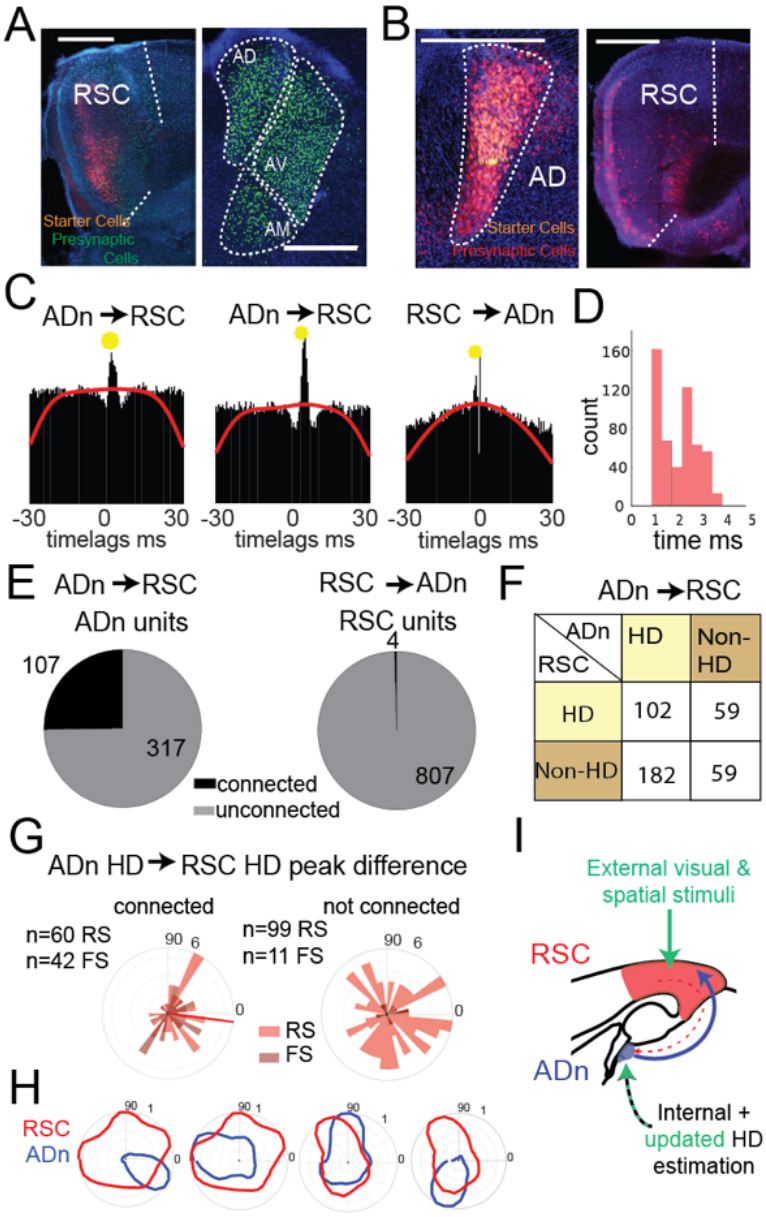

Figure 2.10 Asymmetric connectivity between RSC and ADn.

A: Monosynaptic rabies tracing of inputs to RSC (left, starter cells in red) shows a high density of presynaptic cells in ADn (right, green). **B:** Monosynaptic rabies tracing of inputs to ADn (left, starter cells identified by the overlap of blue, green and red) shows a low density of presynaptic cells in RSC (right, red) and mostly in A29. Scale bar in **A** and **B**, 0.5 mm. **C:** Examples of cross-correlograms with putative excitatory connections (yellow circle) from ADn to RSC (first 2 examples) and RSC to ADn (third example), showing a sharp peak between 1 and 5 ms time lag above the baseline (red line) at more than 99.9% of the cumulative Poisson distribution. **D:** Distribution of the latencies of the peaks in the cross-correlograms for ADn-to-RSC connections. **E:** Pie charts showing the number of ADn units that are functionally connected to RSC (left) and of RSC units that are functionally connected to ADn (right). **F:** Breakdown into HD- and non-HD coding of the putative pre- and post- synaptic partners of connected ADn-to-RSC pairs. **G:** Polar plot distributions of the differences between PFDs (calculated as circular means of the tuning curves) of connected ADn HD units and their putative HD-coding synaptic partners in RSC (N=102 units, 60 RS and 42 FS, 6 mice, left) and the same ADn HD units and all other HD-coding non-synaptic partners (N=110, 99 RS and 11 FS, 6 mice, right). Red line on the left plot indicates the circular mean (-7.44°) of the RS peak differences; Rayleigh test for non-uniformity $p=0.0086$ for the RS synaptic partner, $p<0.001$ for RS and FS, $p=0.1290$ of the non-synaptic partners (right plot). **H:** Polar plots of tuning curves of 4 example pairs of connected ADn to RSC HD units with variable PFDs. **I:** Adapted schematic from Fig. 2.3 showing that the connectivity from RSC to ADn is nearly absent and that the visually-guided updates in the HD frame emerge from a strong feedforward HD input from ADn.

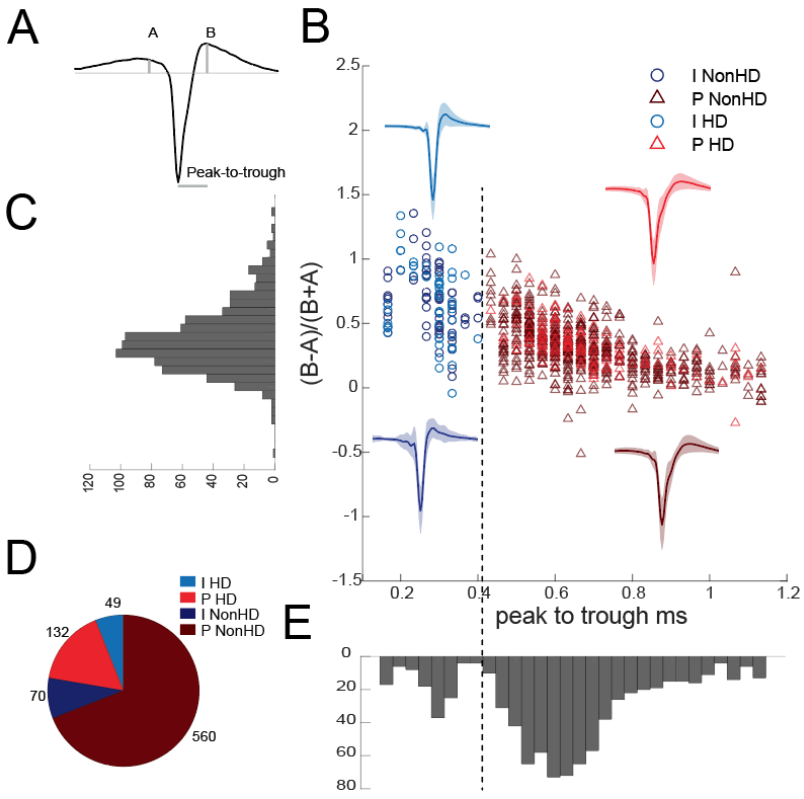

Figure 2.11 Separation of Putative Pyramidal Neurons and FS Interneurons in Cortex.

A: Example putative RS neuron spike waveform with A (pre-polarization) and B (after hyperpolarization) heights and the peak to trough distance metrics used for separating RS (~pyramidal) and FS (~interneurons) spiking neurons in RSC. **B:** Scatter plot of all 811 RSC units according to the metrics calculated as in A. Dashed line indicates the <0.42 ms peak-to-trough duration discrimination. Units are shape- and color-coded to reflect the unit type classification and whether they were HD tuned or not. The plot includes the mean and SD of the combined spike waveforms for the 4 classes of units. **C:** Unimodal distribution of the spike waveform symmetry values across all units. **D:** Counts of the 4 classes of units. **E:** Bimodal distribution of the peak-to-trough values, indicative of two clusters.

ADn units and all other non-synaptically connected HD-coding units, whose distribution was uniform (Fig. 2.10 G right polar plot, n=110, 99 RS and 11 FS units, p=0.1290 Rayleigh test for the RS units). Together, these results suggest that ADn sustains the RSC HD code with a widespread feedforward connectivity to both RS and FS units, that targets not only clearly HD-tuned units, directly shaping their PFDs (Fig. 2.10 H), but also units with more complex, possibly multimodal, receptive fields. On the other hand, the very sparse RSC-to-ADn connections are an unlikely circuit mechanism to drive the change, or the stability in the presence of visual cues, in HD PFD alone (Fig. 2.10 I).

Discussion

Our data shows that the HD representation in ADn and RSC was closely coordinated, both during visual cue stability and during adaptation to a new reference in response to cue rotation (Fig. 2.6 C,F,G). This was also true for HD drift in darkness (Fig. 2.8 E,F), showing that visual input is not necessary for maintaining this coordination, and that other sensory modalities, such as angular velocity, optic flow, and motor efference copy, possibly influence ADn and RSC HD. Finally, the underlying functional connectivity indicated that RSC is likely not wired to drive visual updates, or even maintain visual anchoring, via direct corticothalamic input to ADn. The latter, however, provides strong feedforward input driving the HD code in RSC (Fig. 2.10 E-H). Together, our results provide direct evidence against the hypothesis that visually-triggered updates in the HD reference would first appear in RSC, as a result of visual integration, and then be conveyed to ADn. We conclude that the visually-driven updating of HD is a more complex process that privileges coordination across brain regions over sustained error signals with mismatched representations.

With a simple generalized linear encoding model of HD (Fig. 2.4) on a trial to trial basis, we decoded quite accurately at a fine temporal scale the HD during the stable cue (Fig. 2.4 C,D), with ensembles of 4 to 30 units ADn and 8 to 90 in RSC. We observed variable and mostly slow drifts of the HD representation to a new target, whose duration and trajectory did not depend on the final angle shift (Fig. 2.7 A-C). These events suggest that an experience- and time-dependent weighting of the internal HD estimation against the egocentric bearing of the cue takes place as the new HD reference is determined. Repeated exposure to the cue and the environment is known to cause landmark devaluation (Knierim, Kudrimoti, Mcnaughton, 1995; Knight *et al.*, 2014) which, in addition to increasing the incidence of under-rotations, may affect the speed of these shifts. Slow, continuous drifts of the HD representation after cue rotation have been observed in flies (Kim, Rouault, Druckmann, and Jayaraman, 2017), rat (Knierim, Kudrimoti, and McNaughton, 1998)and mouse (Ajabi, Keinath, Wei, and Brandon, 2021) ADn, with the exception of one study in the rat ADn (Zugaro, Arleo, Berthoz, and Wiener, 2003) where immediate HD shifting was observed in specific cue-heading configurations. While a recent study (Ajabi, Keinath, Wei, and Brandon, 2021) related fast and slow HD shifts to network gain mechanisms in ADn and average angular velocity differences preceding the cue rotation, we could not determine

categorically different dynamics, likely because of several differences in our behavioral paradigm. First, our mice were free to roam in a wider arena, thus continuously experiencing different egocentric views of the cue; second, two sizes of cue rotations were tested, increasing the variability of the size of the experienced conflicts; third, the cue rotation did not follow a period of darkness. Nonetheless, it remains to be solved if the cause of such slow drifts lies in: 1) the configuration of the polarizing visual stimulus, including the distance between the cue and the mouse, with farther away cues being less impacted by egocentric view and having more control over HD (Zugaro, Berthoz, and Wiener, 2001); 2) the memory of previous experiences of cue rotations (Ajabi, Keinath, Wei, and Brandon, 2021; Knierim, Kudrimoti, and Mcnaughton, 1995);and/or 3) the intrinsic time course of synaptic plasticity associated with the learning of the new landmark orientation (Goodridge, Dudchenko, Worboys, Golob, and Taube, 1998; Hahnloser, 2003; Kim, Hermundstad, Romani, Abbott, and Jayaraman, 2019; Kim, Rouault, Druckmann, and Jayaraman, 2017; Page, Walters, Knight, Piette, Jeffery, and Stringer, 2014; Skaggs, Knierim, Kudrimoti, and McNaughton, 1995; Yan, Burgess, and Bicanski, 2021).

Our anatomical and the functional connectivity experiments between ADn and RSC revealed a striking asymmetry between the strong feedforward ADn-to-RSC HD drive (Fig. 2.10 E-G) and the sparseness of RSC-to-ADn connections. This asymmetry was more extreme than that observed in previously reported ADn-POS connectivity (Peyrache, Lacroix, Petersen, and Buzsaki, 2015; van Groen and Wyss, 1990), but similar to anatomical tracing in the rat (Shibata, 1998), and possibly further exacerbated by the widespread sampling of RSC locations in our recordings (ie: granular vs dysgranular, L2-3 vs L5, Fig 2.1). Furthermore, the general bias toward similar tuning between connected ADn and RSC HD units suggests that ADn HD code might not be simply inherited in RSC, as it has been shown in POS (Peyrache *et al.*, 2015; Peyrache, Schieferstein and Buzsáki, 2017), but likely integrated with other spatial codes and with different circuit organizations, that include recruitment of FS and RS neurons (Simonnet, Nassar, Stella, Cohen, Mathon, Boccara, Miles, and Fricker, 2017).

How would the visual cue integration that anchors HD be reflected in the ensemble representation? We hypothesized that an "error" signal would appear as a temporal offset in the HD of the two regions: specifically, the RSC update, by integration of visual inputs, would precede that of other regions, in our case ADn. Contrary to this hypothesis, our decoding showed no temporal offset in HD representation during shifting (Fig. 2.6 E,F), and similar trajectory dynamics

to the final HD offset were observed in ADn and RSC. Importantly, this was true regardless of the imposed cue rotation and HD mismatch-induced devaluation of the anchoring effect of the cue (Fig. 2.6 C and Fig. 2.5). At the same time, even in the absence of visual cues, RSC and ADn were closely coordinated during small and large HD drifts. A potential mechanism supporting coordination in darkness may originate from the similar anticipatory time interval previously reported in the tuning curves of HD units in ADn and RSC during head rotations (Cho and Sharp, 2001; Lozano, Page, Jacob, Lomi, Street, and Jeffery, 2017), suggesting similar integration of AV signals. Movement related signals may indeed be important for HD coordination, as abnormal cerebellar function decreased the HD coordination in darkness between ADn and RSC, as long-scale spike correlation between ADn and RSC units recently showed (Fallahnezhad, Méro, Xhensjana, Vincent, Rochefort, and Rondi-Reig, 2021).

Together, our data provide direct evidence of HD coordination between ADn and RSC via simultaneous recording under two different visual challenges: cue rotations and darkness. This coordination is sustained by a strong and widespread feedforward ADn-to-RSC connectivity, where the updated HD reference, contrary to the initial hypothesis that it derived from corticothalamic connections, may already be computed upstream of ADn (Yoder, Peck, and Taube, 2015). This framework is consistent with the existing hypothesis that visual update may compete with and, depending on the manipulation, dynamically bias the memory of the internal estimation from angular velocity (Ajabi, Keinath, Wei, and Brandon, 2021).

The HD coordination and the striking sparseness of the RSC-to-ADn connectivity do not preclude, however, that RSC could support the change in reference through selected activity of orienting “landmark” (Bicanski and Burgess, 2016; Mitchell, Czajkowski, Zhang, Jeffery, and Nelson, 2018; Page and Jeffery, 2018) or conjunctive HD-visual coding cells, as previous RSC lesion studies suggested HD instability in ADn (Clark, Bassett, Wang, and Taube, 2010). The dense interconnection between RSC and several regions of the hippocampal formation (Sugar, Witter, van Strien, and Cappaert, 2011; Wyss and Van Groen, 1992) may support coordinated HD representation across the brain, a mechanism that may ensure consistent flexible spatial computations relevant to behavior output. Alternatively, POS, through its reciprocal connections with visual areas and the combined spatial and dominant HD coding, provides the direct HD update concurrently to ADn and RSC. Future experiments using multi-site high-density recordings with laminar probes in RSC should directly assess the activity patterns, at the single unit and population

level, associated with the learning of the new cue orientation. Under tight temporal control between cue rotation and the animal view and limited cue devaluation with repeated trials, these experiments could test the presence of orienting landmark-coding cells. Finally, with reversible inactivation of RSC, it will be possible to determine the role of RSC in visual cue integration.

Methods

Behavior and Subjects

All animal procedures were performed in accordance with NIH and Massachusetts Institute of Technology Committee on Animal care guidelines. We used adult (>8 weeks old) C57BL/6 from Charles River and from Jackson Laboratory RRID: IMSR_JAX:000664 and one Vgat-Ires-Cre C57 BL/6 mice (RRID:IMSR_RBRC10723), 4 females and 8 males, for tetrode recordings, and 2 12-week old mice for rabies tracing experiments. Mice were kept on a 12-hour light/dark cycle with unrestricted access to water. 8 of the implanted mice underwent mild (up to a 10% reduction in body weight) food restriction. Of the implanted mice, 8 were housed isolated in conventional cages, 4 with siblings in rat cages with running wheels. One mouse had channelrhodopsin expression in cortical interneurons, but this aspect was not investigated in the present study.

The behavioral arena was 50 cm in diameter with a 25 cm cylinder wall, surrounded by an outer cylinder of 80 cm diameter and 30 cm height, where a string of 132 white LEDs (Adafruit, APA102) covering the upper circumference provided the only light source. The arena was enclosed in a 78x86x84 cm wooden dark box to shield from lighting and noise. In food deprived mice, pellets (Bioserve) were sprinkled on the floor to allow continuous exploration during long recordings. To provide novelty in the environment and induce exploration, two types of arena walls (black pvc with a white paper at the upper edge and opaque clear plastic) were used and changed when the cue rotation did not produce shifts in the HD tuning.

The visual cue was a set of computer-controlled (teensy 3.2) LEDs spanning an angle of 20°with brightness following a gaussian with peak at the center and sd of 1. 2 weeks after surgery mice were habituated to a single cue or no cue at all while units were monitored. Different starting cue angular positions for the recording sessions were sampled and different sequences of rotations of ±90° and ±45°were played. For recordings with the Open-Ephys ONIX system (Newman, Voigts, Zhang, Kemere, Dakin, Manders, and Rosen, 2019) with the commutator, rotations and

cue on-off switches occurred every 20 to 40 minutes, vs the 5 to 20 minutes for recordings with the first generation Open-Ephys system (Siegle, López, Patel, Abramov, Ohayon, and Voigts, 2017) without commutator. Sessions length varied based on the animals' behavior, with a minimum of 2 up to 11 rotations/ on-off switches. Cue rotations occurred in consecutive "jumps" from one angular position to the next. In 3 mice, periods of darkness were interleaved in some rotation sessions.

Electrodes and Drive Implants Surgeries

Light weight drives for tetrode recordings were fabricated following the guidelines in (Voigts, Newman, Wilson, and Harnett, 2020) for a total of 16 independently-movable tetrodes per drive. Arrays were designed to simultaneously target ipsilateral ADn and RSC, for a total length of 2.8 mm and a width of 0.5 mm. To increase the yield of units especially for ADn, some guide tube positions were occupied by two tetrodes. Tetrodes were constructed from 12.7 μm nichrome wired (Sandvik – Kanthal, QH PAC polyimide coated) with an automated tetrode twisting machine (Newman, 2020) and were gold plated to lower the impedance to a final value between 150-300 Ohm. One mouse was implanted with 32 carbon fiber electrodes (~100 Ohm, (Guitchounts, Markowitz, Liberti, and Gardner, 2013) in ADn only, whose position was fixed since surgery.

All surgeries were performed using aseptic techniques. Mice were anesthetized with isoflurane (2% induction, 0.75%–1.25% maintenance in 1 l/min oxygen) and secured in a stereotaxic apparatus. Body temperature was maintained with a feedback-controlled heating pad (DC Temperature Control System, FHC). Slow-release buprenorphine (1 mg/kg) and dexamethasone (4mg/kg) were pre-operatively injected subcutaneously. After shaving of the scalp, application of hair-removal cream and disinfection with iodine and ethanol, an incision was made to expose the skull. For implants, after cleaning with ethanol, the skull was scored and a base of dental cement (C&B Metabond and Ivoclar Vivadent Tetric EvoFlow) was applied. A burr hole was drilled over prefrontal cortex close to the olfactory bulb for placement of the ground screw (stainless steel) connected to a silver wire. Sometimes an additional burr hole and ground screw, connected to the other with silver epoxy, provided extra stability. For drive implants with tetrode arrays, a large craniotomy from ~0.3 to ~ 3 mm from Bregma, and from the midline to ~0.95 mm ML at the level of M2 and ~ 0.7 mm ML at the level of RSC was drilled. After durotomy, the drive was lowered onto the surface of the brain with one RSC (AP ~ 2.400, ML ~0.150 mm, DV ~0.200

mm) and one ADn (AP ~0.350 mm, ML ~0.975 mm, DV ~1.800 mm) -targeting tetrodes extended for guiding the placement of the array. For the carbon fibers implant, a smaller (~ 1 mm diameter) craniotomy, followed by durotomy, allowed lowering of the bundle of fibers into ADn (AP: 0.68 mm, ML 0.75 mm, DV 2.65 mm). The drive, or the fiber frame, was then secured to the skull with dental cement, the skin incision was partially closed with sutures and the mouse was placed in a clean cage with wet food and a heating pad and monitored until fully recovered. All drive implants were done on the right hemisphere.

Viral Surgeries

The same stereotactic procedures were applied to viral surgeries. For ADn rabies tracing experiments, a burr hole was drilled over AP 0.68 mm, ML 0.75 mm coordinates and 25 nL of 1:1:1 mixture of helper viruses, pAAV-syn-FLEX-splitTVA-EGFP-tTA and pAAV-TREtight-mTagBFP2-B19G (Wickersham) and AAV2/1.hSyn.Cre (Janelia Farms) was delivered at a rate of 60nL/min through a glass pipette lowered to DV 2.65 mm. This injection was followed by 50 nL of (EnvA)SAD-ΔG-mCherry (Wickersham) two weeks later at the same location, and after 7 days the brains were processed for histology. For RSC rabies tracing experiments, the coordinates were AP 2.8 mm, ML 0.45 mm, DV 0.75 and 0.45 mm, and the injection of 50 nL of 1:1 mixture of AAV2/1.hSyn.Cre(Janelia Farms) and AAV1-hsyn-DIO-TVA66T-dTom-CVS-N2C(g) (Allen Institute) was followed 3 weeks later by a 100 nL of EnvA dG CVS-N2C Histone-eGFP (Allen Institute) before histological processing 9 days later. 5 minutes after each injection, the pipette was slowly withdrawn and the incision was sutured.

Immunohistochemistry and confocal imaging

Brain fixation with 4% paraformaldehyde in PBS was achieved with transcardial perfusion for monosynaptic rabies tracing experiments and with drop fix for electrolytic lesions retrieval from the drive-implanted mice. After being left overnight at 4°C, brains were sectioned coronally at 100 μm thickness with a floating section vibratome (Leica VT1000s), washed in PBS and then labeled with 1:1000 DAPI solution (62248; Thermo Fisher Scientific). All sections were mounted and coverslipped with clear-mount with tris buffer (17985-12; Electron Microscopy Sciences). Confocal images were captured using a Leica TCS SP8 microscope with a 10X objective (NA 0.40) and a Zeiss LSM 710 with a 10x objective (NA 0.45). ML and DV coordinates for cortical

tetrode rotations (Fig. 2.1) were measured in ImageJ/FIJI (National Institutes of Health) from the midline and the pia to the center of the lesions and aligned to 4 matching coronal slices from the Mouse Brain Atlas (Allen Institute) for AP axis reference.

Electrophysiology and Data Acquisition

Electrophysiology signals were acquired continuously at 30 kHz, while the behavioral tracking was acquired at 30 Hz with one or two lighthouse tracking stations (HTC Vive Base Station, Amazon). An additional camera (FFY-U3-16S2M-S, FLIR) was placed on the ceiling of the behavior box for behavior monitoring. 3 mice were recorded on a first generation Open-Ephys system (Siegle, López, Patel, Abramov, Ohayon, and Voigts, 2017) with an Intan 64 or Intan 32 (for the carbon fiber-implanted mouse) headstage. In these mice, tracking provided by two lighthouse receivers (TS4231, Digikey) attached at the base of the headstage, whose signal was recorded and powered through a teensy 3.6. The other 9 mice were recorded on a new-generation Open-Ephys ONIX (Newman, Voigts, Zhang, Kemere, Dakin, Manders, and Rosen, 2019) system with 64 channel headstages with a powered commutator, that integrated electrophysiology and behavior tracking using the Bonsai software (Lopes et al., 2015).

Spikes were sorted on 300-6000Hz band pass filtered continuous traces, using MountainSort (https://github.com/flatironinstitute/mountainsort, Chung *et al.*, 2017). Units were then manually selected based on the spike template shapes and interspike interval (ISI) distribution. After implant surgery, ADn-targeting tetrodes were lowered until HD-coding cells were identified based on their tuning obtained from brief recordings, and RSC targeting tetrodes were slowly lowered until well-isolated units appeared. When at least 3 HD cells in ADn were first detected, recordings of cue rotation or cue on-cue off sessions were collected over a minimum of 2 weeks and up to 8 months. Tetrodes in ADn and RSC were regularly moved by ~20-40 um increments, followed by recordings of short stable cue-on sessions to verify if the yield was improved. To avoid sampling of the same units for HD neurons quantifications and spike correlations for monosynaptic connections, sessions recorded at least 4 days apart and only one session for the carbon fiber-implanted mouse were included in these analyses. At the end of the experiments, electrolytic lesions were obtained by passing positive and negative current (20-25 uA) on each electrode contact for 5 s with a stimulus isolator (A365RC, WPI) while the animal

was under isofluorane-induced anesthesia. After 30-60 min of recovery, the brains were extracted for histology.

Data Analysis

HD units selection

HD was quantified as the relative orientation of two or three infrared lighthouse receivers present on the integrated headstage, after their (x,y) coordinates were linearly interpolated to align to the same 50Hz timestamps. For each session, HD tuning curves were quantified as the histogram of the spike trains over HD angles of 10-degree bins divided by the occupancy. For HD units selection and information metrics for other spatial correlates, data from a stable cue-on period was used. Information was calculated as bits/spike as

$$I = \frac{\sum_i^N \lambda(x_i) \times log_2\left(\frac{\lambda(x_i)}{\lambda}\right) \times p(x_i)}{\lambda}$$

following the methods of (Skaggs, McNaughton, Gothard, and Markus, 1993) where x is the binned HD (N=36 bins), p(x) is the occupancy, and λ is the mean firing rate and $\lambda(x_i)$ is the firing rate for each angular bin. Cells in ADn and RSC were selected as HD-coding if the amount of directional information was more than the 95th percentile of the shuffle distribution and the resultant of the smoothed tuning curve was more than the 90th percentile of the shuffle distribution. Shuffling of the spikes was obtained by shifting 500 times the spike trains by random amounts with respect to the HD from tracking. The peak number was obtained from matlab's "*findpeaks.m*", with a minimum peak distance of 1.2, width of 0.7 and prominence of 4. For units with more than one peak (Fig. 2.2) and with prominence more than 10, we applied Matlab's "*fitnlm.m*" with a basic von Mises model function with one peak

$$coeff_1 + coeff_2 \times \frac{1}{2pi * besseli(0, coeff_4)} \times e^{coeff_4} \times \cos(angles - coeff_3)$$

where *besseli* is the modified Bessel function of the first kind, *angles* is the range of possible angles between 0 and *2pi* in 3600 bins, and the subscripted coefficients correspond to: 1 a baseline constant offset, 2 a scaling factor for the peak height, 3 the peak location, 4 the concentration parameter in the Von Mises probability distribution. For instances were up to 3 peaks were identified, the model function was expanded with a linear sum combining additional sets of height,

location and concentration coefficients. Starting values for coefficients estimation were obtained from the *findpeaks.m* and 0 for the constant offset. The aim of this strategy was to identify a von Mises distribution anchored to the largest peak in tuning curves, whose resultant would have otherwise been much lower despite a strong directional information (Fig. 2.3 E 3rd example from top, and Fig. 2.2 A-C,H).

Decoding HD

We decoded HD using a linear-Gaussian GLM based on the 20 ms-binned firing rates of ADn and RSC neurons, separately (Fig. 2.4 A). A Butterworth filter with cutoff normalized frequency of 0.2 was applied to the firing rates, which were then normalized. Maximum a posteriori (MAP) estimation coefficients of the neuronal ensembles (the predictors) via ridge regression regularization was applied on the sine and cosine of HD, binned in 10° bins. The segments for the training were taken from a cue-on period at least 50 s away from rotation. Decoding was performed using matlab's "*glmval.m*" with the corresponding identity link function and HD reconstructed as the $\tan^{-1}(\frac{\sin HD}{\cos HD})$ from the decoded bins. With this strategy, we obtained the HD representation, which was linked to the neuronal ensembles via the learned coefficients during training, in a test period following the training session and in the period after cue rotation. For testing drift in dark and light, shorter training sessions during a stable cue on (up to 8 min of data) were used and evaluated on the subsequent cue-on period and after the cue was turned off.

Detection of mono-synaptic connections

We performed spike cross-correlation between all unique possible pairs of simultaneously recorded ADn-RSC neurons to detect putative monosynaptic connections. Excitatory connections appear as peaks in the cross-correlogram in the short time scale (1-5 ms) above baseline (Fujisawa, Amarasingham, Harrison, and Buzsáki, 2008; Stark and Abeles, 2009). We focused on excitatory connectivity since corticothalamic and thalamocortical projections are excitatory and negative deviations from the baseline are often resulting from large positive deviations in the other direction. Cross correlograms were constructed in bins of 0.5 ms by taking all spikes occurring during cue-on trials in a session (or only during cue-off trials). The baseline correlation, simulating homogeneous firing, was constructed by convolving the cross correlogram with a 10 ms s.d. Gaussian window. Significant connections were detected if at least 2 consecutive bins in the 1 to

5 ms window of the cross correlogram were above the 99.9th percentile of the cumulative Poisson distribution at the baseline rate.

Timing of the decoded rotations

To investigate the dynamics of the decoded HD shift in response to cue rotations, we calculated the time it took between the putative entry of the new cue in the mouse visual field (within ±154° from the snout) and the stabilization of the target ADn decoded HD error, namely the circular mean error between 100 and 400 s after vision of the new cue. With a sliding window of 10 s from the new cue vision, the HD shifting was considered completed when the circular variance, normalized by that observed in the previous cue-on period, and the difference between the target offset and the circular mean decoded error were respectively less than 2 and less than 0.1 for least 100 consecutive bins (2 s) (See Fig. 2.7 A for examples). In addition, we quantified the rotation trajectory as the sum of the absolute distances between consecutive points of the unwrapped decoded error after rotation, smoothed over a 5 s window, as an indicator of how continuous the HD shifts were. We limited this analysis to ADn rotations as the decoding accuracy was significantly higher than in RSC (Fig. 2.4 B-D).

Interneurons and Pyramidal neurons separation

Fast spiking (FS) interneurons and regular spiking (RS, pyramidal) neurons have distinct features that appear on the extracellular spike waveforms and can be used for classification (Barthó, Hirase, Monconduit, Zugaro, Harris, and Buzsáki, 2004; Wilson and McNaughton, 1993). We applied the metrics described in (Sirota, Montgomery, Fujisawa, Isomura, Zugaro, and Buzsáki, 2008) on spike waveforms identified from the bandpass filtered continuous traces. Briefly, a mean spike waveform was obtained for each cortical neuron and the peak-to-trough was quantified as the time between the peak of the spike and the maximum point in the afterhyperpolarization, whereas the symmetry around the spike was calculated as the difference between the height at the maximum point after spike peak (B) and the maximum point before spike peak (A), divided by the sum of these two quantities. While in our dataset the symmetry value was unimodally distributed, the peak-to-trough was clearly bimodally distributed, allowing to cluster FS and RS with a previously reported (Peyrache, Lacroix, Petersen, and Buzsaki, 2015) cutoff duration of 0.42 ms, which

resulted in average spike waveforms with a slow repolarization decay for RS and faster repolarization in FS (Fig. 2.11).

Quantifications and Statistical Analysis

All statistical analyses were performed in Matlab (MathWorks, R2020a). All spiking and behavioral data, with exception of the spike times for the detection of monosynaptic connections, was binned in 20 ms bins. Behavioral tracking from the light receivers was linearly interpolated. Circular Statistic Toolbox (Berens, 2009) functions were employed for quantifications of HD units' PFDs as circular means, as well as population mean rotations, variance, confidence interval, and circular correlations between decoded errors, phase-offsets between HD cell pairs, and rotations between regions. Correlation between the size and time of rotation and between the absolute egocentric bearing of the cue and the size of the rotation were calculated as Pearson correlations coefficient. Information for spatial correlates was calculated as bits/spike (Skaggs et al 1993) from periods with speed larger than 1.2 cm/s, except for the movement-related variables where all indices were taken, and compared across regions and HD-coding groups with Kruskal Wallis test, followed by Bonferroni-corrected multiple comparisons. Two-tailed Kolmogorov Smirnov tests were used to compare the distribution of the time lags of peak correlation between ADn and RSC decoded errors vs the null distribution obtained from 100 shuffles, and Wilcoxon Signed-Rank tests to compare the peak correlation values before and after cue rotation. Shuffle distributions for the decoded errors (both for dark and cue-rotation drifts) were obtained by shifting the tracked HD by random amounts. Significant ensemble PFDs rotations were determined if at least half of the HD cells experienced PFDs shifts larger than the 98^{th} percentile of a distribution obtained by randomly reassigning 500 times the indices from that trial. Unless otherwise stated, summary data was presented as mean and 95% confidence intervals and P-values threshold of 0.05 were used for statistical non-parametric tests.

Chapter 3 : Anterodorsal Nucleus of Thalamus lacks excitatory recurrence and local inhibition

Introduction

In recent years, work on the structure and function of the thalamus has shown that it is more than a relay station of information to cortex. Anatomical, electrophysiological and behavioral characterizations of thalamic nuclei have hinted at the complexity of this region and reassessed the role it plays in cortical function and cognition (Halassa and Kastner, 2017; Halassa and Sherman, 2019; Rikhye, Wimmer, and Halassa, 2018; Shepherd and Yamawaki, 2021; Sherman, 2016; Sherman and Guillery, 1996). Distinct cellular and synaptic properties, but also the intra-thalamic and long-range circuit architecture, defined classical sensory thalamic nuclei into first and higher order. The first order nuclei have strong feedforward and reduced feedback connectivity with cortex, largely topographical organization of the thalamocortical connections. Diverse thalamocortical loops form circuit motifs involving inhibition from Thalamic Reticular Nucleus (TRN) (Shepherd and Yamawaki, 2021). TRN has been shown to play an important role in shaping thalamic responses in an activity-dependent manner (Crandall, Cruikshank, and Connors, 2015) and during behavioral tasks (Wimmer, Schmitt, Davidson, Nakajima, Deisseroth, and Halassa, 2015), in addition to regulating arousal and sleep waves (Lewis, Voigts, Flores, Ian Schmitt, Wilson, Halassa, and Brown, 2015).

Recently thalamic nuclei outside of classical sensory systems have received more attention, in particular the role of Mediodorsal Thalamus and nuclei of the anterior group, of which ADn is part. They make connections with associative cortices and have been shown to be involved in cognitive functions, including flexible use and context-depend switch of task rules (Rikhye, Gilra, and Halassa, 2018; Schmitt, Wimmer, Nakajima, Happ, Mofakham, and Halassa, 2017; Wolff and Vann, 2018). ADn receives HD and angular velocity (AV) input from LMN and DTN, the HD generative circuitry integrating optic flow, motor, oculomotor and vestibular "sensory" signals (Angelaki and Laurens, 2020; Peyrache, Duszkiewicz, Viejo, and Angeles-Duran, 2019). Evidence

from slice electrophysiology of the all-or-none nature of mamillothalamic synapses and the graded facilitating nature of descending cortical afferents recapitulate the driver and modulator role of these two excitatory inputs, respectively (Petrof and Sherman, 2009). Despite HD not being strictly a sensory signal, these features make ADn comparable to other first order thalamic nuclei, such as the lateral geniculate nucleus. There are, however, some differences from canonical sensory thalamic nuclei: one is the low level of burstiness observed even during NREM sleep (Viejo and Peyrache, 2020), the other is the organization of cortical synaptic targeting. In fact, ADn axons target the L1 and 3 in both POS (Nassar, Simonnet, Huang, Mathon, Cohen, Bendels, Beraneck, Miles, and Fricker, 2018; Simonnet and Fricker, 2018) and granular RSC (Brennan, Jedrasiak-Cape, Kailasa, Rice, Sudhakar, and Ahmed, 2021) vs the traditional L4 of the extensively characterized visual, auditory and somatosensory thalamus.

The persistent activity of ADn HD neurons in the absence of movement or of external sensory input (Peyrache, Lacroix, Petersen, and Buzsaki, 2015) has posited the idea that recurrent excitatory connections might support this feature (Knierim and Zhang, 2012; Skaggs, Knierim, Kudrimoti, and McNaughton, 1995; Zhang, 1996). Recent studies in the fly central complex compass neurons concluded that ring architectures with local recurrent excitation and global inhibition best modeled the experimental observations (Kim, Rouault, Druckmann, and Jayaraman, 2017). Given the similarities in tuning properties of compass (EP-G) and AV (P-EN) neurons and in the dynamics of the activity packet shifts in response to head movement (Green, Adachi, Shah, Hirokawa, Magani, and Maimon, 2017) between the fly and the rodent HD system, it is possible that similar circuit architectures exist. However alternative computational models without recurrent excitatory connectivity have been proposed (Boucheny, Brunel, and Arleo, 2005; Song and Wang, 2005), to reflect the general notion that no direct excitatory connections have been reported within thalamus (Jones, 2007) or in LMN (Allen and Hopkins, 1988). There is however no evidence that ADn follows the same local connectivity as other thalamic nuclei. Moreover, whether the inhibitory input to ADn neurons, included in all model of HD, originates exclusively from TRN is not yet resolved. We therefore tested whether the ADn local circuit contains features reminiscent of these attractor network models.

Results

Thalamic Reticular Nucleus provides inhibition to ADn

To test that no *Gaba*-ergic neurons were present in the mouse ADn, we performed immunohistochemical staining for the Gaba-producing enzymes Gad67 and Gad65. From coronal slices containing ADn, we could find evidence of somatic localization of amplified Gad67 immunoreactivity only in TRN (Fig. 3.1 A,C). ADn did no show any somatic localization of Gad 67 Fig.3.1 B) or Gad65 (Fig.3.1 D), excluding the possibility that inhibitory neurons were part of ADn local connectivity. However dense bouton-like fluorescence was detected in ADn for both Gad67 and Gad65 staining, consistent with enzymatic activity at axon terminals, suggesting that ADn neurons receive dense inhibition. In line with previous and recent findings about the source of inhibition to ADn, monosynaptic rabies tracing in ADn revealed labeling of presynaptic partners in Dorsal Anterior TRN, with axon bundles leaving TRN across AVn (Fig. 3.1 E).

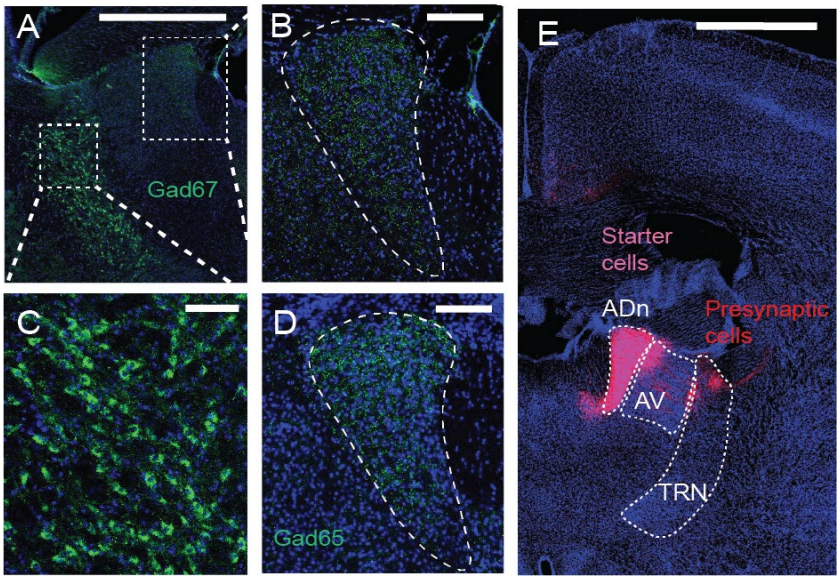

Figure 3.1 Thalamic Reticular Nucleus provides inhibition to ADn.

A: Coronal slice containing TRN and ADn stained for Gad67 (green) and Dapi (blue), scale bar 1 mm. **B,** Zoomed-in square from A showing ADn (outlined) with axon terminals stained for Gad67, but no cellular fill, 200 µm. **C,** Zoomed-in square from A showing a portion of TRN with cytosolic staining for Gad67, 100 µm. **D,** Axon terminal staining for Gad65 from another experiment, from a coronal slice containing ADn, scale bar 200 µm. **E,** Coronal slice from a monosynaptic rabies tracing experiment in ADn showing starter cells in ADn (co-localization of red, green and blue), fiber tracts in red leaving ADn and presynaptic cells in dorsal TRN, with more fiber tracts leaving the internal capsule, scale bar 1 mm.

Absence of recurrent connectivity in ADn

To detect if possible connections between ADn neurons were present, we performed a channelrhodopsin-assisted-circuit-mapping experiment (cracm) for local connections. We sparsely injected AAV1-ChR2-eYFP (or -mCherry) into adult mouse ADn, and after 3-4 weeks of expression we performed whole cell patch clamp experiments on coronal slices containing ADn in combination with widefield LED stimulation with blue 473 nm wavelength (Fig. 3.2 A). ChR2-eYFP positive cells were easily identified by the membrane-bound expression of eYFP observed under the 2-photon microscope (Fig. 3.2 B left). Brief wide field stimulation of these cells readily evoked action potentials, confirming the expected effect of fast depolarization by Chr2- channel opening (Fig.3.2 B right). We hypothesized that if recurrent excitatory connections existed between ADn neurons, light excitation of the axon collaterals would induce short latency excitatory post-synaptic potentials (EPSPs) in ChR2-eYFP negative cells (Fig. 3.2 C, left). When we patched these neurons, however we never observed EPSPs (Fig. 3.2 C, right), under different stimulation regimes, from short, 1 ms to 500 ms-long pulses, or 10 Hz pulses of 2 ms width (out of 31 cells, from 5 injected mice). The average voltage difference between the peak during the light stimulation and the baseline was close to 0 and significantly lower than three standard deviations away from the mean of the baseline voltage distribution (Fig. 3.2 D, left) (n=17 cells tested under 100 and 50 ms long pulses, $p<0.001$ Mann-Whitney test between stimulation and baseline). These experiments were performed in standard ACSF. To exclude the possibility that some TRN-mediated inhibition could still be intact in our coronal slices, for a subset of these cells we also perfused picrotoxin (PTX, 100 μmol) and repeated the stimulation procedure. This strategy did not reveal any evoked EPSP. However, while the mean voltage difference was similar to that under standard ACSF, the change from baseline was not significantly different from our predicted effect from baseline (n=7, $p>0.05$) (Fig. 3.2 D, right). We concluded that ADn neurons do not form recurrent connections, consistently with other sensory thalamic nuclei architecture (Jones, 2007).

Discussion

Canonical features of thalamic circuitry based on findings in sensory thalamic nuclei seemed in contrast with the original attractor network models proposed for HD coding, namely the presence

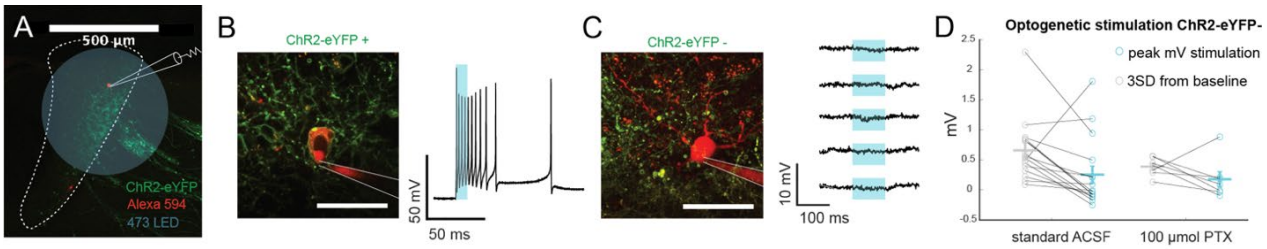

Figure 3.2 Absence of recurrent connectivity in ADn.

A: Set-up for testing recurrent connections between ADn neurons using optogenetic stimulation: a wide field 473 LED pulse during whole cell patch clamp electrophysiology. Confocal image of a coronal slice containing ADn (white outline) sparsely infected with ChR2-eYFP (green) obtained after immunohistochemical enhancement of the eYFP-infected neurons and axons collaterals. 2 cells were filled with 0.15% Biocytin during the CRACM experiment and subsequently immunolabeled with Streptavidin conjugated with Alexa-594. **B,** Left, 2-photon image at 60x of an ADn cell filled with Alexa 594 via a patch pipette. The yellow colocalization on the cell membrane indicates expression of ChR2-eYFP, similarly to the surrounding cells. Scale bar 100 µm. Right, example burst of action potentials triggered by a 10 ms wide-field 473 LED pulse. **C,** Left, same as in B, but for a cell that does not express ChR2-eYFP. Right, voltage traces in response to 100 ms continuous showing no evoked EPSP locked to the stimulus. **D,** Quantification of the responses to optogenetic stimulation in ChR2-eYFP negative cells. Grey, individual and mean of 3 times the SD of the baseline voltage distribution prior to stimulation; cyan, baseline-subtracted peak voltage response during 50-100 ms stimulation. Left, standard ACSF, n=17 cells, from 5 mice, Wilcoxon Signed-rank test $p<0.05$; right, 100 µmol PTX, n= 7 cells from 3 mice, Wilcoxon Signed-Rank test $p<0.1$).

of locally restricted recurrent connections, necessary for maintaining the persistent firing for encoding the current orientation, while maintaining the activity localized. The experiments outlined here show that indeed in ADn there are no recurrent excitatory connections that could be identified through rapid recruitment of action potential firing in neighboring cells with optogenetic stimulation. Moreover, ADn does not contain any local interneurons, but is densely innervated by TRN, the canonical source of thalamic inhibition. These two findings are consistent with attractor network models that include only external excitatory inputs and reciprocal inhibition.

However, these models were designed to make predictions on the generative circuitry of HD, with specific vestibular and AV inputs to the DTN (Boucheny, Brunel, and Arleo, 2005; Song and Wang, 2005). Given that AV does not have a processing stream through thalamus like vision and hearing, but it is rather distributed and integrated with proprioceptive, HD and motor signals

(Wijesinghe, Protti, and Camp, 2015), it is unclear how similar networks can be implemented for different HD processing nodes throughout the brain. DTN is a crucial component of the HD signal throughout the brain (Bassett, Tullman and Taube, 2007) as it receives vestibular input and encodes AV (Sharp, Tinkelman and Cho, 2001). In contrast, brief suppression of anterodorsal TRN increases the gain of ADn firing (Duszkiewicz, Carrasco, Orhan, Brown, Owczarek, Vite, Wood, and Peyrache, 2022) and long term suppression through the DREADD/CNO approach also widens HD tuning curves (Vantomme, Rovó, Cardis, Béard, Katsioudi, Guadagno, Perrenoud, Fernandez, and Lüthi, 2020), suggesting that TRN provides widespread inhibition, without affecting the HD tuning. It is not known yet whether anterodorsal TRN, as a result of its reciprocal connections with ADn and the input from descending cortical regions in the HD circuitry, is HD tuned. Answering this first question through targeted in vivo electrophysiology, with high density silicon or neuropixel probes in TRN, would help generate testable hypotheses about the wiring pattern between ADn-TRN-POS connectivity.

Recent evidence has pointed to a role of inhibition in modulating ADn network gain during fast or long-range HD shifts in response to cue rotations (Ajabi, Keinath, Wei, and Brandon, 2021). Stimulation of RSC/POS subcortical afferents also readily recruit TRN-mediated inhibition of HD units (Vantomme, Osorio-Forero, Lüthi, and Fernandez, 2019). Exactly what synaptic mechanisms regulate the HD reference shift, both in terms of size and timescale, in the mammalian is unknown. It is possible that multiple mechanisms can be engaged depending on the behavioral conditions and the competing signals in place, such as the size of the mismatch between the internal HD and the new orientation bearing of the cue. Future studies should address what connectivity map and potential inhibitory plasticity mechanisms regulate HD tuning in ADn. These could be achieved by employing patch clamp electrophysiology, granted that axon fibers between ADn and TRN are preserved in coronal slices, and single cell anatomical tracing of the ADn-TRN wiring diagram. Altogether, these results could provide tremendous insights into the connectivity architecture and the role of TRN plays in the HD circuitry.

Methods

Experimental Models and Subject Details

All animal procedures were carried out in accordance with NIH and Massachusetts Institute of Technology Committee on Animal care guidelines. C57BL/6 male and female mice were used in approximately equal numbers. 5 adult mice (between 8 and 12 weeks of age) were used for the electrophysiology experiments. 2 12-week old mice were used for rabies tracing experiments and 5 12-week old mice were used for the GAD staining experiments. Mice were kept on a 12-hour light/dark cycle in conventional housing and had unrestricted access to food and water.

Stereotactic Surgeries

All viral surgeries were performed using the same aseptic techniques described in the methods section in Chapter 2. The same ADn rabies tracing experiment shown in Fig. 2.4 was used for the identification of presynaptic cells in TRN. Briefly, after the mice were anesthetized with 2% isofluorane, the eyes were protected with ointment, the scalp was shaved and hair was wiped after hair removal. After disinfection of the skin and exposure of the skull, a burr hole was drilled to target viral injections at the same ADn coordinates, AP 0.68 mm, ML 0.75 mm. 25 nL of 1:1:1 mixture of helper viruses, pAAV-syn-FLEX-splitTVA-EGFP-tTA and pAAV-TREtight-mTagBFP2-B19G (Wickersham) was delivered at a rate of 60nL/min through a glass pipette lowered to DV 2.65 mm. This injection was followed by 50 nL of (EnvA)SAD-ΔG-mCherry (Wickersham) two weeks later at the same location, and after 7 days the brains were processed for histology. For sparse ChR2-experiments bilateral injections of 25 nL of AAV2-hSyn-hChR2(H134R)-mCherry or - eYFP (UNC Vector Core, 5.7 e11 particles per mL, diluted in water) were targeted at ADn (AP: 0.85; ML: +/- 0.75; DV: 2.65). Virus was allowed to express for 3 weeks before the start of slice electrophysiology experiments.

Immunohistochemistry and confocal imaging

For monosynaptic rabies tracing experiments, brains of injected mice were fixed by transcardial perfusion with 4% paraformaldehyde in PBS and left overnight at 4°C. Brains were sectioned coronally at 100 μm thickness with a floating section vibratome (Leica VT1000s). Sections from rabies tracing experiments were rinsed in PBS and then immunolabeled with 1:1000 DAPI solution

(62248; Thermo Fisher Scientific). A similar procedure was followed for GAD-65 and GAD-67 staining experiments, however, after fixation, sections were rinsed in PBS, blocked in 5% normal goat serum in PBS for 1 hour at RT, and immunolabeled with 1:1000 mouse anti-GAD67 (MAB5406; Millipore Sigma) or rabbit anti-GAD-65/67 (AB1511;Millipore Sigma) overnight at 4°C. Sections were rinsed 3 times for 10 minutes with PBS, incubated in 1:500 Alexa Fluor 488 secondary antibodies, Alexa 488 conjugated goat anti-rabbit (AB_143165; Thermo Fisher Scientific) or goat-anti-mouse (AB_2536161; Thermo Fisher Scientific) in 5% goat serum in PBS for 3 hours at RT, rinsed and finally labeled with 1:1000 DAPI solution for 5 minutes.

For verification of ADn injection sites spread in the sparse channelrhodopsin injections, slices from optogenetics experiments were fixed in 4% paraformaldehyde and left overnight at 4°C. After 3 10 minutes PBS washes, sections were first blocked in 2% normal goat serum and 0.4% Triton x-100 for 1 hour, and subsequently immunolabeled with chicken anti-GFP (89138426, Fisher Scientific) or rabbit anti-RFP (632475; Takara), respectively, for ChR2-eYFP and ChR2-mCherry injections and left at 4°C overnight. After a second round of 0.4% Triton x-100 in PBS (PBST) washing (3 times, 10 minutes each), sections were incubated with secondary antibodies (respectively, Alexa 488 goat anti-chicken, Thermo Fisher A11039, and Alexa 568 goat anti-rabbit A11036 Thermo Fisher) for 3 hours. Biocytin staining with streptavidin with alexa-568 (Thermo Fisher, S11226) or alexa-488 (Thermo Fisher, S32354) conjugated, in opposition to the secondary staining of the ChR2-fibers, Finally, after 3X 10 minutes PBST washes, they were immunolabeled with 1:1000 DAPI solution for 5 minutes. All sections were mounted and coverslipped with clear-mount with tris buffer (17985-12; Electron Microscopy Sciences). Confocal images were captured using a Leica TCS SP8 microscope with a 10X objective (NA 0.40) and a Zeiss LSM 710 with a 10x objective (NA 0.45).

Acute slice preparation

Coronal brain slices (300 μm) containing ADn were prepared from 11-12-week-old injected C57/BL6 mice. Animals were deeply anesthetized with isoflurane prior to cardiac perfusion with cold slicing solution. Brain slices were obtained with a vibratome (Leica VT1200s) in ice-cold solution containing (in mM): sucrose 90, NaCl 60, $NaHCO_3$ 26.5, KCl 2.75, NaH_2PO_4 1.25, $CaCl_2$ 1.1, $MgCl_2$ 5, glucose 9, sodium pyruvate 3, and ascorbic acid 1, saturated with 95% O_2 and 5% CO_2. Slices were then incubated in artificial cerebrospinal fluid (aCSF) containing (in mM): NaCl

120, KCl 3, $NaHCO_3$ 25, NaH_2PO_4 1.25, $CaCl_2$ 1.2, $MgCl_2$ 1.2, glucose 11, sodium pyruvate 3, and ascorbic acid 1, saturated with 95% O_2 and 5% CO_2 at 35.5 °C for 45 min and then stored at 18 °C. All recordings were performed at 33–37 °C in aCSF.

Electrophysiological recordings and optogenetics stimulation

Cells were visualized through an Olympus BX-61 microscope with infrared Dodt optics and a water-immersion lens (60X, 0.9 NA; Olympus). Current-clamp recordings were performed in bridge mode with a Dagan BVC-700 amplifier with bridge fully balanced. After break-in, the recording chamber was illuminated with a full-field 473 nm LED (ThorLabs) with a 10 ms pulse to determine if the cell was connected or expressed ChR2, in which case it readily fired bursts of action potentials. Continuous or 10 Hz LED pulses of 10 to 500 ms were used to trigger responses in ChR2 eYFP-negative cells. In a subset of recordings, 100 μmol of PTX was washed over the slices. Current and voltage signals were filtered at 10 kHz and digitized at 20 kHz. Patch pipettes were made from thin-wall glass (1.5 O.D., 1.1 I.D.), with resistances ranging from 3 to 6 MΩ. The capacitance was fully neutralized prior to break in. The standard intracellular solution contained (in mM): potassium gluconate 134, KCl 6, HEPES buffer 10, NaCl 4, Mg_2ATP 4, NaGTP 3, and phosphocreatine di (tris) 14. Biocytin (1%) (Invitrogen, B1582) and, depending on the experiment, 0.05 Alexa 594 or 0.1 Alexa 488, were added to the internal solution. Liquid junction potential was not corrected for.

Chapter 4 : Long-Range Thalamic and Cortico-Cortical Connectivity to Retrosplenial Cortex[2]

Introduction

RSC is an associative cortical area playing a fundamental role in spatial cognition. It is densely interconnected with cortical and subcortical regions (Sugar, Witter, van Strien, and Cappaert, 2011; Van Groen and Wyss, 2003; Wyss and Van Groen, 1992) and displays a variety of visuo-spatial but also contextual and task-related receptive fields. Lesions to RSC have distinct consequences on spatial tasks, with the majority pointing to an inability to form or use spatial cognitive maps to guide navigation (Maguire, 2001; Vann, Aggleton, and Maguire, 2009). Several studies on cognitive tasks with high-density recordings in associative areas have suggested that neuronal mixed selectivity and nonlinear neuronal encoding enables diverse task representations at the ensemble level, which can be easily decoded by linear classifiers and conveyed for downstream processing (Fusi, Miller, and Rigotti, 2016; Mante, Sussillo, Shenoy, and Newsome, 2013; Rigotti, Barak, Warden, Wang, Daw, Miller, and Fusi, 2013; Rigotti, Rubin, Wang, and Fusi, 2010). Such high dimensional neuronal representations could serve as a potential mechanism for solving navigational tasks in RSC, for example by tying egocentric and allocentric frames to the same spatial map and giving rise to landmark code (Auger, Mullally, and Maguire, 2012; Fischer, Soto-Albors, Buck, and Harnett, 2019).

The presence of multiple converging sources of inputs may give rise to the characteristic mixed selectivity in single neurons, but it is still unknown whether synaptic contacts from different input streams are mixed and scattered across the dendritic arbor or not. Constrained L1 targeting in RSCg (or A29) has been shown to be a powerful strategy to shape neuronal activity either via

[2] Partially adapted from "Differential dendritic integration of long-range inputs in association cortex via subcellular changes in synaptic AMPA-to-NMDA receptor ratio", (Neuron, 2022) authored by Mathieu Lafourcade, **Marie-Sophie H. van der Goes**, Dimitra Vardalaki, Norma J. Brown, Jakob Voigts, Dae Hee Yun,Minyoung E. Kim, Taeyun Ku, and Mark T. Harnett (Lafourcade, Van Der Goes, Vardalaki, Brown, Voigts, Yun, Kim, Ku, and Harnett, 2022)

distinct inputs with opposing effects on L5 pyramidal neuron and behavioral output (Yamawaki, Li, Lambot, Ren, Radulovic, and Shepherd, 2019) or by differential post-synaptic cell-type recruitment with profound effects on tuning (Brennan, Jedrasiak-Cape, Kailasa, Rice, Sudhakar, and Ahmed, 2021). Moreover, inputs with similar tuning properties seem clustered on dendritic branches of individual neurons in sensory cortices (Iacaruso, Gasler, and Hofer, 2017; Ju, Li, Liu, Jiang, Macknik, Martinez-Conde, and Tang, 2020; Scholl, Wilson, and Fitzpatrick, 2017), but it is not known to what extent this is the case for associative cortices.

Studies on single neurons in RSC have showed how very different types of information, such as movement, which can be classified as a self-centered signal, as well as location within an environment, or world-centered signal, can be combined to shape their responses (Alexander and Nitz, 2015). HD information, crucial for determining self-location and forming spatial maps, is also found in RSC in conjunction with other signals. Specifically, a study found that while most allocentric HD was encoded in the granular portion of RSC, HD bound to a local environmental set of features was discovered in the dorsal, dysgranular portion of RSC (RSCd, or A30) (Jacob, Casali, Spieser, Page, Overington, and Jeffery, 2017; Zhang, Grieves, and Jeffery, 2021). This type of conjunctive encoding was theorized to play a fundamental role in the formation of visual landmarks in RSC (Page and Jeffery, 2018). Furthermore, this model required connections from diverse input sources signaling different kinds of information, making RSCd an attractive model region for testing the organization of inputs at the single neuron level.

Using monosynaptic rabies tracing to identify different input structures converging onto thick-tufted L5 pyramidal neurons in RSCd and Subcellular Channelrhodopsin Circuit Mapping (SCRACM) (Petreanu, Mao, Sternson, and Svoboda, 2009), we found evidence of spatial organization of synaptic inputs onto different dendritic domains. We conclude that this connectivity logic, in combination with domain-specific integration rules and different input pattern statistics, provides a potential substrate for mixed selectivity through input-specific decoding schemas.

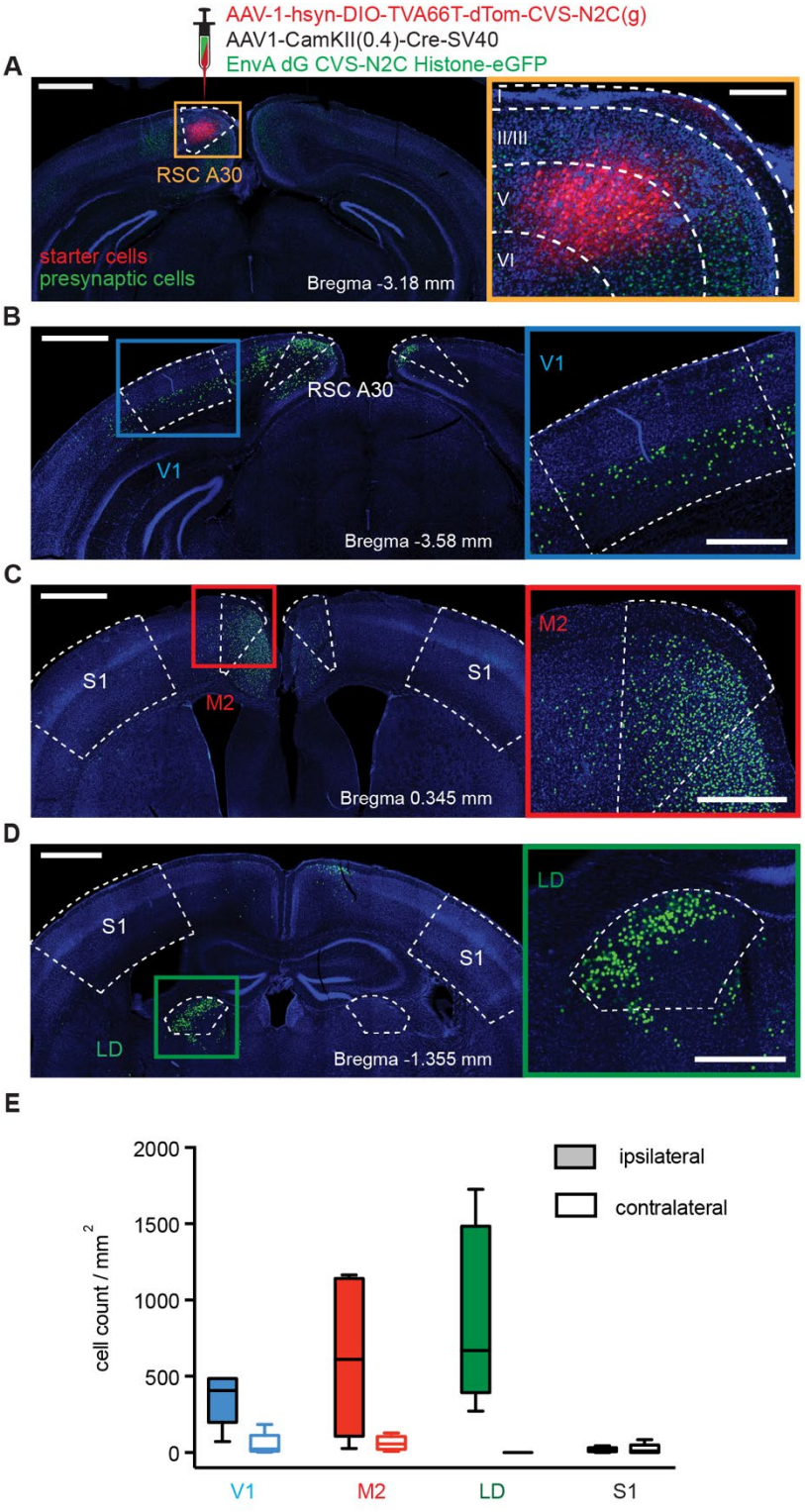

Figure 4.1 RSC layer 5 cells receive monosynaptic input from V1, M2, and LD

(A) Unilateral injection of monosynaptic rabiesbased retrograde tracing viruses in RSC A30. Left, confocal image of a coronal brain slice at the injection site, starter cells are labeled with tdTomato (red) and presynaptic cells with eGFP (green). Scale bar, 0.5 mm. Right: magnified orange square from left overlaid with cortical layer boundaries (adapted from Allen Brain Atlas) showing starter cell infection localized to layer 5. Scale bars, 200 mm. **(B–D)** Presynaptic cells were found in the deep layers of V1, all layers of M2, and LD, respectively. Left images scale bars, 1.0 mm. Right insets: magnified area of interest from right, scale bars, 0.5 mm. **(E)** Quantification of presynaptic cells (normalized by area) for V1, M2, LD, and S1 for both ipsi- (filled bars) and contra-lateral (empty bars) hemispheres (median ipsilateral S1: 14.06, V1: 406.5, M2: 612.0, LD: 669.9; $p < 0.05$ for ipsilateral S1 versus V1, M2, and LD; Mann-Whitney, n = 5 mice). Whisker plots include the medians (center lines), the first interquartile range (boxes), and the ± 1.5 X interquartile range (whiskers). Values out of the 99.3% coverage (outliers) have been excluded.

Results

The emergence of diverse visuo-spatial receptive fields associated with vision, self-motion, and HD (Alexander, Carstensen, Hinman, Raudies, Chapman, and Hasselmo, 2020; Alexander and Nitz, 2015; Cho and Sharp, 2001; Fischer, Soto-Albors, Buck, and Harnett, 2019; Jacob, Casali, Spieser, Page, Overington, and Jeffery, 2017) suggests that RSC A30 receives inputs from visual and motor cortices as well as thalamic areas (Shibata, 1993; Sugar, Witter, van Strien, and Cappaert, 2011; Van Groen and Wyss, 2003; Wyss and van Groen, 1992). To identify areas that provide direct inputs to RSC A30 in mice, we performed monosynaptic rabies tracing (Wickersham and Sullivan, 2015) in C57/BL6 mice (Fig. 4.1). Our data shows substantial long-range inputs to A30 from ipsilateral primary visual cortex (V1), secondary motor cortex (M2), and lateral dorsal thalamus (LD), consistent with classical anatomical studies in rats showing that RSC A30 receives direct inputs from multiple discrete cortical and subcortical regions (Shibata, 1993; Sugar, Witter, van Strien, and Cappaert, 2011; Van Groen and Wyss, 2003). As a control, we

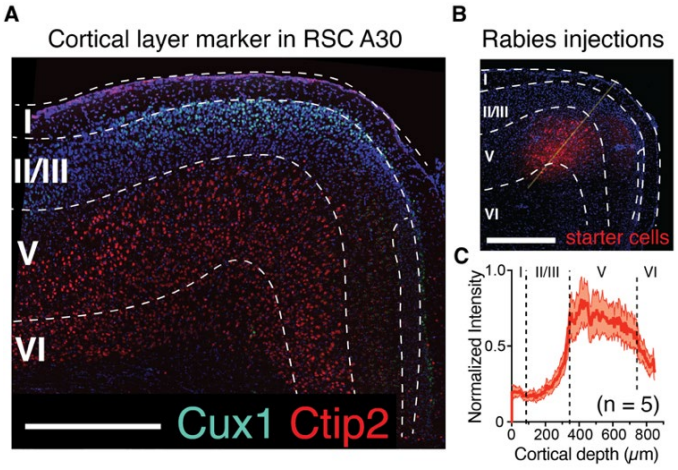

Figure 4.2 Rabies injections target RSC A30 L5.

A, Superposition of Allen Atlas cortical layers outline with an immunostaining image for Cux1 (layer 2 marker, green) and Ctip2 (layer 5/6 marker, red) with cell bodies stained with DAPI (blue). Scale bar 500 μm. **B**, Example of starter cells localization in RSCA30 (different example than in Fig. 1A) with layer outlines. Yellow line represents line intensity profile. Scale bar: 500 μm. **C**, Normalized averaged red fluorescence intensity profile for 5 mice used for monosynaptic rabies experiments. Line and shaded areas are mean±sem.

observed little to no input from a region previously shown not to project to RSC: primary somatosensory cortex ($p<0.05$ for S1 versus V1, M2, & LD; Mann Whitney, n=5 mice, all ipsilateral comparisons). While we did observe other inputs to A30 including A29 RSC (the medial, granular subdivision), anterior cingulate cortex, primary motor cortex, and other thalamic areas, we focused on V1, M2, and LD as key inputs for RSC's function in visuospatial navigation. Specifically, LD might carry important visually-modulated HD signal (Mizumori and Williams, 1993) to A30, the more "visual" subdivision of RSC (Mitchell, Czajkowski, Zhang, Jeffery, and Nelson, 2018), while ADn feeds vestibular-driven HD to the more "self-motion" -dominated RSCg. Although our monosynaptic rabies tracing was performed with synapsin and CamKII promoters in wild-type mice, our injections mostly infected L5 neurons (Fig. 4.1 A and Fig. 4.2).

To assess how V1, M2, and LD inputs were organized at the level of single neurons, we used Subcellular Channelrhodopsin Assisted Circuit Mapping (SCRACM) (Petreanu, Mao, Sternson, and Svoboda, 2009) to reveal the functional synaptic density of a specified input across the dendritic arbor of individual neurons. We first targeted ChR2-expressing AAV injections to V1 in adult mice (Fig. 4.3 A and Fig. 4.4). After 4 weeks of ChR2 expression, we performed patch clamp recordings of L5b PCs in acute slices of RSC that contained ChR2-infected axons from V1 (Fig. 4.3). We activated ChR2 in V1 axons using a grid of ~50 μm diameter spots of 473 nm laser light, sequentially delivered across the dendritic arbor of the recorded neuron in the presence of TTX to block axonal conduction (Fig. 4.3 B). We observed EPSPs when the laser spot was near the soma, as opposed to the apical trunk dendrite or tuft (Fig. 4.3 C,D), indicating that V1 axon terminals preferentially made functional synapses at the basal and proximal oblique dendrites of L5b PCs in RSC A30. All neurons receiving direct V1 input (16 neurons from 11 mice) displayed a similar perisomatic connectivity pattern (Fig. 4.3 E). Different patterns were observed for M2 and LD inputs (Fig. 4.3 F-O). M2 axons preferentially made functional synapses at the proximal trunk and oblique dendrites (n=18 neurons from 13 mice), while LD axons made the vast majority of their synaptic contacts in the distal apical dendritic tuft (n=7 neurons from 5 mice; two-way ANOVA: p=0.0228 input source, p=2.77e-06 distance from pia, p=2.03e-30 input source*distance from pia; see Fig. 4.5 for laminar profiles used for statistical analyses).

Does the functional organization of synaptic inputs to L5b neurons in RSC A30 simply reflect the laminar distribution of axonal fibers from the different regions (i.e. does it follow Peters'

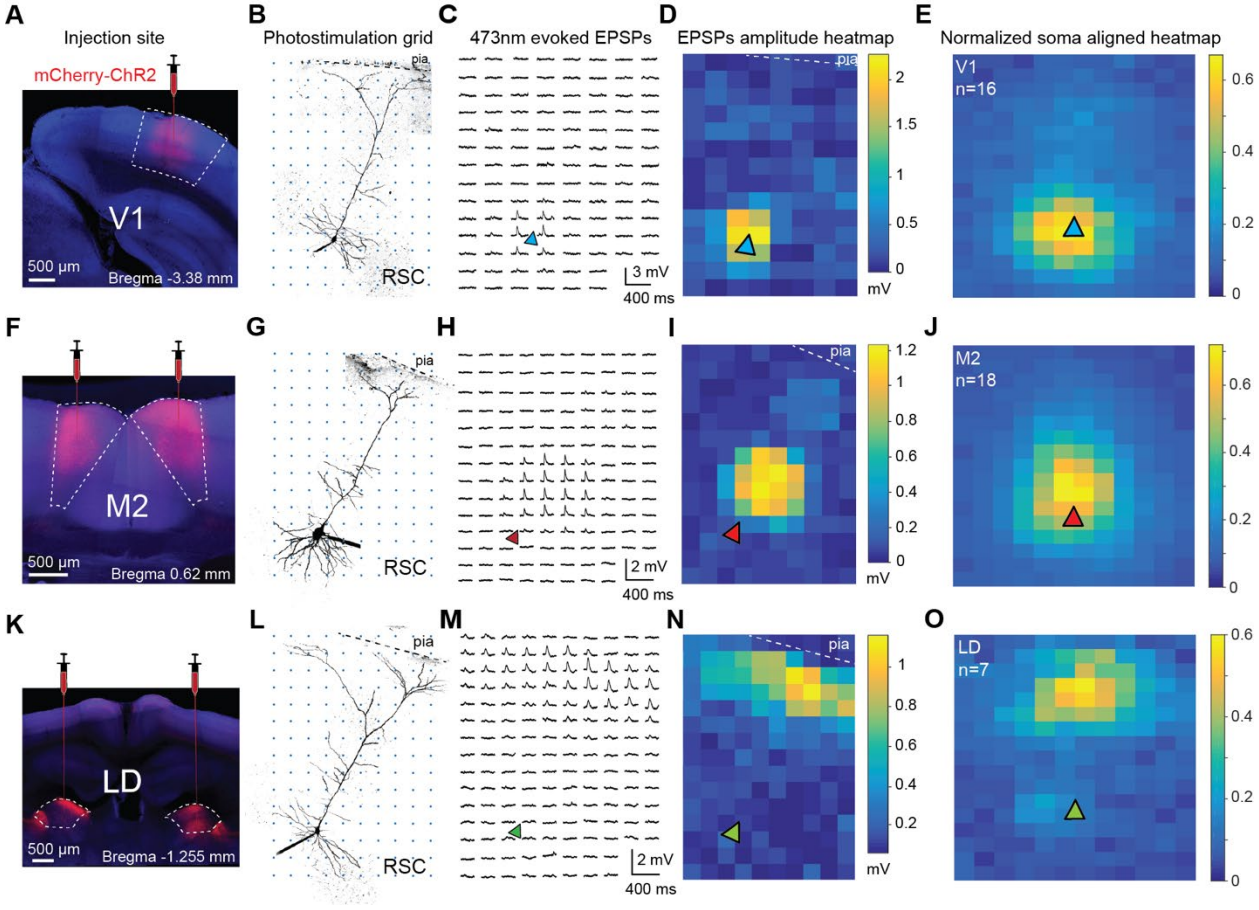

Figure 4.3 Excitatory monosynaptic inputs from V1, M2, and LD target distinct dendritic domains of RSC A30 L5b PCs.

A, F, K, Coronal slices showing injection sites of AAV2.hSyn-mCherry-ChR2 in V1, M2, and LD, respectively. See Fig. S2 for a summary of injection sites per region. **B, G, L**, Two-photon z-stacks of exemplar RSC A30 L5b PCs from animals injected in V1 (top), M2 (middle), and LD (bottom). Axons from injected brain regions were excited by a 473 nm photo-stimulation grid (50 µm spacing) over the recorded neurons, which were filled with Alexa-488 for post-hoc two-photon reconstruction. **C, H, M**, ChR2-evoked EPSPs from the exemplar cells at left recorded at each photo-stimulation location. EPSPs are only apparent when photo-stimulation spots activate functional synaptic contacts between injected brain regions and recorded cells in RSC. **D, I, N**, Corresponding exemplar heatmaps of EPSP amplitudes for the cells at left. **E, J, O,** Average normalized EPSP amplitude heatmaps aligned to soma position (triangle) for V1 (16 cells from 11 mice), M2 (18 cells from 13 mice), and LD (7 cells from 5 mice).

connectivity pattern (Peters and Feldman, 1976; Rees, Moradi, and Ascoli, 2017))? To address this, we quantified the axonal fiber density in RSC A30 from cells in V1, M2, and LD that expressed tdTomato or mCherry (Fig. 4.5). We observed a substantial discrepancy between laminar fiber density and functional connectivity on L5b cells (Fig. 4.5 B and C). Despite no functional connectivity in the tuft dendrites of L5b cells, V1 and M2 axons ramify in L1, suggesting they make numerous synapses at other cell types. Additionally, LD axons display two narrow, dense bands of fibers in L1 and L3. However, only the band in L1 appears to form synapses on L5b cells in RSC A30. This is in contrast to a recent report in which anterior thalamic axons project specifically to L1 of RSC A29 and form most of their synapses onto L5 neurons in this zone (Yamawaki, Li, Lambot, Ren, Radulovic, and Shepherd, 2019). Our results instead provide further evidence that, in general, axo-dendritic anatomical overlap is not an accurate predictor of functional synaptic connections. Instead, a highly selective connectivity program seems to control the functional architecture of long-range excitatory inputs to L5b PCs.

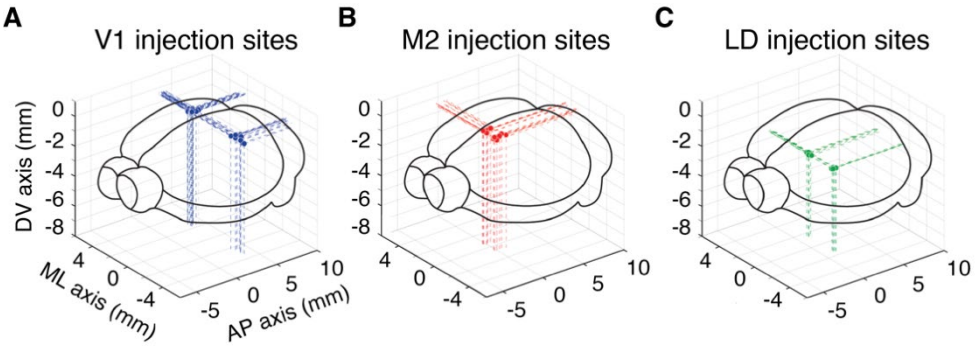

Figure 4.4 Injection site locations for SCRACM experiments.

A Center of the V1-targeted ChR2-mCherry injection volumes, reconstructed with ImageJ software from the recovered brain slices from sCRACM experiments, plotted in 3D space with the corresponding coordinate projections on the 3 axes and aligned to a 3D mouse brain outline. **B**, Center of the M2-targeted ChR2-mCherry injection volumes. **C**, Center of the LD-targeted ChR2-mCherry injection volumes.

Discussion

Our data shows that inputs from different regions converge onto RSCd L5b neurons with a spatially segregated organization along the dendritic arbors. While V1 makes mostly perisomatic connections, M2 preferentially targets the apical obliques and LD the distal tuft. This organization was not entirely predicted by the density of axons terminals in RSCd. V1, M2 or LD may target diverse cell subgroups, for example interneurons or other dendritic compartments for cells in other layers. While a full laminar or cell type-specific map for each input source is out of the scope of this work, results from these kinds of experiments may provide important insights for local computations of visual, motor or directional information in RSC.

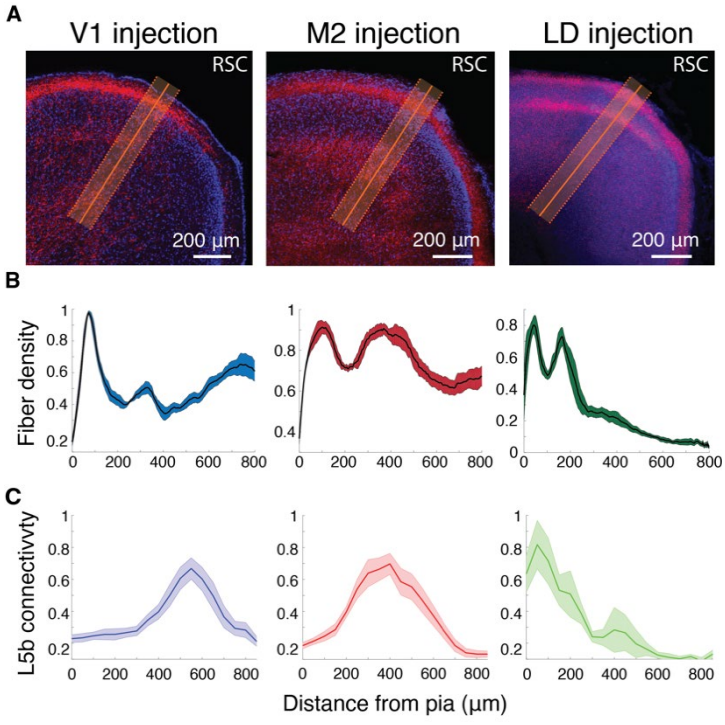

Figure 4.5 Fiber density versus connectivity density profiles for V1, M2, and LD inputs.

A, Confocal images of representative coronal sections containing RSC A30 showing different distributions of axon terminals from V1 (left), M2 (middle), and LD (right) expressing tdTomato (V1 and M2) or ChR2-mCherry (LD). DAPI counterstain in blue. Orange oblique lines indicate the region used for fiber density quantifications of V1 (blue), M2 (red), and LD (green) inputs. **B**, Laminar profile of averaged normalized fiber density distribution for V1 (left), M2 (middle), and LD (right) ($p<0.00001$ for input source, distance from pia, and input source*distance from pia, two-way ANOVA on 3 mice for each input source). **C**, Laminar profile of averaged normalized EPSP amplitudes evoked by 473 nm focal ChR2 stimulation of V1 (left), M2 (middle), and LD (right) terminals over the dendritic arbors of L5b neurons in RSC; n=16/16/11, 18/18/13, and 7/7/5 neurons/slices/mice, respectively ($p=0.0228$ input source; $p=2.77e-06$ distance from pia, $p=2.03e-30$ input source*distance from pia, two-way ANOVA). In panels B and C lines and shaded areas are mean±sem.

The results here presented, along with the findings on distinct dendritic integration rules in the 3 main dendritic domains described in Lafourcade et al (Lafourcade, Van Der Goes, Vardalaki, Brown, Voigts, Yun, Kim, Ku, and Harnett, 2022), provide a new insight into how single cortical neurons in association cortex receive and process their inputs at the subcellular level before final integration at the axon. The striking segregation of inputs we observed may be particularly important for implementing compartment- and/or input-specific plasticity rules and mechanisms. First, segregated inputs are less likely to interact in terms of synaptic plasticity, due to the spatial compartmentalization of electrical and chemical signals (Harvey and Svoboda, 2007), a feature that enables tuning of independent computations. Second, by spatially segregating different inputs in distinct dendritic compartments, single neurons can more easily implement discrete postsynaptic mechanisms for input-specific decoding.

Similar input mapping experiments have been performed in RSCg, which revealed localized anterior thalamic inputs to the tufts of L5 somas (Yamawaki, Li, Lambot, Ren, Radulovic, and Shepherd, 2019) and to L3 somas, which might provide a synaptic substrate for cortical HD tuning (Brennan, Jedrasiak-Cape, Kailasa, Rice, Sudhakar, and Ahmed, 2021) and circuit mechanisms contributing to specific spatial behaviors (Yamawaki, Li, Lambot, Ren, Radulovic, and Shepherd, 2019). The nonoverlapping but striking similarity between the axonal distribution of ADn/AVn in RSCg and that of LD/LP in RSCd (Fig. 4.5) suggests that a structured thalamic-HD pathway is established in these cortical sub-regions. The similarity in the axonal distribution, and potentially dendritic targeting, suggests a parallel pathway for HD modulation of RSC neuronal output. The different identity of the thalamic HD inputs might contribute to diverse spatial representations and encoding between RSCg and RSCd (Mitchell and Dalrymple-Alford, 2006). In fact, a higher density of environment-driven bi- or pluri-directional HD tuning was found in the dysgranular portion of RSC compared to the granular portion, where allocentric HD is encoded (Jacob, Casali, Spieser, Page, Overington, and Jeffery, 2017; Zhang, Grieves, and Jeffery, 2021). LD, which has been reported to encode HD in combination with light or visual cues (Mizumori and Williams, 1993), might indeed provide RSCd with a cue-relevant directional input.

Compartmentalization of tuft dendrites, which occupy L1, may endow cortical pyramidal neurons with distinct integrative properties that influence neuronal output (Harnett, Magee, and Williams, 2015; Harnett, Xu, Magee, and Williams, 2013). Independent HD signals in the distal dendrites of L5 neurons in RSCd have been observed in freely head-rotating mice (Voigts and

Harnett, 2020). This activity might play an important role in learning cue orientation and possibly form landmark representations, specifically if in conjunction with other visual and motor inputs. Future experiments, with specific optical manipulations of tuft dendritic activity, should establish whether these distal inputs can act as teaching signals for the presence of stable orienting cues useful for navigation.

Methods

Experimental Models and Subjects Details

All animal procedures were carried out in accordance with NIH and Massachusetts Institute of Technology Committee on Animal care guidelines. C57BL/6 male and female mice were used in approximately equal numbers. Adult mice (between 8 and 16 weeks of age) were used for all electrophysiology experiments. 5 12-week old mice were used for rabies tracing experiments. Mice were kept on a 12-hour light/dark cycle in conventional housing and had unrestricted access to food and water.

Stereotactic Surgery Procedures

Viral injection surgeries were performed using aseptic techniques. Mice were anesthetized with isoflurane and head-secured in a stereotaxic apparatus. Body temperature was maintained with a feedback-controlled heating pad (DC Temperature Control System, FHC). Slow-release buprenorphine (1 mg/kg) was pre-operatively injected subcutaneously. After incision of the scalp, a small burr hole was made using a dental air drill. Virus was delivered at a slow rate (max. 50 nL/min) to prevent tissue damage through a small beveled injection pipette. After a five-minute rest, the pipette was slowly withdrawn and the incision was sutured. For sCRACM experiments, bilateral injections of 100 nL of AAV2-hSyn-hChR2(H134R)-mCherry (UNC Vector Core) were made over M2 (AP: -0.5; ML: +/- 0.65; DV: 0.50), LD (AP: -1.3; ML: +/- 1.4; DV: 2.45), or V1 (AP -3 and -3.8, ML +/-2.4 and +/- 2.8, DV: 0.45 and 0.5). For V1 injections, two small burr holes were drilled to increase the spread of infection (see Fig. 4.4 for 3D reconstructions of the injection coordinates for all sites from recovered brain slices). Virus was allowed to express for 4-8 weeks before slice electrophysiology experiments commenced. For anterograde fiber tracing from V1 and M2, mice received bilateral stereotaxic injections in V1 and M2 with same coordinates as

described above of 100 nL of pENN-AAV-CAG-tdTomato-WPRE-SV40 (105554-AAV1; Addgene). The virus expressed for 10 days before perfusion.

Immunohistochemistry and confocal imaging

For monosynaptic rabies tracing and M2 and V1 fiber density quantification experiments, brains of injected mice were fixed by transcardial perfusion with 4% paraformaldehyde in PBS and left overnight at 4°C. The same procedure was applied for layer markers staining experiments. Brains were sectioned coronally at 100 μm thickness with a floating section vibratome (Leica VT1000s). Sections from rabies tracing experiments were rinsed in PBS and then immunolabeled with 1:1000 DAPI solution (62248; Thermo Fisher Scientific). Sections from M2 and V1 fiber density and layer markers staining experiments were rinsed in PBS, blocked in 2% normal goat serum and 0.4% Triton x-100 for 1 hour, and immunolabeled with 1:500 rabbit anti-RCFP (632475; Takara) for 24 hours at 4°C, or 1:500 rat anti-Ctip2 (Abcam, ab18465, layer 5 marker) and rabbit anti-Cux1 (ABS687, Thermo Fisher Scientific, layer 2/3 marker). Sections were rinsed 3 times for 10 minutes with 0.4% Triton x-100 in PBS (PBST), and for the fiber density they were incubated in 1:250 Alexa Fluor 568 goat anti-rabbit IgG (H+L) (A-11036; Thermo Fisher Scientific) for 3 hours, and raised in PBST. For the layer markers, slices were incubated in 1:1000 goat anti-rabbit Alexa 488 (AB_143165; Thermo Fisher Scientific) and 1:1000 goat anti-rat Alexa 594 (A21471; Thermo Fisher Scientific).

For LD fiber density quantification and sCRACM injection site verification, slices recovered from sCRACM experiments preparations were rapidly transferred to well plates containing 4% paraformaldehyde and left overnight at 4°C. They were subsequently rinsed 1 time with PBS for 10 minutes. Sections containing RSC and the injection areas were immunolabeled with 1:1000 DAPI solution for 5 minutes. All sections were mounted and coverslipped with clear-mount with tris buffer (17985-12; Electron Microscopy Sciences). Confocal images were captured using a Leica TCS SP8 microscope with a 10X objective (NA 0.40) and a Zeiss LSM 710 with a 10x objective (NA 0.45).

Confocal Image Processing

The spread and targeting of V1, M2 and LD areas were verified from the recovered sCRACM brain slices containing the injection sites, visible from high density of cells with mCherry

expression. The center of mass of the injection volumes was determined by visual inspection, aligned with the confocal images of the injection sites to the Mouse Allen Reference Atlas, and measured with ImageJ software for AP, ML and DV coordinates. Mice with restricted and comparable ChR2-mcherry expression in the target areas were included for quantifications LD fiber density and sCRACM analysis. Axonal terminals from LD were readily detectable in RSC both under 2-photon and confocal microscopy, but M2 and V1 fibers required antibody enhancement. Therefore, separate anterograde tracing experiments were performed on an additional set of mice. Columnar distributions of axon terminals from infected LD, V1, and M2 cells were obtained from pixel intensity using ImageJ. An area containing a width of 60 pixels and a length of 800 μm, starting at the pia, was drawn across RSC A30. This analysis was divided into anterior (AP=-2.055 to -2.555 mm) and posterior (AP= -2.78 to -3.68 mm) A30. Both hemispheres were sampled for fiber density analysis in each brain section. The average pixel fluorescence was extracted across the area using the plot profile tool.

Successful monosynaptic rabies tracing experiments were determined by restriction of the td-Tomato-labeled starter cells to layer 5 in A30. After alignment to the Allen Mouse Brain Reference Atlas and background removal, presynaptic cells (green) from V1, M2 and LD areas from the same AP coordinates across the 5 mice were counted by segmenting the image using MatLab's watershed function.

Acute slice preparation

Coronal brain slices (300 μm) from retrosplenial cortex were prepared from 8 to 16-week-old C57/BL6 mice of both sexes (Jackson) using the same procedure described in the Chapter 3 methods section. Animals were deeply anesthetized with isoflurane prior to cardiac perfusion (using slicing solution described below) or decapitation. Slicing was performed with a vibratome (Leica VT1200s) in ice-cold slicing solution containing (in mM): sucrose 90, NaCl 60, $NaHCO_3$ 26.5, KCl 2.75, NaH_2PO_4 1.25, $CaCl_2$ 1.1, $MgCl_2$ 5, glucose 9, sodium pyruvate 3, and ascorbic acid 1, saturated with 95% O_2 and 5% CO_2. Slices were incubated in artificial cerebrospinal fluid (aCSF) containing (in mM): NaCl 120, KCl 3, $NaHCO_3$ 25, NaH_2PO_4 1.25, $CaCl_2$ 1.2, $MgCl_2$ 1.2, glucose 11, sodium pyruvate 3, and ascorbic acid 1, saturated with 95% O_2 and 5% CO_2 at 35.5 °C for 45 min and then stored at 18 °C. All recordings were performed at 33–37 °C in aCSF.

Electrophysiological recordings

An Olympus BX-61 microscope with infrared Dodt optics and a water-immersion lens (60X, 0.9 NA; Olympus) was used to visualize cells. Patch-clamp recordings were performed from morphologically and electrophysiologically identified L5b RSC pyramidal cells. Current-clamp recordings were performed in bridge mode with a Dagan BVC-700 amplifier with bridge fully balanced. Current and voltage signals were filtered at 10 kHz and digitized at 20 kHz. Patch pipettes were prepared with thin-wall glass (1.5 O.D., 1.1 I.D.). Pipettes had resistances ranging from 6 to 12 MΩ and the capacitance was fully neutralized prior to break in. The standard intracellular solution contained (in mM): potassium gluconate 134, KCl 6, HEPES buffer 10, NaCl 4, Mg_2ATP 4, NaGTP 3, and phosphocreatine di (tris) 14. Depending on the experiment, 0.05 Alexa 594, 0.1 Alexa 488, and/or 0.1 OGB 6F mM (Invitrogen) were added to the internal solution. Liquid junction potential was not corrected for.

Subcellular Channelrhodopsin Assisted Circuit Mapping (sCRACM)

Prior to starting each sCRACM experiment, we verified viral targeting with 2-photon imaging by visualizing fluorescently labeled cell bodies at injection locations in acute slices. For all recordings TTX (500 nM), 4-AP (100 μM), and CPP (5 μM) were added to the bath perfusion to limit spatial activation of presynaptic terminals. After whole-cell break in, a full-field 473 nm LED (ThorLabs) was used to determine if the cell received inputs to the region where the injection was performed. If a reliable EPSP could be obtained with the full-field LED, we proceeded to sCRACM. The position of a 473 nm laser beam (OptoEngine LLC, 100mW) was controlled with galvanometer scanners (Bruker). The beam passed through an air objective (4x, 0.16 NA; UPlanApo, Olympus). The duration of the light pulses was controlled via TTL input to the laser. Duration was adjusted to obtain small EPSPs (1-4 mV); the interstimulus interval between each spot was 1 s. Stimulation used a 50 μm spot spacing in a grid of 15 × 20 spot (750 μm × 1000 μm), which covered the dendritic arbor. Grids were repeated 2–6 times and averaged. sCRACM pixel values (EPSP amplitude) were calculated as the difference between local baseline (mean voltage 50ms before stimulation) and maximum voltage in a 50 ms window after photo stimulation. Population data of the spatial distribution of inputs were analyzed by first rotating the maps to align all neurons (to vertical trunk dendrites), then peak-normalizing the maps, and finally averaging across cells within a given experiment (LD vs. V1 vs. M2).

Quantification and Statistical Analysis

Analyses were performed using custom-written MATLAB code. Current and voltage signals were filtered at 2 kHz with zero-phase filtering using the MATLAB function filtfilt. Statistical analysis was performed in GraphPad Prism and/or MatLab. Statistical details can be found in the text and/or figure legends. Reported n values refer to number of branches unless indicated otherwise.

Chapter 5 : Conclusions and Future Directions

The past few decades have seen advancements in the understanding of the circuit components of the HD system and their contributions to spatial codes and navigation. Particularly, in recent years, studies focused on cortical regions involved in spatial navigation have unraveled the diversity and complexity of cortical spatial receptive fields (Alexander, Carstensen, Hinman, Raudies, Chapman, and Hasselmo, 2020; Alexander and Nitz, 2017, 2015; Jacob, Casali, Spieser, Page, Overington, and Jeffery, 2017; LaChance, Todd, and Taube, 2019; Laurens, Abrego, Cham, Popeney, Yu, Rotem, Aarse, Asprodini, Dickman, and Angelaki, 2019; Sargolini, Fyhn, Hafting, McNaughton, Witter, Moser, and Moser, 2006) and their role in spatial cognition by integrating allocentric and/or egocentric stimuli (Auger, Mullally, and Maguire, 2012; Campbell, Ocko, Mallory, Low, Ganguli, and Giocomo, 2018; Clark, Simmons, Berkowitz, and Wilber, 2019; Epstein, Patai, Julian, and Spiers, 2017; Fischer, Soto-Albors, Buck, and Harnett, 2019; Mao, Kandler, McNaughton, and Bonin, 2017a; Mao, Molina, Bonin, and McNaughton, 2020; van Wijngaarden, Babl, and Ito, 2020; Wilber, Clark, Forster, Tatsuno, and McNaughton, 2014). A large body of evidence points to RSC as a key region for associative spatial computations that guide navigation (Auger, Zeidman, and Maguire, 2017; Mitchell, Czajkowski, Zhang, Jeffery, and Nelson, 2018; Vann, Aggleton, and Maguire, 2009). Visual reorientation, thought to depend on RSC activity, is a particularly important problem in navigation. In fact, HD signals contribute to the formation of several spatial codes in the brain and correct use of orienting cues allows successful navigation within an environment. I hypothesized that corticothalamic circuits of RSC are crucial to this process and asked how local and long-range circuit mechanisms can support spatial reorientation by: 1) comparing the simultaneous HD representation of ADn and RSC during cue manipulations and assess the functional connectivity; 2) testing what components predicted by attractor network architectures exist in the ADn local circuitry to sustain the HD code; 3) identifying the spatial organization of thalamic HD and cortico-cortical synaptic inputs in individual RSC neurons that possibly underlie the associative spatial computations. I summarize below the main findings of this thesis in the context of the current understanding of the HD system and visually-guided reorientation. I also consider experimental and technical limitations and

suggest potential avenues to overcome them in future studies, with the goal to provide useful insights on how research in this system can improve human health.

5.1 Coordinated HD representation updates

I showed that the prominent visual cue-based reorientation, a spatial computation thought to depend on intact RSC and POS (Clark, Bassett, Wang, and Taube, 2010; Goodridge and Taube, 1997), is characterized by matching HD referencing of RSC and ADn, despite variability in RSC HD coding (Fig. 2.3). This variability is consistent with the high-dimensional tuning observed in RSC, but whether this region contains specific functional subgroups with distinct HD and visual or environment-driven responses, as previously reported in the parahippocampal region (Kornienko, Latuske, Bassler, Kohler, and Allen, 2018), is unknown. Nonetheless, despite the specific tuning properties, which may play a fundamental role in detecting complex scenes or other stimulus modalities for real world navigation, a global HD representation in our simple task can be extracted from the RSC ensemble activity (Fig. 2.4). With a decoding strategy based on neuronal activity, I found dynamics of the RSC HD reference shift that are closely matched to those of simultaneously recorded ADn neurons (Fig. 2.6). This coordination was not dependent on the presence of visual cues, and persisted in drift from the true HD in darkness (Fig. 2.8). This suggests that, at least at our temporal and HD angle resolution, other velocity, angular acceleration and visual signals present in RSC do not noticeably affect the global HD encoding (which is likely sustained by a strong feedforward connectivity from ADn to RSC; Fig. 2.10), or actually contribute to maintaining this coordination.

POS is the other major ADn target, exhibiting a high density of HD coding cells directly influenced by ADn tuning (Peyrache, Lacroix, Petersen, and Buzsaki, 2015). Specific recurrent local excitatory-inhibitory loops in POS appear to be involved in sustaining this representation (Nassar, Simonnet, Huang, Mathon, Cohen, Bendels, Beraneck, Miles, and Fricker, 2018; Simonnet, Nassar, Stella, Cohen, Mathon, Boccara, Miles, and Fricker, 2017). POS is required for stability of HD and visually-guided updating (Goodridge, Dudchenko, Worboys, Golob, and Taube, 1998; Goodridge and Taube, 1997). It also receives input from RSC and visual areas, suggesting that updated HD reference signals may also emerge at this level. Given that ADn HD coding anticipates POS HD consistently both during awake free foraging as well as during sleep by 20-50 ms, a feedforward model of HD update would predict that this temporal offset would not

be altered by visual cue changes as those shown in this work. This would not, however, exclude that POS may integrate visual, HD and RSC orienting information to drive the update through a spatially biased code. No electrophysiological recording of such cells during cue rotation has been performed to date. However, a direct and dedicated POS projection to LMN exists (Huang, Simonnet, Nassar, Richevaux, Lofredi, and Fricker, 2017), originating from deep POS layers, where HD coding cells are sparser, suggesting a possible anatomical route for this kind of information. Indeed, lesions of this descending axon fiber tract produced instability and loss of visual cue control of HD similar to either POS or RSC lesions (Yoder, Peck, and Taube, 2015). Engagement of this visual-update pathway is consistent with a potential update of the HD frame upstream of ADn, at the level of AV integration, as already suggested by the persistent HD rotation from dynamic cue biasing of HD even after cue omission (Ajabi, Keinath, Wei, and Brandon, 2021). Moreover, this hypothesis corroborates the notion that the HD signal, despite its low-dimensionality and tractability from a behavioral and computational perspective, is actually the product of simultaneous distributed processing of multiple sensory inputs.

5.2 The role of corticothalamic connections to ADn

A major hurdle of untangling the neural mechanisms underlying the use of visual and self-motion cues in the HD system is the complexity of the navigation circuitry, as it comprises multiple nodes for integration of different streams of information. In Chapter 2, I showed that putative functional connections from RSC to ADn were dwarfed by the dense and divergent connections in the thalamo-cortical direction and that this striking asymmetry likely biased the direction of HD information flow from ADn to RSC, even upon landmark-driven update of the HD reference (Fig. 2.10). This observation is consistent with a coordinated HD representation across brain structures, but leaves several open questions.

The few RSC to ADn connections might originate from a small dedicated subgroup of RSC neurons, namely the granular L6, (Shibata, 1998), which we sparsely recorded given the widespread sampling of RSC locations (Fig. 2.1). In sensory thalamo-cortical loops, descending cortical information to first order thalamic nuclei is sparse and plays a modulatory role, as a result of transmission via unmyelinated L6 axons. Whether this is also the case for RSC is unknown. However, descending cortical inputs to ADn, which likely include both POS and RSC projections, form synapses that can potentiate via metabotropic glutamate receptors, consistent with a

modulatory pathway (Petrof and Sherman, 2009). Moreover, L6 POS neurons also send direct projections to ADn (Huang, Simonnet, Nassar, Richevaux, Lofredi, and Fricker, 2017), in a less striking, but nonetheless asymmetric fashion (Peyrache, Lacroix, Petersen, and Buzsaki, 2015). What is the role of these few descending corticothalamic projections and what kind of information do they convey to ADn? Future studies using viral techniques to restrict inhibitory opsins expression to these neurons could be used to test what role they play during navigation in the behaving mice, both with stable cues and during visual cue rotation. Conversely, by combining excitatory opsins with dense tetrode or silicone probe recordings, the tuning of these neurons could be identified and mapped with optotagging. Anatomical tracing experiments could also determine whether these neuron populations have axon collaterals targeting other brain regions, for example TRN (Vantomme, Rovó, Cardis, Béard, Katsioudi, Guadagno, Perrenoud, Fernandez, and Lüthi, 2020).

5.3 The role of TRN in shaping ADn HD

Another major target of descending cortical inputs affecting thalamic computations is the TRN. Several circuit motifs involving inhibition in thalamocortical loops have been identified in sensory systems (Cruikshank, Lewis, and Connors, 2007; Shepherd and Yamawaki, 2021), with important roles in shaping sensory responses and learning. It is not surprising that they are implicated in anterior thalamic nuclei function as well. TRN is reciprocally connected with ADn (Wang, Gonzalo-Ruiz, Sanz, Campbell, and Lieberman, 1999) and receives descending cortical input from RSCg/POS (Vantomme, Rovó, Cardis, Béard, Katsioudi, Guadagno, Perrenoud, Fernandez, and Lüthi, 2020). Given that no recurrent connectivity is found in ADn (Fig. 3.2), cellular properties and strong synaptic inputs from LMN that relay HD tuning with all or nothing properties (Petrof and Sherman, 2009) likely sustain persistent activity in ADn. External excitatory inputs, together with reciprocal inhibitory inputs, in theoretical LMN-DTN attractor networks have been shown to recapitulate properties of HD coding (Boucheny, Brunel, and Arleo, 2005; Song and Wang, 2005). One fundamental difference between the LMN-DTN anatomy and that of downstream HD targets is that the DTN inhibitory inputs are necessary for HD coding, as shown by the ablation of directional tuning in anterior thalamic nuclei upon DTN lesions (Bassett, Tullman, and Taube, 2007), but, on the contrary, brief or long term inhibition of TRN does not completely ablate HD tuning (Duszkiewicz, Carrasco, Orhan, Brown, Owczarek, Vite, Wood, and Peyrache, 2022;

Vantomme, Rovó, Cardis, Béard, Katsioudi, Guadagno, Perrenoud, Fernandez, and Lüthi, 2020). TRN, instead, may play a modulatory role on the gain of ADn HD neurons, possibly as sharpening of the tuning curves in comparison to LMN (Taube and Bassett, 2003). However, whether ADn HD coding is influenced by other features has not been thoroughly tested. TRN's involvement in arousal and attention may be recruited in response to task demands and affect ADn HD coding, attributing therefore to ADn a larger role in the HD circuitry beyond simply relaying HD to cortex.

Furthermore, inhibitory control may be critical for adaptive responses to external sensory stimuli other than self-movement. Indeed, in the fly central complex visual "ring" neurons, whose responses tile the visual space, make inhibitory synapses onto compass neurons and through coordinated pre and post-synaptic plasticity mechanisms can regulate the pinning offset of the HD activity packet to changing visual cues (Fisher, Lu, D'Alessandro, and Wilson, 2019). Whether a similar mechanism involving TRN control of anterior thalamic nuclei responses occurs, in isolation or in parallel to upstream HD circuitry involving LMN-DTN synapses, is unknown. Preliminary evidence of reduced network gain following visual cue changes indicates that strong inhibition in ADn, especially during either fast or large resets, may indeed mediate visual control of HD (Ajabi, Keinath, Wei, and Brandon, 2021). This finding is also consistent with the fast recruitment of inhibition in response to RSC/POS activation (Vantomme, Rovó, Cardis, Béard, Katsioudi, Guadagno, Perrenoud, Fernandez, and Lüthi, 2020). How descending POS, or other cortical, excitatory inputs converge and modulate this activity is however unknown.

Moreover, no studies have yet addressed what connectivity layout or synaptic mechanisms may account for TRN-mediated inhibition of ADn both during the stable cue and during learning of the new cue orientation. The finding that in the fly only specific visual cue positions inhibit some compass neurons (Fisher, Lu, D'Alessandro, and Wilson, 2019) suggests that some topographical mapping of the descending cortical input to TRN, and/or to the upstream LMN/DTN circuitry, may exist. However, no studies have specifically looked at tuning in the anterodorsal TRN portion, connected to ADn. Future anatomical experiments with single cell tracing and expansion microscopy could potentially yield valuable insight into the connectivity logic and cell type specificity (parvalbumin- or somatostatin- expressing) of TRN-mediated inhibition.

5.4 Angular velocity and HD representation

The linear-gaussian GLM decoding based on the neuronal firing rates that I used in the present work may not account for differences in behavioral states, such as speed, arousal or attention modulation, and more complex interactions. Testing how other decoding methods impact HD estimation in ADn and RSC around the cue rotation may provide further insights into the instantaneous population activity readout (Xu et al., 2019). Indeed, nonlinear encoders, applied to large scale ADn - POS recordings revealed both in awake as well as in sleeping mice that ADn leads POS activity by 25 to 50 ms (Viejo, Cortier, and Peyrache, 2018). The state-invariant relationship indicates that this anticipatory HD coding is not dependent on AV or active head turns as initially proposed (Blair and Sharp, 1995), but rather controlled by local circuit and cellular properties for improved current HD decoding by downstream targets (Zirkelbach, Stemmler, and Herz, 2019). Whether the anticipatory RSC HD coding observed during head turns (Lozano, Page, Jacob, Lomi, Street, and Jeffery, 2017) is also preserved during sleep is currently unknown. In awake behavior, it is likely to arise from mixed coding as a result of the strong AV and HD by AV that have been observed in RSC (Hennestad, Witoelar, Chambers, and Vervaeke, 2021; Keshavarzi, Bracey, Faville, Campagner, Tyson, Lenzi, Branco, and Margrie, 2021) and inputs from motor cortex. The leading ADn activity with respect to POS is consistent with a feedforward ADn signal, whereby HD tuning in POS is largely inherited (Peyrache, Lacroix, Petersen, and Buzsaki, 2015). In contrast, the observation in Chapter 2, Fig. 2.10 G that the HD tuning in RSC is biased by direct ADn input, but is not entirely aligned, is suggestive of integration of complex and potentially multi-modal inputs. These may include local AV input and be influenced by the degree of conjunctive encoding present in these neurons in RSC. Neuronal mixed selectivity has been proposed to increase the decoding reliability of fast-changing high-precision variables (Finkelstein, Ulanovsky, Tsodyks, and Aljadeff, 2018), such as HD, which rapidly changes as a function of AV in a manner that depends on the encoding timescales and the size of the ensemble.

As pointed out, the size of the ensemble population is a critical factor in accurately decoding fast-changing signals, especially in mixed-selective populations, contrary to “pure” cells, for which fewer units are needed. Because of the limited number of simultaneous units I recorded in ADn and RSC, and the uneven HD coverage especially for the fewer HD-coding units in RSC, I implemented two strategies to increase the decoding accuracy: 10° binning of HD and 20 ms binning of the time series to convert spike times into firing rates. Future experiments with high

density recordings, for example using silicon or neuropixel probes simultaneously targeting RSC and ADn units in freely moving mice, could reveal whether the coordination is still preserved at finer timescales than 20 ms. Subsequent cross correlation analyses from the two regions might also be applied to smaller HD remapping windows than the 75 s presented in Fig 2.6 E-F. These would also provide more detailed mechanistic insights into the initial phases of the HD remapping. Higher neuronal sampling and shorter but numerous continuous trials would also allow to investigate the relationship between the HD representation and different egocentric and head velocity conjunctions, for example when the cue appears in the visual field both during and after cue rotations. Such analyses would provide mechanistic insights into the possible modulatory variables that contribute to the HD reference shift dynamics.

AV signals may have a differential weight in establishing the final HD reference depending on previous experience of the visual cue and the size of the internal and external cue conflict (Knierim, Kudrimoti, and McNaughton, 1998). Moreover, given RSC's role in the stability of ADn HD, constant integration of movement and visual signals may emerge at this cortical level as well as in upstream regions. RSC lesions prevent not only visual anchoring of HD but also lead to instability, both in the presence of visual cues acting as landmarks (Clark, Bassett, Wang, and Taube, 2010; Clark, Simmons, Berkowitz, and Wilber, 2019) as well as in darkness (Elduayen and Save, 2014). This suggests that RSC is not only important for visual processing of spatial information, but also for forming coherent representations of self-location from motion signals. To test whether visual transformations carried by RSC are in fact necessary for visually-driven changes in the HD reference, future studies could implement phasic optical inhibition of visual inputs synapsing onto RSC neurons at different time points during rotation of the visual cue.

5.5 Circuit organization for landmark coding in RSC

External sensory (particularly visual) stimuli can anchor the HD representation if they are deemed stable and reliable (Knierim, Kudrimoti, and Mcnaughton, 1995). Distal cues, that are less affected by motion parallax, fit these requirements (Zugaro, Berthoz, and Wiener, 2001) and can eventually function as landmarks. Neural signals encoding for landmarks have been recorded in RSC and are particularly relevant for goal-directed behavior and for strategic route planning and motor output (Auger, Mullally, and Maguire, 2012; Marchette, Vass, Ryan, and Epstein, 2014). However, exactly how RSC transforms visual, or external cues, into stable landmarks is unknown.

Mixed-selectivity of RSC neurons provides a candidate mechanisms for understanding these transformations, whereby different gradients of mapping allocentric and egocentric features for navigation can be signaled to downstream decoding regions (Alexander and Nitz, 2015). Recently, different environment-driven multidirectional HD tuning curves have been described in dysgranular RSC (Jacob, Casali, Spieser, Page, Overington, and Jeffery, 2017; Zhang, Grieves, and Jeffery, 2021). This finding suggests that other features can intersect with a global allocentric directional frame at the single cell level, thus providing a cellular coding substrate for learning of stable landmarks. Our findings expand on this notion by showing a highly organized long-range input targeting to L5b pyramidal neurons in RSC (Fig. 4.3). This organization, together with specific dendritic integration rules (Lafourcade, Van Der Goes, Vardalaki, Brown, Voigts, Yun, Kim, Ku, and Harnett, 2022), may represent a subcellular mechanism for input specific decoding.

Independent HD encoding in the distal dendrites compared to their respective somas has been recorded in RSC L5 pyramidal neurons (Voigts and Harnett, 2020), which is where thalamic LD inputs make synapses (Fig. 4.3 K-O) (Lafourcade, Van Der Goes, Vardalaki, Brown, Voigts, Yun, Kim, Ku, and Harnett, 2022). Moreover, precise coupling of visual and motor inputs are hypothesized to nonlinearly combine to form landmark responses in a linear environment in individual RSC neurons (Fischer, Soto-Albors, Buck, and Harnett, 2019). These suggest that high-dimensional spatial information about the environment likely requires conjunction and transformation of specific inputs. Future investigations using optical imaging and manipulations of precisely timed and localized inputs suggested by the work presented here are needed to reveal how these local dendritic operations are linked to landmark encoding.

5.6 Cue control of the HD representation

Previous studies have indicated that visual-cue driven HD remapping can occur on very short time scales, with slight differences for units shifting their PFD to be aligned with the prominent cue orientation versus units that became silent (Zugaro, Arleo, Berthoz, and Wiener, 2003). Such fast dynamics were hypothesized to be driven by direct input from the retina or visual thalamus. These events, however, represented a subset of HD remapping sessions, where specific heading and behavior configurations were required. In contrast we observed variable, but mostly slow remapping dynamics, more similar to those previously reported (Ajabi, Keinath, Wei, and Brandon, 2021; Knierim, Kudrimoti, and McNaughton, 1998). The variability of remapping

dynamics that we observed could result from several factors, including cue devaluation, size of the HD mismatch, and AV at the time of cue rotation. Long time scales, similar to our observations, are however characteristic of the learning of landmark orientation via exploration of the arena (Goodridge, Dudchenko, Worboys, Golob, and Taube, 1998).

Cue devaluation could result from repeated behavioral manipulations, which bias the HD reference to the current, internally-anchored HD representation. Large rotations were more dramatically affected, as they carried larger mismatches with the ongoing HD representations and lead to landmark instability (Fig. 2.5). In my experiments it is unclear if the decreased or null HD shifts after cue rotations resulted from anchoring to other features of the environment, rejection of the prominent cue rotation and preference for the self-motion HD, or simply uncertainty over the only prominent cue. Moreover, potential odor cues, despite having a local bearing and thus being less reliable for allocentric HD, can emerge during exploration of the arena, causing further mismatches with the updated orientations of the prominent visual cue. Strategies to reduce landmark devaluation could include having separate training and testing arenas and reducing the length of the testing sessions, or interleaving cue rotations with prolonged dark sessions or changing arena designs, such as addition of paths or corridors.

I have shown that the egocentric bearing of the new and the previous cue do not influence the size of the rotation, but it is not obvious if other aspects of the egocentric experience may influence the time course of the neural rotation. It is also possible that previous HD activity or AV at the time of the rotation play a role in the HD reference shift speed (Ajabi, Keinath, Wei, and Brandon, 2021). Exactly what neural mechanisms and pathways in the complex HD system underlie different learning timescales and competition among different signals, not only limited to instantaneous body-, vestibular-, optic-flow-based signals, but also including memory of previous cues and devaluation, is unknown.

Despite the simplicity of the classical behavioral settings, originally designed to isolate specific variables and minimize noise or complex responses, there are several caveats to the behavioral relevance of the neural processes described. First of all, in a natural behavior, most likely a visual landmark is embedded in a complex visual scene, where multiple sensory modalities interact. Second, landmarks emerge and are mostly used in goal-directed behavior, a process which requires, together with higher levels of arousal and attention, spatial computations necessary for creating motor plans and engages reward responses. Third, in realistic navigation most landmarks

are cues that agents navigate by and that are deemed stable in their allocentric mapping as multiple but coherent egocentric views of them are sampled during exploration with constant changes in the relative distance and heading. Such local landmarks are known to be encoded as vectorial representations by object vector cells in MEC (Høydal, Skytøen, Andersson, Moser, and Moser, 2019), which support positioning and landmark-based navigation (Bicanski and Burgess, 2018; Yan, Burgess, and Bicanski, 2021). Even though this thesis work and previous studies have highlighted the importance of anchoring signals for HD coding by using external or distal cues, it is unclear whether the free foraging behavior here presented engages the same circuitry, and the same remapping dynamics, as in goal-directed or more naturalistic navigation behavior.

Interestingly, while ADn has been characterized to exclusively encode allocentric HD, few studies have tested wider ranges of cue manipulations and the flexibility of HD encoding in this thalamic region. One study (Taube and Burton, 1995) showed that, by having rats navigate between two environments through a passageway without external cues, ADn and POS HD switched between reference frames, depending on the context, after cue rotation in the familiar environment. These observations suggested that ADn and POS HD cells discharged according to the perceived directional heading and, while they were preferentially tied to stable landmarks, they also integrated idiothetic cues. On the other hand, RSC neurons have been shown to respond to multiple spatial coordinate systems, from allocentric head direction and positional signals to the egocentric boundary vector cells (Alexander, Carstensen, Hinman, Raudies, Chapman, and Hasselmo, 2020). In MEC, HD cells can temporarily track internal and changing external HD reference frames, suggesting that navigation signals in this region are not fixed to single external references (Park, Keeley, Savin, Ranck, and Fenton, 2019).

How different reference frames affect ADn HD coding during navigation is still unknown, however distal cues do exert a stronger anchoring power over ADn HD cells than foreground cues (Zugaro, Berthoz, and Wiener, 2001). Furthermore, no studies have yet investigated whether local stable cues that act as landmarks have similar bearings on thalamic HD as those reported for external or distal cues. Future work should address how more complex cue manipulations scenarios engaging multiple frames of reference, known to evoke with various spatial responses in cortex, affect thalamic HD coding with simultaneous recordings in ADn and RSC or MEC. Altogether, findings from these studies could also reveal potential roles of ADn beyond simply relaying allocentric HD to cortex.

5.7 Implications for human spatial navigation

Rodent and fly navigation systems have been excellent model organisms for testing cellular and circuit properties of the HD system. Recent studies in the macaques have also recapitulated the properties of HD coding in the anterior thalamus (Laurens, Kim, Dickman, and Angelaki, 2016), and functional magnetic resonance imaging studies in humans have revealed several similarities in the cortical and thalamic HD encoding and use of landmarks for navigation (Auger, Mullally, and Maguire, 2012; Knight and Hayman, 2014; Shine, Valdés-Herrera, Hegarty, and Wolbers, 2016; Shine and Wolbers, 2021). The similarity in the HD tuning properties and the presence of analogous local circuit components, such as the reciprocal and global inhibition, between the fly brain and the rodent brain suggest that the implementation of the HD coding is at least partially conserved across species.

However, several features of long-range circuit organization are likely to be very different as a result of: 1) the organization and the weight of sensory systems processing in the different species, from the highly developed vestibular system in rodents versus the visual system in monkeys and humans versus the simpler visually-driven computations in the fly; 2) the complexity of spatial representations, memory capacity and the cognitive tasks that different species are able to carry. Given that humans, like macaques, heavily rely on vision, one would hypothesize that human navigation is likely to privilege landmark-based or route-following navigation rather than path integration, compared to more dark-dwelling animals such as rodents. However body-based cues do contribute to global-frame HD coding in human anterior thalamus (Shine, Valdés-Herrera, Hegarty, and Wolbers, 2016). Moreover, the commonly reported VR-induced motion sickness, even with stationary movement, over a prolonged period of time is suggestive of an accumulated mismatch between oculomotor and visual flow input with velocity integration, which is worse for uncalibrated VR headsets. Recent studies have applied Mobile Brain/Body Imaging technology to allow participants to move through virtual environments while high-density EEG were recorded (Do, Lin, and Gramann, 2021; Gramann, Hohlefeld, Gehrke, and Klug, 2021), an approach that can circumvent the limitations of functional magnetic imaging. Results from future investigations leveraging on this technology will be of particular interest toward understanding spatial, and non-spatial, memory processes in diseases such as Alzheimer's and developing targeted therapies.

Research in the spatial navigation field has profound implications for understanding human cognition in health and disease. Rodent models have played a tremendous role in the discovery of

the biological substrates of spatial cognition. Spatial deficits in human disease can range from general disorientation to memory formation and recall, to inability to form spatial maps, use of landmarks or understand links between routes and goal locations. Such deficits in humans can emerge following stroke or focal brain lesions (Maguire, Burke, Phillips, and Staunton, 1996) or be symptoms of cognitive disorders such as Schizophrenia and neurodegenerative disorders such as Alzheimer's disease (Coughlan, Laczó, Hort, Minihane, and Hornberger, 2018). In the early stages of AD, the brain regions associated with HD computations from AV and visual inputs are the first to be affected (Baloyannis, Mavroudis, Baloyannis, and Costa, 2016; Grossi, Lopez, and Martinez, 1989; Nestor, Fryer, Ikeda, and Hodges, 2003), with profound effects on memory and cognitive mapping. To this date, the mechanisms that lead to the disruption of neuronal activity in these regions are still unknown, but these studies have further brought attention to the link between visual space-heading computations occurring in these regions and memory processes. Recently, therapies based on virtual reality training have also been shown to enhance spatial-motor coordination and alleviate the spatial disorientation seen in patients with brain damage (Kober, Wood, Hofer, Kreuzig, Kiefer, and Neuper, 2013). Altogether, research in the mechanisms underlying visual control of the HD signal and the intrinsic circuit architecture that shapes these codes can have a great impact on designing treatments that can alleviate spatial deficits.

Bibliography

Aggleton, J.P., Nelson, A.J.D., 2015. Why do lesions in the rodent anterior thalamic nuclei cause such severe spatial deficits? Neurosci. Biobehav. Rev. 54, 131–144. https://doi.org/10.1016/j.neubiorev.2014.08.013

Aggleton, J.P., O'Mara, S.M., Vann, S.D., Wright, N.F., Tsanov, M., Erichsen, J.T., 2010. Hippocampal-anterior thalamic pathways for memory: Uncovering a network of direct and indirect actions. Eur. J. Neurosci. 31, 2292–2307. https://doi.org/10.1111/j.1460-9568.2010.07251.x

Ajabi, Z., Keinath, A.T., Wei, X.-X., Brandon, M.P., 2021. Population dynamics of the thalamic head direction system during drift and reorientation. bioRxiv 1–53.

Alexander, A.S., Carstensen, L.C., Hinman, J.R., Raudies, F., Chapman, W.G., Hasselmo, M.E., 2020. Egocentric boundary vector tuning of the retrosplenial cortex. Sci. Adv. 6. https://doi.org/10.1126/sciadv.aaz2322

Alexander, A.S., Nitz, D.A., 2017. Spatially Periodic Activation Patterns of Retrosplenial Cortex Encode Route Sub-spaces and Distance Traveled. Curr. Biol. 27, 1551-1560.e4. https://doi.org/10.1016/j.cub.2017.04.036

Alexander, A.S., Nitz, D.A., 2015. Retrosplenial cortex maps the conjunction of internal and external spaces. Nat. Neurosci. 18, 1143–1151. https://doi.org/10.1038/nn.4058

Allen, G. V., Hopkins, D.A., 1988. Mamillary body in the rat: A cytoarchitectonic, golgi, and ultrastructural study. J. Comp. Neurol. 275, 39–64. https://doi.org/10.1002/cne.902750105

Allen, G. V, Hopkins, D.A., 1989. Mamillary body in the rat: Topography and synaptology of projections from the subicular complex, prefrontal cortex, and midbrain tegmentum. J. Comp. Neurol. 286, 311–336. https://doi.org/10.1002/cne.902860303

Anastasiades, P.G., Collins, D.P., Carter, A.G., 2021. Mediodorsal and Ventromedial Thalamus Engage Distinct L1 Circuits in the Prefrontal Cortex. Neuron 109, 314-330.e4. https://doi.org/10.1016/j.neuron.2020.10.031

Angelaki, D.E., Laurens, J., 2020. The head direction cell network: attractor dynamics, integration within the navigation system, and three-dimensional properties. Curr. Opin. Neurobiol. 60, 136–144. https://doi.org/10.1016/j.conb.2019.12.002

Angelaki, D.E., Ng, J., Abrego, A.M., Cham, H.X., Asprodini, E.K., Dickman, J.D., Laurens, J., 2020. A gravity-based three-dimensional compass in the mouse brain. Nat. Commun. 11. https://doi.org/10.1038/s41467-020-15566-5

Auger, S.D., Maguire, E.A., 2017. Dissociating Landmark Stability from Orienting Value Using

Functional Magnetic Resonance Imaging. J. Cogn. Neurosci. 139. https://doi.org/10.1162/jocn_a_01231

Auger, S.D., Mullally, S.L., Maguire, E.A., 2012. Retrosplenial cortex codes for permanent landmarks. PLoS One 7. https://doi.org/10.1371/journal.pone.0043620

Auger, S.D., Zeidman, P., Maguire, E.A., 2017. Efficacy of navigation may be influenced by retrosplenial cortex-mediated learning of landmark stability. Neuropsychologia 104, 102–112. https://doi.org/10.1016/j.neuropsychologia.2017.08.012

Baloyannis, S.J., Mavroudis, I., Baloyannis, I.S., Costa, V.G., 2016. Mammillary Bodies in Alzheimer's Disease: A Golgi and Electron Microscope Study. Am. J. Alzheimers. Dis. Other Demen. 31, 247–256. https://doi.org/10.1177/1533317515602548

Banino, A. et al., 2018. Vector-based navigation using grid-like representations in artificial agents. Nature 26. https://doi.org/10.1038/s41586-018-0102-6

Barry, C., Burgess, N., 2014. Neural mechanisms of self-location. Curr. Biol. 24, R330-9. https://doi.org/10.1016/j.cub.2014.02.049

Barthó, P., Hirase, H., Monconduit, L., Zugaro, M., Harris, K.D., Buzsáki, G., 2004. Characterization of neocortical principal cells and interneurons by network interactions and extracellular features. J. Neurophysiol. 92, 600–608. https://doi.org/10.1152/jn.01170.2003

Bassett, J.P., Tullman, M.L., Taube, J.S., 2007. Lesions of the Tegmentomammillary Circuit in the Head Direction System Disrupt the Head Direction Signal in the Anterior Thalamus. J. Neurosci. 27, 7564–7577.

Ben-Yishay, E., Krivoruchko, K., Ron, S., Ulanovsky, N., Derdikman, D., Gutfreund, Y., 2021. Directional tuning in the hippocampal formation of birds. Curr. Biol. 31, 2592-2602.e4. https://doi.org/10.1016/j.cub.2021.04.029

Berens, P., 2009. CircStat: A MATLAB Toolbox for Circular Statistics. J. Stat. Softw. 31. https://doi.org/10.18637/jss.v031.i10

Bicanski, A., Burgess, N., 2018. A neural-level model of spatial memory and imagery. Elife 7. https://doi.org/10.7554/eLife.33752

Bicanski, A., Burgess, N., 2016. Environmental Anchoring of Head Direction in a Computational Model of Retrosplenial Cortex. J. Neurosci. 36, 11601–11618. https://doi.org/10.1523/JNEUROSCI.0516-16.2016

Bjerknes, T.L., Langston, R.F., Kruge, I.U., Moser, E.I., Moser, M.B., 2015. Coherence among head direction cells before eye opening in rat pups. Curr. Biol. 25, 103–108. https://doi.org/10.1016/j.cub.2014.11.009

Blair, H.T., Cho, J., Sharp, P.E., 1998. Role of the Lateral Mammillary Nucleus in the Rat Head Direction Circuit : A Combined Single Unit Recording and Lesion Study. Neuron 21, 1387–1397.

Blair, H.T., Lipscomb, B.W., Sharp, P.E., 1997. Anticipatory time intervals of head-direction cells in the anterior thalamus of the rat: Implications for path integration in the headdirection circuit. J. Neurophysiol. 78, 145–159. https://doi.org/10.1152/jn.1997.78.1.145

Blair, H.T., Sharp, P.E., 1995. Anticipatory head direction signals in anterior thalamus: evidence for a thalamocortical circuit that integrates angular head motion to compute head direction. J. Neurosci. 15, 6260–6270.

Boccara, C.N., Nardin, M., Stella, F., O'Neill, J., Csicsvari, J., 2019. The Entorhinal Cognitive Map is Attracted to Goals. Science (80-.). 1447, 1443–1447.

Boccara, C.N., Sargolini, F., Thoresen, V.H., Solstad, T., Witter, M.P., Moser, E.I., Moser, M.B., 2010. Grid cells in pre-and parasubiculum. Nat. Neurosci. 13, 987–994. https://doi.org/10.1038/nn.2602

Bonnevie, T., Dunn, B., Fyhn, M., Hafting, T., Derdikman, D., Kubie, J.L., Roudi, Y., Moser, E.I., Moser, M.B., 2013. Grid cells require excitatory drive from the hippocampus. Nat. Neurosci. 16, 309–317. https://doi.org/10.1038/nn.3311

Born, G., Schneider-Soupiadis, F.A., Erisken, S., Vaiceliunaite, A., Lao, C.L., Mobarhan, M.H., Spacek, M.A., Einevoll, G.T., Busse, L., 2021. Corticothalamic feedback sculpts visual spatial integration in mouse thalamus. Nat. Neurosci. 24, 1711–1720. https://doi.org/10.1038/s41593-021-00943-0

Boucheny, C., Brunel, N., Arleo, A., 2005. A continuous attractor network model without recurrent excitation: Maintenance and integration in the head direction cell system. J. Comput. Neurosci. 18, 205–227. https://doi.org/10.1007/s10827-005-6559-y

Brandon, M.P., Boogard, A.R., Schultheiss, N.W., Hasselmo, M.E., 2013. Segregation of cortical head direction cell assemblies on alternating theta cycles. Nat. Neurosci. 16, 739–748. https://doi.org/10.1038/nn.3383

Brennan, E.K.W., Jedrasiak-Cape, I., Kailasa, S., Rice, S.P., Sudhakar, S.K., Ahmed, O.J., 2021. Thalamus and claustrum control parallel layer 1 circuits in retrosplenial cortex. Elife 10, 1–42. https://doi.org/10.7554/eLife.62207

Burak, Y., Fiete, I.R., 2009. Accurate path integration in continuous attractor network models of grid cells. PLoS Comput. Biol. 5. https://doi.org/10.1371/journal.pcbi.1000291

Burgess, N., Barry, C., O'Keefe, J., 2009. An oscillatory interference model of grid cell firing. Hippocampus 17, 801–812. https://doi.org/10.1002/hipo.20327.An

Butler, W.N., Hardcastle, K., Giocomo, L.M., 2019. Remembered reward locations restructure entorhinal spatial maps. Science (80-.). 363, 1447–1452. https://doi.org/10.1126/science.aav5297

Butler, W.N., Smith, K.S., van der Meer, M.A.A., Taube, J.S., 2017. The Head-Direction Signal Plays a Functional Role as a Neural Compass during Navigation. Curr. Biol. 27, 1259–1267. https://doi.org/10.1016/j.cub.2017.03.033

Buzsáki, G., 2015. Hippocampal sharp wave-ripple: A cognitive biomarker for episodic memory and planning. Hippocampus 25, 1073–1188. https://doi.org/10.1002/hipo.22488

Buzsáki, G., 2002. Theta oscillations in the hippocampus. Neuron 33, 325–340. https://doi.org/10.1016/S0896-6273(02)00586-X

Byrne, P., Becker, S., Burgess, N., 2007. Remembering the past and imagining the future: a neural model of spatial memory and imagery. Psychol. Rev. 114, 340–75. https://doi.org/10.1037/0033-295X.114.2.340

Calton, J.L., Stackman, R.W., Goodridge, J.P., Archey, W.B., Dudchenko, P.A., Taube, J.S., 2003. Hippocampal place cell instability after lesions of the head direction cell network. J. Neurosci. 23, 9719–9731. https://doi.org/23/30/9719 [pii]

Campbell, M.G., Ocko, S.A., Mallory, C.S., Low, I.I.C., Ganguli, S., Giocomo, L.M., 2018. Principles governing the integration of landmark and self-motion cues in entorhinal cortical codes for navigation. Nat. Neurosci. 21, 1096–1106. https://doi.org/10.1038/s41593-018-0189-y

Chaudhuri, R., Gerçek, B., Pandey, B., Peyrache, A., Fiete, I., 2019. The intrinsic attractor manifold and population dynamics of a canonical cognitive circuit across waking and sleep. Nat. Neurosci. 22, 1512–1520. https://doi.org/10.1038/s41593-019-0460-x

Chen, G., King, J. a, Burgess, N., O'Keefe, J., 2013. How vision and movement combine in the hippocampal place code. Proc. Natl. Acad. Sci. U. S. A. 110, 378–83. https://doi.org/10.1073/pnas.1215834110

Chen, L.L., Lin, L.H., Green, E.J., Barnes, C.A., McNaughton, B.L., 1994a. Head-direction cells in the rat posterior cortex - I. anatomical distribution and behavioral modulation. Exp. Brain Res. 101, 8–23. https://doi.org/10.1007/BF00243212

Chen, L.L., Lin, L.H., Green, E.J., Barnes, C.A., McNaughton, B.L., 1994b. Head-direction cells in the rat posterior cortex - II. Contributions of visual and ideothetic information to the directional firing. Exp. Brain Res. 101, 24–34. https://doi.org/10.1007/BF00243213

Cho, J., Sharp, P.E., 2001. Head direction, place, and movement correlates for cells in the rat retrosplenial cortex. Behav. Neurosci. 115, 3–25. https://doi.org/10.1037/0735-7044.115.1.3

Chung, J.E., Magland, J.F., Barnett, A.H., Tolosa, V.M., Tooker, A.C., Lee, K.Y., Shah, K.G., Felix, S.H., Frank, L.M., Greengard, L.F., 2017. A Fully Automated Approach to Spike Sorting. Neuron 95, 1381-1394.e6. https://doi.org/10.1016/j.neuron.2017.08.030

Clark, B.J., Bassett, J.P., Wang, S.S., Taube, J.S., 2010. Impaired head direction cell representation in the anterodorsal thalamus after lesions of the retrosplenial cortex. J. Neurosci. 30, 5289–302. https://doi.org/10.1523/JNEUROSCI.3380-09.2010

Clark, B.J., Brown, J.E., Taube, J.S., 2012. Head direction cell activity in the anterodorsal thalamus requires intact supragenual nuclei. J. Neurophysiol. 108, 2767–2784. https://doi.org/10.1152/jn.00295.2012

Clark, B.J., Simmons, C.M., Berkowitz, L.E., Wilber, A.A., 2019. The Retrosplenial-Parietal Network and Reference Frame Coordination for Spatial Navigation. Behav. Neurosci. 132, 416–429. https://doi.org/10.1037/bne0000260.The

Clark, B.J., Taube, J.S., 2012. Vestibular and attractor network basis of the head direction cell signal in subcortical circuits. Front. Neural Circuits 6, 7. https://doi.org/10.3389/fncir.2012.00007

Colgin, L.L., 2016. Rhythms of the hippocampal network. Nat. Rev. Neurosci. 17, 239–249. https://doi.org/10.1038/nrn.2016.21

Commins, S., Fey, D., 2019. Understanding the role of distance, direction and cue salience in an associative model of landmark learning. Sci. Rep. 9, 1–13. https://doi.org/10.1038/s41598-019-38525-7

Connelly, W.M., Laing, M., Errington, A.C., Crunelli, V., 2016. The Thalamus as a Low Pass Filter: Filtering at the Cellular Level does Not Equate with Filtering at the Network Level. Front. Neural Circuits 9, 1–10. https://doi.org/10.3389/fncir.2015.00089

Corcoran, K. a, Frick, B.J., Radulovic, J., Kay, L.M., 2016. Analysis of coherent activity between retrosplenial cortex, hippocampus, thalamus, and anterior cingulate cortex during retrieval of recent and remote context fear memory. Neurobiol. Learn. Mem. 127, 93–101. https://doi.org/10.1016/j.nlm.2015.11.019

Coughlan, G., Laczó, J., Hort, J., Minihane, A.M., Hornberger, M., 2018. Spatial navigation deficits — Overlooked cognitive marker for preclinical Alzheimer disease? Nat. Rev. Neurol. 14, 496–506. https://doi.org/10.1038/s41582-018-0031-x

Crandall, S.R., Cruikshank, S.J., Connors, B.W., 2015. A Corticothalamic Switch: Controlling the Thalamus with Dynamic Synapses. Neuron 86, 768–782. https://doi.org/10.1016/j.neuron.2015.03.040

Cruikshank, S.J., Lewis, T.J., Connors, B.W., 2007. Synaptic basis for intense thalamocortical activation of feedforward inhibitory cells in neocortex. Nat. Neurosci. 10, 462–468.

https://doi.org/10.1038/nn1861

Cullen, K.E., Taube, J.S., 2017. Our sense of direction: Progress, controversies and challenges. Nat. Neurosci. https://doi.org/10.1038/nn.4658

Darwin, C., 1873. Origin of certain instincts. Nature 7, 417–418. https://doi.org/10.1038/007417a0

Diekelmann, S., Born, J., 2010. The memory function of sleep. Nat. Rev. Neurosci. 11, 114–126. https://doi.org/10.1038/nrn2762

Do, T.T.N., Lin, C.T., Gramann, K., 2021. Human brain dynamics in active spatial navigation. Sci. Rep. 11, 1–12. https://doi.org/10.1038/s41598-021-92246-4

Dräger, U.C., Olsen, J.F., 1980. Origins of crossed and uncrossed retinal projections in pigmented and albino mice. J. Comp. Neurol. 191, 383–412. https://doi.org/10.1002/cne.901910306

Duszkiewicz, A.J., Carrasco, S.S., Orhan, P., Brown, E., Owczarek, E., Vite, R., Wood, E.R., Peyrache, A., 2022. Reciprocal representation of encoded features by cortical excitatory and inhibitory neuronal populations . bioRxiv.

Ekstrom, A.D., Kahana, M.J., Caplan, J.B., Fields, T.A., Isham, E.A., Newman, E.L., Fried, I., 2003. Cellular networks underlying human spatial navigation. Nature 425, 184–187. https://doi.org/10.1038/nature01964

El Jundi, B., Warrant, E.J., Byrne, M.J., Khaldy, L., Baird, E., Smolka, J., Dacke, M., 2015. Neural coding underlying the cue preference for celestial orientation. Proc. Natl. Acad. Sci. U. S. A. 112, 11395–11400. https://doi.org/10.1073/pnas.1501272112

Elduayen, C., Save, E., 2014. The retrosplenial cortex is necessary for path integration in the dark. Behav. Brain Res. 272, 303–307. https://doi.org/10.1016/j.bbr.2014.07.009

Epstein, R.A., Patai, E.Z., Julian, J.B., Spiers, H.J., 2017. The cognitive map in humans: Spatial navigation and beyond. Nat. Neurosci. 20, 1504–1513. https://doi.org/10.1038/nn.4656

Etienne, A.S., Jeffery, K.J., 2004. Path integration in mammals. Hippocampus 14, 180–192. https://doi.org/10.1002/hipo.10173

Fallahnezhad, M., Méro, J. Le, Xhensjana, Z., Vincent, J., Rochefort, C., Rondi-Reig, L., 2021. Cerebellar Control of a Unitary Head Direction Sense. bioRxiv 6.

Finkelstein, A., Derdikman, D., Rubin, A., Foerster, J.N., Las, L., Ulanovsky, N., 2014. Three-dimensional head-direction coding in the bat brain. Nature 517, 159–164. https://doi.org/10.1038/nature14031

Finkelstein, A., Ulanovsky, N., Tsodyks, M., Aljadeff, J., 2018. Optimal dynamic coding by mixed-dimensionality neurons in the head-direction system of bats. Nat. Commun. 9.

https://doi.org/10.1038/s41467-018-05562-1

Fischer, L.F., Soto-Albors, R.M., Buck, F., Harnett, M.T., 2019. Representation of visual landmarks in retrosplenial cortex. Elife 1–25. https://doi.org/10.7554/eLife.51458

Fischler, W.M., Joshi, N.R., Devi-Chou, V., Kitch, L.J., Schnitzer, M.J., Abbott, L.F., Axel, R., 2019. Olfactory Landmarks and Path Integration Converge to Form a Cognitive Spatial Map. bioRxiv 752360. https://doi.org/10.1101/752360

Fisher, Y.E., Lu, J., D'Alessandro, I., Wilson, R.I., 2019. Sensorimotor experience remaps visual input to a heading-direction network. Nature 576. https://doi.org/10.1038/s41586-019-1772-4

Franconville, R., Beron, C., Jayaraman, V., 2018. Building a functional connectome of the drosophila central complex. Elife 7, 1–24. https://doi.org/10.7554/eLife.37017

Frost, B.E., Martin, S.K., Cafalchio, M., Islam, M.N., Aggleton, J.P., O'Mara, S.M., 2021. Anterior thalamic inputs are required for subiculum spatial coding, with associated consequences for hippocampal spatial memory. J. Neurosci. 41, 6511–6525. https://doi.org/10.1523/JNEUROSCI.2868-20.2021

Fuhs, M.C., Touretzky, D.S., 2006. A spin glass model of path integration in rat medial entorhinal cortex. J. Neurosci. 26, 4266–4276. https://doi.org/10.1523/JNEUROSCI.4353-05.2006

Fuhs, M.C., VanRhoads, S.R., Casale, A.E., McNaughton, B.L., Touretzky, D.S., 2005. Influence of path integration versus environmental orientation on place cell remapping between visually identical environments. J. Neurophysiol. 94, 2603–2616. https://doi.org/10.1152/jn.00132.2005

Fujisawa, S., Amarasingham, A., Harrison, M.T., Buzsáki, G., 2008. Behavior-dependent short-term assembly dynamics in the medial prefrontal cortex. Nat. Neurosci. 11, 823–833. https://doi.org/10.1038/nn.2134

Fusi, S., Miller, E.K., Rigotti, M., 2016. Why neurons mix: High dimensionality for higher cognition. Curr. Opin. Neurobiol. 37, 66–74. https://doi.org/10.1016/j.conb.2016.01.010

Fyhn, M., Hafting, T., Treves, A., Moser, M.-B., Moser, E.I., 2007. Hippocampal remapping and grid realignment in entorhinal cortex. Nature 446, 190–4. https://doi.org/10.1038/nature05601

Gent, T.C., Bandarabadi, M., Herrera, C.G., Adamantidis, A.R., 2018. Thalamic dual control of sleep and wakefulness. Nat. Neurosci. 21, 974–984. https://doi.org/10.1038/s41593-018-0164-7

Geva-Sagiv, M., Las, L., Yovel, Y., Ulanovsky, N., 2015. Spatial cognition in bats and rats: from sensory acquisition to multiscale maps and navigation. Nat. Rev. Neurosci. 16, 94–108.

https://doi.org/10.1038/nrn3888

Ginosar, G., Aljadeff, J., Burak, Y., Sompolinsky, H., Las, L., Ulanovsky, N., 2021. Locally ordered representation of 3D space in the entorhinal cortex, Nature. Springer US. https://doi.org/10.1038/s41586-021-03783-x

Giocomo, L.M., Stensola, T., Bonnevie, T., Van Cauter, T., Moser, M.B., Moser, E.I., 2014. Topography of head direction cells in medial entorhinal cortex. Curr. Biol. 24, 252–262. https://doi.org/10.1016/j.cub.2013.12.002

Golob, E.J., Taube, J.S., 1999. Head direction cells in rats with hippocampal or overlying neocortical lesions: Evidence for impaired angular path integration. J. Neurosci. 19, 7198–7211. https://doi.org/10.1523/jneurosci.19-16-07198.1999

Goodridge, J.P., Dudchenko, P.A., Worboys, K.A., Golob, E.J., Taube, J.S., 1998. Cue control and head direction cells. Behav. Neurosci. 112, 749–761. https://doi.org/10.1037/0735-7044.112.4.749

Goodridge, J.P., Taube, J.S., 1997. Interaction between the postsubiculum and anterior thalamus in the generation of head direction cell activity. J. Neurosci. 17, 9315–9330. https://doi.org/10.1523/jneurosci.17-23-09315.1997

Gramann, K., Hohlefeld, F.U., Gehrke, L., Klug, M., 2021. Human cortical dynamics during full-body heading changes. Sci. Rep. 11, 1–12. https://doi.org/10.1038/s41598-021-97749-8

Green, J., Adachi, A., Shah, K.K., Hirokawa, J.D., Magani, P.S., Maimon, G., 2017. A neural circuit architecture for angular integration in Drosophila. Nature 546, 101–106. https://doi.org/10.1038/nature22343

Grieves, R.M., Jedidi-Ayoub, S., Mishchanchuk, K., Liu, A., Renaudineau, S., Duvelle, É., Jeffery, K.J., 2021. Irregular distribution of grid cell firing fields in rats exploring a 3D volumetric space. Nat. Neurosci. 24, 1567–1573. https://doi.org/10.1038/s41593-021-00907-4

Grossi, D., Lopez, O.L., Martinez, A.J., 1989. Mamillary bodies in Alzheimer's disease. Acta Neurol. Scand. 80, 41–45. https://doi.org/10.1111/j.1600-0404.1989.tb03840.x

Guitchounts, G., Markowitz, J.E., Liberti, W.A., Gardner, T.J., 2013. A carbon-fiber electrode array for long-term neural recording. J. Neural Eng. 10. https://doi.org/10.1088/1741-2560/10/4/046016

Guitchounts, G., Masís, J., Wolff, S.B.E., Cox, D., 2020. Encoding of 3D Head Orienting Movements in the Primary Visual Cortex. Neuron 108, 512-525.e4. https://doi.org/10.1016/j.neuron.2020.07.014

Hafting, T., Fyhn, M., Molden, S., Moser, M.B., Moser, E.I., 2005. Microstructure of a spatial map in the entorhinal cortex. Nature 436, 801–806. https://doi.org/10.1038/nature03721

Hahnloser, R.H.R., 2003. Emergence of neural integration in the head-direction system by visual supervision. Neuroscience 120, 877–891. https://doi.org/10.1016/S0306-4522(03)00201-X

Halassa, M.M., Kastner, S., 2017. Thalamic functions in distributed cognitive control. Nat. Neurosci. 20, 1669–1679. https://doi.org/10.1038/s41593-017-0020-1

Halassa, M.M., Sherman, S.M., 2019. Thalamocortical Circuit Motifs: A General Framework. Neuron 103, 762–770. https://doi.org/10.1016/j.neuron.2019.06.005

Hanesch, U., Fischbach, K.F., Heisenberg, M., 1989. Neuronal architecture of the central complex in Drosophila melanogaster. Cell Tissue Res. 257, 343–366. https://doi.org/10.1007/BF00261838

Harnett, M.T., Magee, J.C., Williams, S.R., 2015. Distribution and function of HCN channels in the apical dendritic tuft of neocortical pyramidal neurons. J. Neurosci. 35, 1024–1037. https://doi.org/10.1523/JNEUROSCI.2813-14.2015

Harnett, M.T., Xu, N.L., Magee, J.C., Williams, S.R., 2013. Potassium channels control the interaction between active dendritic integration compartments in layer 5 cortical pyramidal neurons. Neuron 79, 516–529. https://doi.org/10.1016/j.neuron.2013.06.005

Harris, R.A., Graham, P., Collett, T.S., 2007. Visual Cues for the Retrieval of Landmark Memories by Navigating Wood Ants. Curr. Biol. 17, 93–102. https://doi.org/10.1016/j.cub.2006.10.068

Harvey, C.D., Svoboda, K., 2007. Locally dynamic synaptic learning rules in pyramidal neuron dendrites. Nature 450, 1195–1200. https://doi.org/10.1038/nature06416

Hasselmo, M.E., Bodelón, C., Wyble, B.P., 2002. A proposed function for hippocampal theta rhythm: Separate phases of encoding and retrieval enhance reversal of prior learning. Neural Comput. 14, 793–817. https://doi.org/10.1162/089976602317318965

Hennestad, E., Witoelar, A., Chambers, A.R., Vervaeke, K., 2021. Mapping vestibular and visual contributions to angular head velocity tuning in the cortex. Cell Rep. 37, 110134. https://doi.org/10.1016/j.celrep.2021.110134

Hindley, E.L., Nelson, a J.D., Aggleton, J.P., Vann, S.D., 2014. The rat retrosplenial cortex is required when visual cues are used flexibly to determine location. Behav. Brain Res. 263, 98–107. https://doi.org/10.1016/j.bbr.2014.01.028

Honkanen, A., Adden, A., Da Silva Freitas, J., Heinze, S., 2019. The insect central complex and the neural basis of navigational strategies. J. Exp. Biol. 222, 1–32. https://doi.org/10.1242/jeb.188854

Hori, E., Nishio, Y., Kazui, K., Umeno, K., Tabuchi, E., Sasaki, K., Endo, S., Ono, T., Nishijo, H., 2005. Place-related neural responses in the monkey hippocampal formation in a virtual space. Hippocampus 15, 991–996. https://doi.org/10.1002/hipo.20108

Høydal, Ø.A., Skytøen, E.R., Andersson, S.O., Moser, M.B., Moser, E.I., 2019. Object-vector coding in the medial entorhinal cortex. Nature. https://doi.org/10.1038/s41586-019-1077-7

Huang, L.W., Simonnet, J., Nassar, M., Richevaux, L., Lofredi, R., Fricker, D., 2017. Laminar localization and projection-specific properties of presubicular neurons targeting the lateral mammillary nucleus, thalamus, or medial entorhinal cortex. eNeuro 4, 1–11. https://doi.org/10.1523/ENEURO.0370-16.2017

Iacaruso, M.F., Gasler, I.T., Hofer, S.B., 2017. Synaptic organization of visual space in primary visual cortex. Nature 547, 449–452. https://doi.org/10.1038/nature23019

Jacob, P.-Y., Casali, G., Spieser, L., Page, H., Overington, D., Jeffery, K., 2017. An independent, landmark-dominated head-direction signal in dysgranular retrosplenial cortex. Nat. Neurosci. 20, 173–175. https://doi.org/10.1038/nn.4465

Jacobs, J. et al., 2013. Direct recordings of grid-like neuronal activity in human spatial navigation. Nat. Neurosci. 16, 1188–1190. https://doi.org/10.1038/nn.3466

Jankowski, M.M., Ronnqvist, K.C., Tsanov, M., Vann, S.D., Wright, N.F., Erichsen, J.T., Aggleton, J.P., O'Mara, S.M., 2013. The anterior thalamus provides a subcortical circuit supporting memory and spatial navigation. Front. Syst. Neurosci. 7, 45. https://doi.org/10.3389/fnsys.2013.00045

Jayakumar, R.P., Madhav, M.S., Savelli, F., Blair, H.T., Cowan, N.J., Knierim, J.J., 2019. Recalibration of path integration in hippocampal place cells. Nature. https://doi.org/10.1038/s41586-019-0939-3

Jeffery, K.J., 1998. Learning of landmark stability and instability by hippocampal place cells. Neuropharmacology 37, 677–687.

Jeffery, K.J., Page, H.J.I., Stringer, S.M., 2016. Optimal cue combination and landmark-stability learning in the head direction system. J. Physiol. 594, 6527–6534. https://doi.org/10.1113/JP272945

Jenkins, T.A., Vann, S.D., Amin, E., Aggleton, J.P., 2004. Anterior thalamic lesions stop immediate early gene activation in selective laminae of the retrosplenial cortex: Evidence of covert pathology in rats? Eur. J. Neurosci. 19, 3291–3304. https://doi.org/10.1111/j.0953-816X.2004.03421.x

Ji, D., Wilson, M.A., 2007. Coordinated memory replay in the visual cortex and hippocampus during sleep. Nat. Neurosci. 10, 100–107. https://doi.org/10.1038/nn1825

Jones, E.G., 2007. The Thalamus. Cambridge University Press.

Jones, M.W., Wilson, M.A., 2005. Theta rhythms coordinate hippocampal-prefrontal interactions in a spatial memory task. PLoS Biol. 3, 1–13. https://doi.org/10.1371/journal.pbio.0030402

Ju, N., Li, Y., Liu, F., Jiang, H., Macknik, S.L., Martinez-Conde, S., Tang, S., 2020. Spatiotemporal functional organization of excitatory synaptic inputs onto macaque V1 neurons. Nat. Commun. 11. https://doi.org/10.1038/s41467-020-14501-y

Kay, K., Chung, J.E., Sosa, M., Schor, J.S., Karlsson, M.P., Larkin, M.C., Liu, D.F., Frank, L.M., 2020. Constant Sub-second Cycling between Representations of Possible Futures in the Hippocampus. Cell 180, 552-567.e25. https://doi.org/10.1016/j.cell.2020.01.014

Keshavarzi, S., Bracey, E.F., Faville, R.A., Campagner, D., Tyson, A.L., Lenzi, S.C., Branco, T., Margrie, roy W., 2021. Multisensory coding of angular head velocity in the retrosplenial cortex. Neuron 1–12. https://doi.org/10.1016/j.neuron.2021.10.031

Kheradmand, B., Nieh, J.C., 2019. The role of landscapes and landmarks in bee navigation: A review. Insects 10. https://doi.org/10.3390/insects10100342

Kim, M., Maguire, E.A., 2019. Encoding of 3D head direction information in the human brain. Hippocampus 29, 619–629. https://doi.org/10.1002/hipo.23060

Kim, S.S., Hermundstad, A.M., Romani, S., Abbott, L.F., Jayaraman, V., 2019. Generation of stable heading representations in diverse visual scenes. Nature 576. https://doi.org/10.1038/s41586-019-1767-1

Kim, S.S., Rouault, H., Druckmann, S., Jayaraman, V., 2017. Ring attractor dynamics in the Drosophila central brain. Science (80-.). 356, 849–853. https://doi.org/10.1126/science.aal4835

Klukas, M., Lewis, M., Fiete, I., 2020. Efficient and flexible representation of higher-dimensional cognitive variables with grid cells. PLoS Comput. Biol. 16, 1–15. https://doi.org/10.1371/journal.pcbi.1007796

Knierim, J.J., Kudrimoti, H.S., Mcnaughton, B.L., 1995. Place Cells , Head Direction Cells , and the Learning of Landmark Stability. J. Neurosci. 15, 1648–1659.

Knierim, J.J., Kudrimoti, H.S., McNaughton, B.L., 1998. Interactions Between Idiothetic Cues and External Landmarks in the Control of Place Cells and Head Direction Cells. J. Neurophysiol. 80, 425–446. https://doi.org/10.1152/jn.1998.80.1.425

Knierim, J.J., Zhang, K., 2012. Attractor dynamics of spatially correlated neural activity in the limbic system. Annu. Rev. Neurosci. 35, 267–85. https://doi.org/10.1146/annurev-neuro-062111-150351

Knight, R., Hayman, R., 2014. Allocentric directional processing in the rodent and human retrosplenial cortex. Front. Hum. Neurosci. 8, 1–5. https://doi.org/10.3389/fnhum.2014.00135

Knight, R., Piette, C.E., Page, H., Walters, D., Marozzi, E., Nardini, M., Stringer, S., Jeffery, K.J.,

2014. Weighted cue integration in the rodent head direction system. Philos. Trans. R. Soc. B Biol. Sci. 369. https://doi.org/10.1098/rstb.2012.0512

Kober, S.E., Wood, G., Hofer, D., Kreuzig, W., Kiefer, M., Neuper, C., 2013. Virtual reality in neurologic rehabilitation of spatial disorientation. J. Neuroeng. Rehabil. 10, 1–13. https://doi.org/10.1186/1743-0003-10-17

Kononenko, N.L., Witter, M.P., 2012. Presubiculum layer III conveys retrosplenial input to the medial entorhinal cortex. Hippocampus 22, 881–895. https://doi.org/10.1002/hipo.20949

Kornienko, O., Latuske, P., Bassler, M., Kohler, L., Allen, K., 2018. Non-rhythmic head-direction cells in the parahippocampal region are not constrained by attractor network dynamics. Elife 7, 1–25. https://doi.org/10.7554/elife.35949

Krapp, H.G., 2007. Polarization Vision: How Insects Find Their Way by Watching the Sky. Curr. Biol. 17, 557–560. https://doi.org/10.1016/j.cub.2007.05.007

Kropff, E., Carmichael, J.E., Moser, M.B., Moser, E.I., 2015. Speed cells in the medial entorhinal cortex. Nature 523, 419–424. https://doi.org/10.1038/nature14622

Kulkarni, M., Zhang, K., Kirkwood, A., 2011. Single-cell persistent activity in anterodorsal thalamus. Neurosci. Lett. 498, 179–84. https://doi.org/10.1016/j.neulet.2011.02.051

LaChance, P.A., Todd, T.P., Taube, J.S., 2019. A sense of space in postrhinal cortex. Science (80-.). 365. https://doi.org/10.1126/science.aax4192

Lafourcade, M., Van Der Goes, M.H., Vardalaki, D., Brown, N.J., Voigts, J., Yun, D.H., Kim, M.E., Ku, T., Harnett, M.T., 2022. Differential dendritic integration of long-range inputs in association cortex via subcellular changes in synaptic AMPA-to-NMDA receptor ratio. Neuron 1–15. https://doi.org/10.1016/j.neuron.2022.01.025

Langston, R.F., Ainge, J.A., Couey, J.J., Canto, C.B., Bjerknes, T.L., Witter, M.P., Moser, E.I., Moser, M.-B., 2010. Development of the Spatial Representation System in the Rat. Science (80-.). 328. https://doi.org/10.1017/cbo9781139167291.033

Laurens, J., Abrego, A., Cham, H., Popeney, B., Yu, Y., Rotem, N., Aarse, J., Asprodini, E.K., Dickman, J.D., Angelaki, D.E., 2019. Multiplexed code of navigation variables in anterior limbic areas. bioRxiv 684464. https://doi.org/10.1101/684464

Laurens, J., Angelaki, D.E., 2019. A model-based reassessment of the three-dimensional tuning of head direction cells in rats. J. Neurophysiol. 122, 1274–1287. https://doi.org/10.1152/jn.00136.2019

Laurens, J., Angelaki, D.E., 2018. The Brain Compass: A Perspective on How Self-Motion Updates the Head Direction Cell Attractor. Neuron 97, 275–289. https://doi.org/10.1016/j.neuron.2017.12.020

Laurens, J., Kim, B., Dickman, J.D., Angelaki, D.E., 2016. Gravity orientation tuning in macaque anterior thalamus. Nat. Neurosci. 19, 1566–1568. https://doi.org/10.1038/nn.4423

Lee, A.K., Wilson, M.A., 2002. Memory of sequential experience in the hippocampus during slow wave sleep. Neuron 36, 1183–1194. https://doi.org/10.1016/S0896-6273(02)01096-6

Lever, C., Burton, S., Jeewajee, A., O'Keefe, J., Burgess, N., 2009. Boundary vector cells in the subiculum of the hippocampal formation. J. Neurosci. 29, 9771–9777. https://doi.org/10.1523/JNEUROSCI.1319-09.2009

Lewis, L.D., Voigts, J., Flores, F.J., Ian Schmitt, L., Wilson, M.A., Halassa, M.M., Brown, E.N., 2015. Thalamic reticular nucleus induces fast and local modulation of arousal state. Elife 4, 1–23. https://doi.org/10.7554/eLife.08760

Lohmann, K.J., Lohmann, C.M.F., Ehrhart, L.M., Bagley, D.A., Swing, T., 2004. Geomagnetic map used in sea-turtle navigation. Nature 428, 909–910. https://doi.org/10.1038/428909a

Lomi, E., Mathiasen, M.L., Cheng, H.Y., Zhang, N., Aggleton, J.P., Mitchell, A.S., Jeffery, K., 2021. Evidence for two Distinct Thalamocortical Circuits in Retrosplenial Cortex. Neurobiol. Learn. Mem. 185, 6. https://doi.org/https://doi.org/10.1016/j.nlm.2021.107525

Long, X., Young, C.K., Zhang, S.J., 2020. Sharp tuning of head direction by somatosensory fast-spiking interneurons. bioRxiv.

Lopes, G. et al., 2015. Bonsai: An event-based framework for processing and controlling data streams. Front. Neuroinform. 9, 1–14. https://doi.org/10.3389/fninf.2015.00007

Lozano, Y.R., Page, H., Jacob, P.-Y., Lomi, E., Street, J., Jeffery, K., 2017. Retrosplenial and postsubicular head direction cells compared during visual landmark discrimination. Brain Neurosci. Adv. 1, 239821281772185. https://doi.org/10.1177/2398212817721859

Maguire, E.A., 2001. The retrosplenial contributions to human navigation: A review of lesion and neuroimaging findings. Scand. J. Psychol. 225–238.

Maguire, E.A., Burke, T., Phillips, J., Staunton, H., 1996. Topographical disorientation following unilateral temporal lobe lesions in humans. Neuropsychologia 34, 993–1001. https://doi.org/https://doi.org/10.1016/0028-3932(96)00022-X

Manita, S. et al., 2015. A Top-Down Cortical Circuit for Accurate Sensory Perception. Neuron 86, 1304–1316. https://doi.org/10.1016/j.neuron.2015.05.006

Mante, V., Sussillo, D., Shenoy, K. V., Newsome, W.T., 2013. Context-dependent computation by recurrent dynamics in prefrontal cortex. Nature 503, 78–84. https://doi.org/10.1038/nature12742

Mao, D., Kandler, S., McNaughton, B.L., Bonin, V., 2017a. Sparse orthogonal population

representation of spatial context in the retrosplenial cortex. Nat. Commun. 8, 243. https://doi.org/10.1038/s41467-017-00180-9

Mao, D., Kandler, S., McNaughton, B.L., Bonin, V., 2017b. Sparse orthogonal population representation of spatial context in the retrosplenial cortex. Nat. Commun. 8, 243. https://doi.org/10.1038/s41467-017-00180-9

Mao, D., Molina, L.A., Bonin, V., McNaughton, B.L., 2020. Vision and Locomotion Combine to Drive Path Integration Sequences in Mouse Retrosplenial Cortex. Curr. Biol. 30, 1680-1688.e4. https://doi.org/10.1016/j.cub.2020.02.070

Marchette, S.A., Vass, L.K., Ryan, J., Epstein, R.A., 2014. Anchoring the neural compass: Coding of local spatial reference frames in human medial parietal lobe. Nat. Neurosci. 17, 1598–1606. https://doi.org/10.1038/nn.3834

Mcnaughton, B.L. et al., 1996. Deciphering the hippocampal polyglot: The hippocampus as a path integration system. J. Exp. Biol. 199, 173–185. https://doi.org/10.1242/jeb.199.1.173

McNaughton, B.L., Battaglia, F.P., Jensen, O., Moser, E.I., Moser, M.-B., 2006. Path integration and the neural basis of the "cognitive map". Nat. Rev. Neurosci. 7, 663–78. https://doi.org/10.1038/nrn1932

Miller, A.M.P., Mau, W., Smith, D.M., 2019. Retrosplenial Cortical Representations of Space and Future Goal Locations Develop with Learning. Curr. Biol. 29, 2083-2090.e4. https://doi.org/10.1016/j.cub.2019.05.034

Miller, A.M.P., Vedder, L.C., Law, L.M., Smith, D.M., 2014. Cues, context, and long-term memory: the role of the retrosplenial cortex in spatial cognition. Front. Hum. Neurosci. 8, 1–15. https://doi.org/10.3389/fnhum.2014.00586

Miller, J.F. et al., 2013. Neural activity in human hippocampal formation reveals the spatial context of retrieved memories. Science (80-.). 342, 1111–1114. https://doi.org/10.1126/science.1244056

Mitchell, A.S., Czajkowski, R., Zhang, N., Jeffery, K., Nelson, A.J.D., 2018. Retrosplenial cortex and its role in spatial cognition. Brain Neurosci. Adv. 2, 239821281875709. https://doi.org/10.1177/2398212818757098

Mitchell, A.S., Dalrymple-Alford, J.C., 2006. Lateral and anterior thalamic lesions impair independent memory systems. Learn. Mem. 13, 388–396. https://doi.org/10.1101/lm.122206

Mittelstaedt, M.L., Mittelstaedt, H., 1980. Homing by path integration in a mammal. Naturwissenschaften 67, 566–567. https://doi.org/10.1007/BF00450672

Mizumori, S.J., Williams, J.D., 1993. Directionally selective mnemonic properties of neurons in the lateral dorsal nucleus of the thalamus of rats. J. Neurosci. 13, 4015–4028.

Muir, G.M., Brown, J.E., Carey, J.P., Hirvonen, T.P., DellaSantina, C.C., Minor, L.B., Taube, J.S., 2009. Disruption of the Head Direction Cell Signal after Occlusion of the Semicircular Canals in the Freely Moving Chinchilla. J. Neurosci. 29, 14521–14533. https://doi.org/10.1523/JNEUROSCI.3450-09.2009

Müller, M., Wehner, R., 1988. Path integration in desert ants, Cataglyphis fortis . Proc. Natl. Acad. Sci. 85, 5287–5290. https://doi.org/10.1073/pnas.85.14.5287

Muller, R.U., Kubie, J.L., 1987. The effects of changes in the environment on the spatial firing of hippocampal complex-spike cells. J. Neurosci. 7, 1951–1968. https://doi.org/10.1523/jneurosci.07-07-01951.1987

Muller, R.U., Ranck, J.B., Taube, J.S., 1996. Head direction cells: Properties and functional significance. Curr. Opin. Neurobiol. 6, 196–206. https://doi.org/10.1016/S0959-4388(96)80073-0

Nassar, M., Simonnet, J., Huang, L.W., Mathon, B., Cohen, I., Bendels, M.H.K., Beraneck, M., Miles, R., Fricker, D., 2018. Anterior thalamic excitation and feedforward inhibition of presubicular neurons projecting to medial entorhinal cortex. J. Neurosci. 38, 6411–6425. https://doi.org/10.1523/JNEUROSCI.0014-18.2018

Nestor, P.J., Fryer, T.D., Ikeda, M., Hodges, J.R., 2003. Retrosplenial cortex (BA 29/30) hypometabolism in mild cognitive impairment (prodromal Alzheimer's disease). Eur. J. Neurosci. 18, 2663–2667. https://doi.org/10.1046/j.1460-9568.2003.02999.x

Newman, J.P., 2020. Twister3: a simple and fast microwire twister. J. Neural Eng. https://doi.org/doi:10.1088/1741-2552/ab77fa

Newman, J.P., Voigts, J., Zhang, J., Kemere, C., Dakin, P., Manders, T., Rosen, Z., 2019. jonnew/open-ephys-pcie: Release 1.0.0. Zenodo. https://doi.org/doi:10.5281/zenodo.3254431

Nitzan, N., McKenzie, S., Beed, P., English, D.F., Oldani, S., Tukker, J.J., Buzsáki, G., Schmitz, D., 2020. Propagation of hippocampal ripples to the neocortex by way of a subiculum-retrosplenial pathway. Nat. Commun. 11. https://doi.org/10.1038/s41467-020-15787-8

O'Keefe, J., Dostrovsky, J., 1971. The hippocampus as a spatial map. Preliminary evidence from unit activity in the freely-moving rat. Brain Res. 34, 171–175. https://doi.org/10.1016/0006-8993(71)90358-1

Page, H.J.I., Jeffery, K.J., 2018. Landmark-based updating of the head direction system by retrosplenial cortex: A computational model. Front. Cell. Neurosci. 12, 1–17. https://doi.org/10.3389/fncel.2018.00191

Page, H.J.I., Walters, D.M., Knight, R., Piette, C.E., Jeffery, K.J., Stringer, S.M., 2014. A theoretical account of cue averaging in the rodent head direction system. Philos. Trans. R.

Soc. B Biol. Sci. 369. https://doi.org/10.1098/rstb.2013.0283

Park, E.H., Keeley, S., Savin, C., Ranck, J.B., Fenton, A.A., 2019. How the Internally Organized Direction Sense Is Used to Navigate. Neuron 101, 285-293.e5. https://doi.org/10.1016/j.neuron.2018.11.019

Pauzin, F.P., Krieger, P., 2018. A Corticothalamic Circuit for Refining Tactile Encoding. Cell Rep. 23, 1314–1325. https://doi.org/10.1016/j.celrep.2018.03.128

Payne, H.L., Lynch, G.F., Aronov, D., 2021. Neural representations of space in the hippocampus of a food-caching bird. Science (80-.). 373, 343–348. https://doi.org/10.1126/science.abg2009

Peters, A., Feldman, M.L., 1976. The projection of the lateral geniculate nucleus to area 17 of the rat cerebral cortex. I. General description. J. Neurocytol. 5, 63–84. https://doi.org/10.1007/BF01176183

Petreanu, L., Mao, T., Sternson, S.M., Svoboda, K., 2009. The subcellular organization of neocortical excitatory connections, Supplementary Information. Nature 457, 1142–5. https://doi.org/10.1038/nature07709

Petrof, I., Sherman, S.M., 2009. Synaptic properties of the mammillary and cortical afferents to the anterodorsal thalamic nucleus in the mouse. J. Neurosci. 29, 7815–7819. https://doi.org/10.1523/JNEUROSCI.1564-09.2009

Peyrache, A., Duszkiewicz, A.J., Viejo, G., Angeles-Duran, S., 2019. Thalamocortical processing of the head-direction sense. Prog. Neurobiol. 183, 101693. https://doi.org/10.1016/j.pneurobio.2019.101693

Peyrache, A., Lacroix, M.M., Petersen, P.C., Buzsaki, G., 2015. Internally organized mechanisms of the head direction sense. Nat Neurosci 18, 569–575. https://doi.org/10.1038/s41583-019-0153-1

Peyrache, A., Schieferstein, N., Buzsáki, G., 2017. Transformation of the head-direction signal into a spatial code. Nat. Commun. 8. https://doi.org/10.1038/s41467-017-01908-3

Pisokas, I., Heinze, S., Webb, B., 2020. The head direction circuit of two insect species. Elife 9, 1–49. https://doi.org/10.7554/eLife.53985

Pothuizen, H.H.J., Aggleton, J.P., Vann, S.D., 2008. Do rats with retrosplenial cortex lesions lack direction? Eur. J. Neurosci. 28, 2486–2498. https://doi.org/10.1111/j.1460-9568.2008.06550.x

Powell, A., Connelly, W.M., Vasalauskaite, A., Nelson, A.J.D., Vann, S.D., Aggleton, J.P., Sengpiel, F., Ranson, A., 2020. Stable Encoding of Visual Cues in the Mouse Retrosplenial Cortex. Cereb. Cortex 1–42. https://doi.org/10.1093/cercor/bhaa030

Preston-Ferrer, P., Coletta, S., Frey, M., Burgalossi, A., 2016. Anatomical organization of presubicular head-direction circuits. Elife 5, 1–20. https://doi.org/10.7554/eLife.14592

Ranck Jr, J.B., 1984. Head direction cells in the deep layer of dorsal presubiculum in freely moving rats. Soc. Neurosci. Abstr. 10, 599.

Raudies, F., Brandon, M.P., Chapman, G.W., Hasselmo, M.E., 2014. Head direction is coded more strongly than movement direction in a population of entorhinal neurons. Brain Res. 1621, 355–367. https://doi.org/10.1016/j.physbeh.2017.03.040

Redish, A.D., Elga, A.N., Touretzky, D.S., 1996. A coupled attractor model of the rodent Head Direction system. Netw. Comput. Neural Syst. 7, 671–685. https://doi.org/10.1088/0954-898X_7_4_004

Rees, C.L., Moradi, K., Ascoli, G.A., 2017. Weighing the Evidence in Peters' Rule: Does Neuronal Morphology Predict Connectivity? Trends Neurosci. 40, 63–71. https://doi.org/10.1016/j.tins.2016.11.007

Rigotti, M., Barak, O., Warden, M.R., Wang, X.J., Daw, N.D., Miller, E.K., Fusi, S., 2013. The importance of mixed selectivity in complex cognitive tasks. Nature 497, 585–590. https://doi.org/10.1038/nature12160

Rigotti, M., Rubin, D.B.D., Wang, X.J., Fusi, S., 2010. Internal representation of task rules by recurrent dynamics: The importance of the diversity of neural responses. Front. Comput. Neurosci. 4, 1–29. https://doi.org/10.3389/fncom.2010.00024

Rikhye, R. V., Gilra, A., Halassa, M.M., 2018. Thalamic regulation of switching between cortical representations enables cognitive flexibility. Nat. Neurosci. 21, 1753–1763. https://doi.org/10.1038/s41593-018-0269-z

Rikhye, R. V., Wimmer, R.D., Halassa, M.M., 2018. Toward an Integrative Theory of Thalamic Function. Annu. Rev. Neurosci. 41, 163–183. https://doi.org/10.1146/annurev-neuro-080317-062144

Rubin, A., Sheintuch, L., Brande-Eilat, N., Pinchasof, O., Rechavi, Y., Geva, N., Ziv, Y., 2019. Revealing neural correlates of behavior without behavioral measurements. Nat. Commun. 10. https://doi.org/10.1038/s41467-019-12724-2

Samsonovich, a, McNaughton, B.L., 1997. Path integration and cognitive mapping in a continuous attractor neural network model. J. Neurosci. 17, 5900–5920. https://doi.org/10.1146/ANNUREV.PSYCH.53.100901.135114

Sargolini, F., Fyhn, M., Hafting, T., McNaughton, B.L., Witter, M.P., Moser, M., Moser, E.I., 2006. Conjunctive Representation of Position, Direction, and Velocity in Entorhinal Cortex. Science (80-.). 312, 758–762. https://doi.org/10.1126/science.1125572

Schmitt, L.I., Wimmer, R.D., Nakajima, M., Happ, M., Mofakham, S., Halassa, M.M., 2017. Thalamic amplification of cortical connectivity sustains attentional control. Nature 545, 219–223. https://doi.org/10.1038/nature22073

Scholl, B., Wilson, D.E., Fitzpatrick, D., 2017. Local Order within Global Disorder: Synaptic Architecture of Visual Space. Neuron 96, 1127-1138.e4. https://doi.org/10.1016/j.neuron.2017.10.017

Schultheiss, N.W., Redish, a D., 2015. The compass within. Nat. Neurosci. 18, 482–3. https://doi.org/10.1038/nn.3977

Schwarz, S., Wystrach, A., Cheng, K., 2017. Ants' navigation in an unfamiliar environment is influenced by their experience of a familiar route. Sci. Rep. 7, 1–7. https://doi.org/10.1038/s41598-017-14036-1

Seelig, J.D., Jayaraman, V., 2015. Neural dynamics for landmark orientation and angular path integration. Nature 521, 186–191.

Sharp, P.E., Blair, H.T., Cho, J., 2001. The anatomical and computational basis of the rat head-direction cell signal. Trends Neurosci. 24, 289–294. https://doi.org/http://dx.doi.org/10.1016/S0166-2236(00)01797-5

Sharp, P.E., Tinkelman, A., Cho, J., 2001. Angular velocity and head direction signals recorded from the dorsal tegmental nucleus of gudden in the rat: Implications for path integration in the head direction cell circuit. Behav. Neurosci. 115, 571–588. https://doi.org/10.1037/0735-7044.115.3.571

Shepherd, G.M.G., Yamawaki, N., 2021. Untangling the cortico-thalamo-cortical loop: cellular pieces of a knotty circuit puzzle. Nat. Rev. Neurosci. 22, 389–406. https://doi.org/10.1038/s41583-021-00459-3

Sherman, S.M., 2016. Thalamus plays a central role in ongoing cortical functioning. Nat. Neurosci. 19, 533–541. https://doi.org/10.1038/nn.4269

Sherman, S.M., Guillery, R.W., 1996. Functional organization of thalamocortical relays. J. Neurophysiol. 76, 1367–1395. https://doi.org/10.1152/jn.1996.76.3.1367

Sheroziya, M., Timofeev, I., 2014. Global intracellular slow-wave dynamics of the thalamocortical system. J. Neurosci. 34, 8875–8893. https://doi.org/10.1523/JNEUROSCI.4460-13.2014

Shibata, H., 1998. Organization of projections of rat retrosplenial cortex to the anterior thalamic nuclei. Eur. J. Neurosci. 10, 3210–3219. https://doi.org/10.1046/j.1460-9568.1998.00328.x

Shibata, H., 1993. Efferent projections from the anterior thalamic nuclei to the cingulate cortex in the rat. J. Comp. Neurol. 330, 533–542. https://doi.org/10.1002/cne.903300409

Shine, J.P., Valdés-Herrera, J.P., Hegarty, M., Wolbers, T., 2016. The Human Retrosplenial Cortex and Thalamus Code Head Direction in a Global Reference Frame. J. Neurosci. 36, 6371–6381. https://doi.org/10.1523/JNEUROSCI.1268-15.2016

Shine, J.P., Wolbers, T., 2021. Global and Local Head Direction Coding in the Human Brain. bioRxiv 43.

Siapas, A.G., Wilson, M.A., 1998. Coordinated Interactions between Hippocampal Ripples and Cortical Spindles during Slow-Wave Sleep of SWS and during behavioral immobility. These high-frequency oscillations constitute a major mode of hippo-campal activity (Buzsaki et al they provide ideal. Neuron 21, 1123–1128.

Siegle, J.H., López, A.C., Patel, Y.A., Abramov, K., Ohayon, S., Voigts, J., 2017. Open Ephys: An open-source, plugin-based platform for multichannel electrophysiology. J. Neural Eng. 14. https://doi.org/10.1088/1741-2552/aa5eea

Simonnet, J., Fricker, D., 2018. Cellular components and circuitry of the presubiculum and its functional role in the head direction system. Cell Tissue Res. 373, 541–556. https://doi.org/10.1007/s00441-018-2841-y

Simonnet, J., Nassar, M., Stella, F., Cohen, I., Mathon, B., Boccara, C.N., Miles, R., Fricker, D., 2017. Activity dependent feedback inhibition may maintain head direction signals in mouse presubiculum. Nat. Commun. 8, 16032. https://doi.org/10.1038/ncomms16032

Sirota, A., Montgomery, S., Fujisawa, S., Isomura, Y., Zugaro, M., Buzsáki, G., 2008. Entrainment of Neocortical Neurons and Gamma Oscillations by the Hippocampal Theta Rhythm. Neuron 60, 683–697. https://doi.org/10.1016/j.neuron.2008.09.014

Skaggs, W.E., Knierim, J.J., Kudrimoti, H.S., McNaughton, B.L., 1995. A model of the neural basis of the rat's sense of direction. Adv. Neural Inf. Process. Syst. 7, 173–180.

Skaggs, W.E., McNaughton, B., Gothard, K.M., Markus, E.J., 1993. Information theoretic approach to deciphering the Hippocampal code. Adv. Neural Inf. Process. Syst. 5, 1030–1038.

Skelton, R.W., Ross, S.P., Nerad, L., Livingstone, S.A., 2006. Human spatial navigation deficits after traumatic brain injury shown in the arena maze, a virtual Morris water maze. Brain Inj. 20, 189–203. https://doi.org/10.1080/02699050500456410

Solstad, T., Boccara, C.N., Kropff, E., Moser, M.-B., Moser, E.I., 2008. Representation of Geometric Borders in the Entorhinal Cortex. Science (80-.). 322, 1865–1868. https://doi.org/10.1126/science.1166466

Song, P., Wang, X.J., 2005. Angular path integration by moving "hill of activity": A spiking neuron model without recurrent excitation of the head-direction system. J. Neurosci. 25, 1002–1014. https://doi.org/10.1523/JNEUROSCI.4172-04.2005

Stackman, R.W., Taube, J.S., 1998. Firing properties of rat lateral mammillary single units: Head direction, head pitch, and angular head velocity. J. Neurosci. 18, 9020–9037. https://doi.org/10.1523/jneurosci.18-21-09020.1998

Stackman, R.W., Taube, J.S., 1997. Firing properties of head direction cells in the rat anterior thalamic nucleus: Dependence on vestibular input. J. Neurosci. 17, 4349–4358. https://doi.org/10.1523/jneurosci.17-11-04349.1997

Stark, E., Abeles, M., 2009. Unbiased estimation of precise temporal correlations between spike trains. J. Neurosci. Methods 179, 90–100. https://doi.org/10.1016/j.jneumeth.2008.12.029

Steriade, M., McCormick, D.A., Sejnowski, T.J., 1993. Thalamocortical oscillations in the sleeping and aroused brain. Science (80-.). 262, 679–685. https://doi.org/10.1126/science.8235588

Sterratt, D.C., Lyngholm, D., Willshaw, D.J., Thompson, I.D., 2013. Standard Anatomical and Visual Space for the Mouse Retina: Computational Reconstruction and Transformation of Flattened Retinae with the Retistruct Package. PLoS Comput. Biol. 9. https://doi.org/10.1371/journal.pcbi.1002921

Stringer, S.M., Rolls, E.T., 2006. Self-organizing path integration using a linked continuous attractor and competitive network: Path integration of head direction. Netw. Comput. Neural Syst. 17, 419–445. https://doi.org/10.1080/09548980601004032

Sugar, J., Witter, M.P., van Strien, N.M., Cappaert, N.L.M., 2011. The Retrosplenial Cortex: Intrinsic Connectivity and Connections with the (Para)Hippocampal Region in the Rat. An Interactive Connectome. Front. Neuroinform. 5, 1–13. https://doi.org/10.3389/fninf.2011.00007

Tan, H.M., Bassett, J.P., O'Keefe, J., Cacucci, F., Wills, T.J., 2015. The development of the head direction system before eye opening in the rat. Curr. Biol. 25, 479–483. https://doi.org/10.1016/j.cub.2014.12.030

Taube, J.S., 2019. Reply to Laurens and Angelaki: A model-based reassessment of the three-dimensional tuning of head direction cells in rats. J. Neurophysiol. 122, 1288–1289. https://doi.org/10.1152/jn.00525.2019

Taube, J.S., Bassett, J.P., 2003. Persistent Neural Activity in Head Direction Cells. Cereb. Cortex 13, 1162–1172. https://doi.org/10.1093/cercor/bhg102

Taube, J.S., Burton, H.L., 1995. Head direction cell activity monitored in a novel environment and during a cue conflict situation. J. Neurophysiol. 74, 1953–1971. https://doi.org/10.1152/jn.1995.74.5.1953

Taube, J.S., Muller, R.U., Ranck, J.B., 1990a. Head-direction cells recorded from the postsubiculum in freely moving rats. I Descriptions and Quantitative Analysis. J. Neurosci.

10, 436–447. https://doi.org/10.1523/jneurosci.10-02-00436.1990

Taube, J.S., Muller, R.U., Ranck, J.B., 1990b. Head-direction cells recorded from the postsubiculum in freely moving rats. II. Effects of environmental manipulations. J. Neurosci. 10, 436–447. https://doi.org/10.1523/jneurosci.10-02-00436.1990

Tolman, E.C., 1948. Cognitive Maps in Rats and Men. Psychol. Rev. 55.

Tsanov, M., Chah, E., Vann, S.D., Reilly, R.B., Erichsen, J.T., Aggleton, J.P., O'Mara, S.M., 2011. Theta-modulated head direction cells in the rat anterior thalamus. J. Neurosci. 31, 9489–9502. https://doi.org/10.1523/JNEUROSCI.0353-11.2011

Tsoar, A., Nathan, R., Bartan, Y., Vyssotskib, A., Dell'Omo, G., Ulanovsky, N., 2011. Large-scale navigational map in a mammal. Proc. Natl. Acad. Sci. U. S. A. 108. https://doi.org/10.1073/pnas.1107365108

Tukker, J.J., Tang, Q., Burgalossi, A., Brecht, M., 2015. Head-Directional Tuning and Theta Modulation of Anatomically Identified Neurons in the Presubiculum. J. Neurosci. 35, 15391–15395. https://doi.org/10.1523/JNEUROSCI.0685-15.2015

Turner-Evans, D., Wegener, S., Rouault, H., Franconville, R., Wolff, T., Seelig, J.D., Druckmann, S., Jayaraman, V., 2017. Angular velocity integration in a fly heading circuit. Elife 6, 1–39. https://doi.org/10.7554/eLife.23496

Ulanovsky, N., Moss, C.F., 2008. What the bat's voice tells the bat's brain. Proc. Natl. Acad. Sci. U. S. A. 105, 8491–8498. https://doi.org/10.1073/pnas.0703550105

Valerio, S., Taube, J.S., 2012. Path integration: how the head direction signal maintains and corrects spatial orientation. Nat. Neurosci. 15, 1445–53. https://doi.org/10.1038/nn.3215

van Groen, T., Wyss, J.M., 1990. The connections of presubiculum and parasubiculum in the rat. Brain Res. 518, 227–243. https://doi.org/10.1016/0006-8993(90)90976-I

Van Groen, T., Wyss, J.M., 2003. Connections of the retrosplenial granular b cortex in the rat. J. Comp. Neurol. 463, 249–263. https://doi.org/10.1002/cne.10757

Van Groen, T., Wyss, J.M., 1990. Connections of the retrosplenial granular a cortex in the rat. J. Comp. Neurol. 300, 593–606. https://doi.org/10.1002/cne.10757

van Wijngaarden, J.B.G., Babl, S.S., Ito, H.T., 2020. Entorhinal-retrosplenial circuits for allocentric-egocentric transformation of boundary coding. Elife 9, 1–25. https://doi.org/10.7554/eLife.59816

Vann, S.D., Aggleton, J.P., 2004. Testing the importance of the retrosplenial guidance system: Effects of different sized retrosplenial cortex lesions on heading direction and spatial working memory. Behav. Brain Res. 155, 97–108. https://doi.org/10.1016/j.bbr.2004.04.005

Vann, S.D., Aggleton, J.P., Maguire, E.A., 2009. What does the retrosplenial cortex do? Nat. Rev. Neurosci. 10, 792–802. https://doi.org/10.1038/nrn2733

Vantomme, G., Osorio-Forero, A., Lüthi, A., Fernandez, L.M.J., 2019. Regulation of local sleep by the thalamic reticular nucleus. Front. Neurosci. 13, 1–8. https://doi.org/10.3389/fnins.2019.00576

Vantomme, G., Rovó, Z., Cardis, R., Béard, E., Katsioudi, G., Guadagno, A., Perrenoud, V., Fernandez, L.M.J., Lüthi, A., 2020. A Thalamic Reticular Circuit for Head Direction Cell Tuning and Spatial Navigation. Cell Rep. 31. https://doi.org/10.1016/j.celrep.2020.107747

Viejo, G., Cortier, T., Peyrache, A., 2018. Brain-state invariant thalamo-cortical coordination revealed by non-linear encoders. PLoS Comput. Biol. 14, 1–25. https://doi.org/10.1371/journal.pcbi.1006041

Viejo, G., Peyrache, A., 2020. Precise coupling of the thalamic head-direction system to hippocampal ripples. Nat. Commun. 11, 1–14. https://doi.org/10.1038/s41467-020-15842-4

Voigts, J., Deister, C.A., Moore, C.I., 2020. Layer ensembles can selectively regulate the behavioral impact and layer-specific representation of sensory deviants. Elife 9, 1–39. https://doi.org/10.7554/eLife.48957

Voigts, J., Harnett, M.T., 2020. Somatic and Dendritic Encoding of Spatial Variables in Retrosplenial Cortex Differs during 2D Navigation. Neuron 105, 237-245.e4. https://doi.org/10.1016/j.neuron.2019.10.016

Voigts, J., Newman, J.P., Wilson, M.A., Harnett, M.T., 2020. An easy-to-assemble, robust, and lightweight drive implant for chronic tetrode recordings in freely moving animals. J. Neural Eng. 17. https://doi.org/10.1088/1741-2552/ab77f9

Wang, B., Gonzalo-Ruiz, A., Sanz, J.M., Campbell, G., Lieberman, A.R., 1999. Immunoelectron microscopic study of γ-aminobutyric acid inputs to identified thalamocortical projection neurons in the anterior thalamus of the rat. Exp. Brain Res. 126, 369–382. https://doi.org/10.1007/s002210050744

Wehner, R., Müller, M., 2006. The significance of direct sunlight and polarized skylight in the ant's celestial system of navigation. Proc. Natl. Acad. Sci. U. S. A. 103, 12575–12579. https://doi.org/10.1073/pnas.0604430103

Whitlock, J.R., Sutherland, R.J., Witter, M.P., Moser, M.B., Moser, E.I., 2008. Navigating from hippocampus to parietal cortex. Proc. Natl. Acad. Sci. U. S. A. 105, 14755–14762. https://doi.org/10.1073/pnas.0804216105

Wickersham, I.R., Sullivan, H.A., 2015. Rabies Viral Vectors for Monosynaptic Tracing and Targeted Transgene Expression in Neurons. Cold Spring Harb. Protoc. 375–386. https://doi.org/10.1101/pdb.prot072389

Wijesinghe, R., Protti, D.A., Camp, A.J., 2015. Vestibular Interactions in the Thalamus. Front. Neural Circuits 9, 1–8. https://doi.org/10.3389/fncir.2015.00079

Wilber, A.A., Clark, B.J., Forster, T.C., Tatsuno, M., McNaughton, B.L., 2014. Interaction of egocentric and world-centered reference frames in the rat posterior parietal cortex. J. Neurosci. 34, 5431–46. https://doi.org/10.1523/JNEUROSCI.0511-14.2014

Wilson, M.A., Mcnaughton, B.L., 1994. Reactivation of Hippocampal Ensemble Memories During Sleep. Science (80-.). 265, 676–679.

Wilson, M.A., McNaughton, B.L., 1993. Dynamics of the hippocampal ensemble code for space. Science (80-.). 261, 1055–1058. https://doi.org/10.1126/science.8351520

Wimmer, R.D., Schmitt, I.L., Davidson, T.J., Nakajima, M., Deisseroth, K., Halassa, M.M., 2015. Thalamic control of sensory selection in divided attention. Nature 526, 705–709. https://doi.org/10.1038/nature15398

Winter, S., Clark, B., Taube, J.S., 2015. Disruption of the head direction cell network impairs the parahippocampal grid cell signal. Science. 347, 1–6.

Wirtshafter, D., Stratford, T.R., 1993. Evidence for GABAergic projections from the tegmental nuclei of Gudden to the mammillary body in the rat. Brain Res. 630, 188–194. https://doi.org/10.1016/0006-8993(93)90656-8

Wolff, M., Vann, S.D., 2018. The Cognitive Thalamus as a Gateway to Mental Representations. J. Neurosci. 39, 3–14. https://doi.org/10.1523/jneurosci.0479-18.2018

Worden, R., Bennett, M.S., Neacsu, V., 2021. The Thalamus as a Blackboard for Perception and Planning. Front. Behav. Neurosci. 15, 1–18. https://doi.org/10.3389/fnbeh.2021.633872

Wu, L.-Q., Dickman, J.D., 2012. Neural Correlates of a Magnetic Sense. Science (80-.). 336, 1054–1058.

Wyss, J.M., van Groen, T., 1992. Connections between the retrosplenial cortex and the hippocampal-formation in the rat - a review. Hippocampus 2, 1–12. https://doi.org/10.1002/hipo.450020102

Wyss, J.M., Van Groen, T., 1992. Connections between the retrosplenial cortex and the hippocampal formation in the rat: A review. Hippocampus 2, 1–11. https://doi.org/10.1002/hipo.450020102

Xie, X., Hahnloser, R.H.R., Seung, H.S., 2002. Double-ring network model of the head-direction system. Phys. Rev. E - Stat. Physics, Plasmas, Fluids, Relat. Interdiscip. Top. 66, 9. https://doi.org/10.1103/PhysRevE.66.041902

Xu, Z. et al., 2019. A Comparison of Neural Decoding Methods and Population Coding Across

Thalamo-Cortical Head Direction Cells. Front. Neural Circuits 13, 1–18. https://doi.org/10.3389/fncir.2019.00075

Yamawaki, N., Li, X., Lambot, L., Ren, L.Y., Radulovic, J., Shepherd, G.M.G., 2019. Long-range inhibitory intersection of a retrosplenial thalamocortical circuit by apical tuft-targeting CA1 neurons. Nat. Neurosci. 22. https://doi.org/10.1038/s41593-019-0355-x

Yamawaki, N., Radulovic, J., Shepherd, G.M.G., 2016. A Corticocortical Circuit Directly Links Retrosplenial Cortex to M2 in the Mouse. J. Neurosci. 36, 9365–9374. https://doi.org/10.1523/JNEUROSCI.1099-16.2016

Yan, Y., Burgess, N., Bicanski, A., 2021. A model of head direction and landmark coding in complex environments, PLOS Computational Biology. https://doi.org/10.1371/journal.pcbi.1009434

Yoder, R.M., Clark, B.J., Brown, J.E., Lamia, M. V., Valerio, S., Shinder, M.E., Taube, J.S., 2011. Both visual and idiothetic cues contribute to head direction cell stability during navigation along complex routes. J. Neurophysiol. 105, 2989–3001. https://doi.org/10.1152/jn.01041.2010

Yoder, R.M., Peck, J.R., Taube, J.S., 2015. Visual landmark information gains control of the head direction signal at the lateral mammillary nuclei. J. Neurosci. 35, 1354–67. https://doi.org/10.1523/JNEUROSCI.1418-14.2015

Yoder, R.M., Taube, J.S., 2014. The vestibular contribution to the head direction signal and navigation. Front. Integr. Neurosci. 8, 1–13. https://doi.org/10.3389/fnint.2014.00032

Yoder, R.M., Taube, J.S., 2011. Projections to the anterodorsal thalamus and lateral mammillary nuclei arise from different cell populations within the postsubiculum: Implications for the control of head direction cells. Hippocampus 21, 1062–1073. https://doi.org/10.1002/hipo.20820.Projections

Yoganarasimha, D., Yu, X., Knierim, J.J., 2006. Head direction cell representations maintain internal coherence during conflicting proximal and distal cue rotations: comparison with hippocampal place cells. J. Neurosci. 26, 622–31. https://doi.org/10.1523/JNEUROSCI.3885-05.2006

Yoshida, M., Chinzorig, C., Matsumoto, J., Nishimaru, H., Ono, T., Yamazaki, M., Nishijo, H., 2021. Configural Cues Associated with Reward Elicit Theta Oscillations of Rat Retrosplenial Cortical Neurons Phase-Locked to LFP Theta Cycles. Cereb. Cortex 31, 2729–2741. https://doi.org/10.1093/cercor/bhaa395

Yoshida, M., Hasselmo, M.E., 2009. Persistent Firing Supported by an Intrinsic Cellular Mechanism in a Component of the Head Direction System. J. Neurosci. 29, 4945–4952. https://doi.org/10.1523/JNEUROSCI.5154-08.2009

Zhang, K., 1996. Representation of spatial orientation by the intrinsic dynamics of the head-direction cell ensemble: A theory. J. Neurosci. 16, 2112–2126. https://doi.org/10.1523/jneurosci.16-06-02112.1996

Zhang, N., Grieves, R.M., Jeffery, K.J., 2021. Environment symmetry drives a multidirectional code in rat retrosplenial cortex. bioRxiv 1–18.

Zhang, W., Bruno, R.M., 2019. High-order thalamic inputs to primary somatosensory cortex are stronger and longer lasting than cortical inputs. Elife 8, 1–22. https://doi.org/10.7554/elife.44158

Zirkelbach, J., Stemmler, M., Herz, A.V.M., 2019. Anticipatory neural activity improves the decoding accuracy for dynamic head-direction signals. J. Neurosci. 39, 2847–2859. https://doi.org/10.1523/JNEUROSCI.2605-18.2019

Zugaro, B., Arleo, A., Berthoz, A., Wiener, S.I., 2003. Rapid Spatial Reorientation and Head Direction Cells. J. Neurosci. 23, 3478–3482.

Zugaro, M.B., Berthoz, A., Wiener, S.I., 2001. Background, but not foreground, spatial cues are taken as references for head direction responses by rat anterodorsal thalamus neurons. J. Neurosci. 21, RC154. https://doi.org/20015390